2012

Implementation And Performance Comparisons For The Crisfield And Stiff Arc Length Methods In FEA

Thomas W. Silvers
University of Central Florida

IMPLEMENTATION AND PERFORMANCE COMPARISONS FOR THE CRISFIELD AND STIFF ARC LENGTH METHODS IN FEA

by

THOMAS W. SILVERS
B.S. University of Central Florida, 2009

A thesis submitted in partial fulfillment of the requirements
for the degree of Master of Science in Mechanical Engineering
in the Department of Mechanical, Materials and Aerospace Engineering
in the College of Engineering and Computer Science
at the University of Central Florida
Orlando, Florida

Spring Term
2012

Major Professors: Ali P. Gordon and David W. Nicholson

ABSTRACT

In Nonlinear Finite Element Analysis (FEA) applied to structures, displacements at which the tangent stiffness matrix $\mathbf{K}_T$ becomes singular are called *critical points,* and correspond to instabilities such as buckling or elastoplastic softening (e.g., necking). Prior to the introduction of Arc Length Methods (ALMs), critical points posed severe computational challenges, which was unfortunate since behavior at instabilities is of great interest as a precursor to structural failure. The original ALM was shown to be capable in some circumstances of continued computation at critical points, but limited success and unattractive features of the formulation were noted and addressed in extensive subsequent research. The widely used Crisfield Cylindrical and Spherical ALMs may be viewed as representing the 'state-of-the-art'. The more recent Stiff Arc Length method, which is attractive on fundamental grounds, was introduced in 2004, but without implementation, benchmarking or performance assessment. The present thesis addresses (a) implementation and (b) performance comparisons for the Crisfield and Stiff methods, using simple benchmarks formulated to incorporate elastoplastic softening. It is seen that, in contrast to the Crisfield methods, the Stiff ALM consistently continues accurate computation at, near and beyond critical points.

To my Grandma, for all her encouragement and support throughout all the years.

ACKNOWLEDGMENTS

First off all I owe a huge thank you to my co-advisor, Dr. David Nicholson. Dr. Nicholson has provided great technical expertise, especially his help in developing some of the equations necessary to complete my thesis. He also provided much insight and support in helping me conduct some of the comparisons mentioned in the thesis. For the past few years, I have been working on this thesis on and off due to my busy work schedule and Dr. Nicholson always remained both patient and flexible in his schedule to accommodate mine, including nights. Without Dr. Nicholson's flexibility in his schedule, finishing this thesis wouldn't have been possible.

Secondly, I would like to thank my advisor Dr. Ali Gordon for all his advice and guidance. Dr. Gordon provided great assistance in the proper formatting required for the thesis and the associated deadlines along with providing several previous example thesis papers to help answer many questions/concerns I had. Dr. Gordon also worked around my work schedule so that we could meet to address any questions I had and to make sure I was remaining on track for finishing the thesis on time. Dr. Gordon's support in reviewing the content and formatting present in the thesis was also a great help and is much appreciated.

Lastly, I would like to thank my family for all their support and guidance throughout the years. My grandma has been a great source of encouragement and always offered her support, even thru all the road blocks that emerged along the way. I also owe my gratitude to my loving fiancée for always being there for me and putting up with the neglection while finishing up my Master's Degree.

TABLE OF CONTENTS

LIST OF FIGURES

LIST OF TABLES

LIST OF NOMENCLATURE

Variable	
K_T	Tangent Stiffness Matrix
n	Numeric Number
$K_T^{\#}$	Augmented Stiffness Matrix
φ	Equilibrium Equation (Unbalanced Force)
p	Displacement
λ	Load Step Parameter
q_i	Internal Force
q_e	External Force
f	Force
S	Arc Length Parameter
Ψ	Load Scaling Parameter
ξ	Arc Length Constraint Equation
ΔS	Approximate to Arc Length Parameter
δ	Iterative Change
Δ	Incremental Change
j	Iterate Counter
k	Increment Counter
$\Delta p_{predictor}$	Displacement Predictor
$\Delta \lambda_{predictor}$	Load Step Parameter Predictor
p_e	Displacement conjugate to q_e

z	Sign Change
ϵ	Error
p^*	Iterative Displacement Change
a	Crisfield Quadratic Equation Scalars
zt	Arc Length Vector
zo	Arc Length Constant
ks	Sub Row or Column of Matrix
Q	Orthogonal Matrix
$K^{\#}$	Transformed Matrix
Λ	Eigenvalue Matrix (Transformed Stiffness Matrix)
q_e^*	Transformed External Force
zt^*	Transformed Arc Length Vector
zo^*	Transformed Arc Length Constant
λe	Eigenvalue
ags	Gram-Schmidt
x	Variable
y	Variable
K_e	Elastic Stiffness Matrix
K_o	Plasticity Onset Stiffness Matrix
K_i	Negative Plasticity Stiffness Matrix
$p\#$	Modified Displacement After Yield
p_y	Displacement At Yield

ko	One Degree-of-Freedom Benchmark Scalar
α	Critical Point Scalar
L	Length
pc	Displacement At Critical Point
C	Constant of Integration
f_y	Yield Force
A	Area
ke	Individual Truss Member Stiffness
ε	Individual Truss Member Strain
E_e	Elastic Modulus
ε_y	Yield Strain
E_{po}	Plasticity Onset Modulus Matrix
E_{p1}	Negative Plasticity Modulus Matrix
E	Incremental Strain Vector
G	Geometric Matrix
D	Incremental Displacement Vector
Γ	Kernal Stiffness Matrix
Ω	Length Matrix
e	Strain Vector
s	Stress Vector
V	Volume
F	Global External Force Vector

J	Jacobian Matrix
ζ	Accelerated Initial Predictor Constant
q	Critical Point Predictor Variable
r	Critical Point Predictor Variable
ke_p	Predicted Stiffness at Critical Point
x_p	Predicted Critical Point
ΔS_T	Total Arc Length

Chapter One : INTRODUCTION

1.1 OBJECTIVES

In nonlinear finite element analysis, many applications exhibit critical points at which the tangent stiffness matrix becomes singular and continued accurate computation becomes very challenging. Arc Length Methods (ALMs) were introduced in the late 1970s to address exhibiting critical points since which time there have been modifications by a number of investigators. The current investigation is intended to review the more widely used methods, implement them in simple benchmark problems, and to compare their advantages, disadvantages and performance with that of the more recently introduced Stiff Arc Length Method (SALM). The situations of interest are structures exhibiting elastoplastic instability (e.g. necking).

More specifically the objectives are:

1. Review widely used Arc Length Methods

   Arc Length Methods developed prior to the SALM have been extensively documented. This investigation is intended to give a unified presentation of the more widely used Arc Length Methods, especially the Crisfield methods, using consistent notation, so that differences are highlighted and conclusions can be more easily drawn.

2. Review the Stiff Arc Length Method

The SALM has several fundamental advantages over previous Arc Length Methods, but has yet to be widely recognized. The article introducing the SALM used different notation from other Arc Length Methods presentations. Also it was not implemented or applied to benchmark examples to demonstrate its validity or its performance compared to previous methods. The current investigation focuses on comparing the formulation and performance of this method to the widely used Arc Length Methods, especially those of Crisfield. To do so, the ALMs have been implemented using benchmark problems formulated to exhibit elastoplastic instability.

3. Formulate a Single Degree-of-Freedom Benchmark Problem with Elastoplastic Instability

   A one degree-of-freedom (1 DOF) elastoplastic benchmark problem has been formulated which exhibits a maximum load and there-after a decreasing load in the plastic region ("softening"). The Crisfield and Stiff ALMs have been implemented using MATHCAD for the benchmark, and a demanding performance comparison has been conducted. The material model embedded in the benchmark has been shown to capture published empirical behavior of several common aluminum alloys.

4. Formulate a Three Degree-of-Freedom Benchmark with Elastoplastic Instability

A 3 DOF benchmark problem, modeling an elastoplastic truss structure, has been formulated; it exhibits several discontinuous stiffness changes as well as softening (negative stiffness) after the maximum load (critical point). The ALMs have been implemented in MATHCAD for this benchmark, and a demanding performance comparison has been conducted.

5. Conduct Performance Comparisons

   Using the elastoplastic benchmarks, performance comparisons have been conducted, addressing:

   1) Continuation of accurate computation at and beyond the critical point load
   2) Consistently improved accuracy with reduced arc length parameter (increment size)
   3) Rate of convergence and computational effort
   4) Minimizing the need for user intervention

   It will be seen that the SALM offers significantly better performance in the benchmark problems than the Crisfield methods

6. Recommendations and Future Work for the Stiff Arc Length Method

   Several recommendations are noted to further enhance the performance of the SALM and to address implementation in a finite element code modeling multi-dof problems.

1.2 REVIEW OF ARC LENGTH METHODS

An extensive review and presentation of ALMs up to 2000 has been given in the first Crisfield monograph (Crisfield, 1991). A very thorough review as of 1999, along with extensive performance assessment, is given in the two articles of Geers (Geers, 1999-a and 1999-b). Also of interest is the more recent review of Memon and Su (Memon and Su, 2004). A recent thesis (Posada, 2007) provides extensive performance assessment of the major ALMs when applied to benchmarks for buckling problems. Finally a recent Arc Length Method proposal for fracture simulation has been given in Verhoosel et al (Verhoosel et al, 2008).

A very brief overview of the basic notion of the Arc Length Method is now given. Prior to the ALM, in nonlinear problems in FEA with n degrees-of-freedom (dofs) the equilibrium relation was expressed as a linear system with an $n \times n$ tangent stiffness matrix $\boldsymbol{K}_T$. Of course this matrix becomes singular at a critical point. The Arc Length Method increases the dimension of the solution space to $n+1$ by (i) introducing an additional degree of freedom, known as the load intensity and (ii) introducing a corresponding (scalar-valued) Arc Length Constraint Equation imposing a restriction on the arc length traversed along the solution path in one increment in the expanded space. Doing so introduces a new linear system containing an augmented tangent stiffness matrix $\boldsymbol{K}_T^*$ which is now $(n+1)\times(n+1)$. With proper selection of the constraint equation, $\boldsymbol{K}_T^*$ remains nonsingular at the critical point of $\boldsymbol{K}_T$. The various ALMs differ in the actual details of the arc length constraint equation and their effect on $\boldsymbol{K}_T^*$ at the

critical point, as well as in aspects of the numerical solution of the augmented linear system.

1.2.1 RIKS AND WEMPNER ARC LENGTH METHOD

The original Arc Length Method was introduced by Riks (Riks, 1972 and Riks, 1979) and Wempner (Wempner, 1971), and is now reviewed. Their formulation was designed to find the solution at the intersection of the arc length constraint equation and the nonlinear equilibrium (FEA) equation. The nonlinear equilibrium equation is shown below as Equation 1.1 (Crisfield, 1991).

$$\boldsymbol{\varphi}(\boldsymbol{p},\lambda) = \boldsymbol{q}_i(\boldsymbol{p}) - \lambda \boldsymbol{q}_e = 0 \tag{1.1}$$

In which $\boldsymbol{\varphi}$ is a function of the displacement vector $\boldsymbol{p}$, and is the out-of-balance force vector which vanishes at equilibrium. The internal force vector $\boldsymbol{q}_i$ is a function of the displacements and is equal to the force vector $\boldsymbol{f}$. The prescribed external force vector is designated as $\boldsymbol{q}_e$ and is scaled by the load intensity parameter λ, which varies between zero and one. Hence $\lambda \boldsymbol{q}_e$ represents the load applied at the current load increment. This representation enables introducing λ as an additional "degree-of-freedom", thereby expanding the dimensions of the solution space by one. Doing so requires introduction of the Arc Length Constraint equation, which is presented below.

The nonlinear equilibrium equation shown in Equation 1.1 assumes proportional loading all the way along the load path until the final prescribed load is attained. The Arc Length Method is intended to continue computation through critical points along proportionally loaded paths.

The arc length parameter *S*, which is a user-specified constant, is shown below in Equation 1.2 (Crisfield, 1991).

$$S = \int \sqrt{d\boldsymbol{p}^T d\boldsymbol{p} + d\lambda^2 \psi^2 \boldsymbol{q}_e{}^T \boldsymbol{q}_e} \tag{1.2}$$

In which ψ is a user-defined *load scaling parameter*. Equation 1.2 can be rewritten in incremental form as Equation 1.3 and may be called the Riks-Wempner Arc Length Constraint equation (Crisfield, 1991).

$$\xi = \Delta\boldsymbol{p}^T \Delta\boldsymbol{p} + \Delta\lambda^2 \psi^2 \boldsymbol{q}_e{}^T \boldsymbol{q}_e - \Delta S^2 = 0 \tag{1.3}$$

Here ΔS is an approximation to the arc length parameter and is equal to the radius of the intersection between the arc length constraint curve and the non-linear equilibrium curve, see Figure 1.1 (Crisfield, 1991). The constraint curve in this case is actually a hypersphere.

With this particular Arc Length Constraint Equation, Newton (also called Newton-Raphson) Iteration may be employed in the expanded space to solve for n displacement variables (dofs) and one load intensity variable (dof). Applying the Newton method to both Equation 1.1 and Equation 1.3 yields two new equations shown below as Equations 1.4 and 1.5 (Crisfield, 1991).

$$\boldsymbol{\varphi}_{new} = \boldsymbol{\varphi}_{old} + \frac{\partial \boldsymbol{\varphi}}{\partial \boldsymbol{p}} \delta\boldsymbol{p} + \frac{\partial \boldsymbol{\varphi}}{\partial \lambda} \delta\lambda = \boldsymbol{\varphi}_{old} + \boldsymbol{K}_T \delta\boldsymbol{p} - \boldsymbol{q}_e \delta\lambda = 0 \tag{1.4}$$

$$\xi_{new} = \xi_{old} + 2\Delta\boldsymbol{p}^T \delta\boldsymbol{p} + 2\Delta\lambda\delta\lambda\psi^2 \boldsymbol{q}_e{}^T \boldsymbol{q}_e = 0 \tag{1.5}$$

Equations 1.4 and 1.5 can be rewritten in matrix form as Equation 1.6 (Crisfield, 1991).

$$\begin{pmatrix} \delta\boldsymbol{p} \\ \delta\lambda \end{pmatrix} = -\begin{bmatrix} \boldsymbol{K}_T & -\boldsymbol{q}_e \\ 2\Delta\boldsymbol{p}^T & 2\Delta\lambda\psi^2 \boldsymbol{q}_e{}^T \boldsymbol{q}_e \end{bmatrix}^{-1} \begin{pmatrix} \boldsymbol{\varphi}_{old} \\ \xi_{old} \end{pmatrix} \tag{1.6}$$

The δ operator represents an *iterative change* (difference between iterates) and the Δ operator represents an *incremental change* (difference from the converged value in the previous increment). The meanings of $\delta\boldsymbol{p}$ and $\Delta\boldsymbol{p}$ are illustrated in Equations 1.7 and 1.8

$$\delta\boldsymbol{p} = \boldsymbol{p}_{k+1}^{j+1} - \boldsymbol{p}_{k+1}^{j} \tag{1.7}$$

$$\Delta\boldsymbol{p} = \boldsymbol{p}_{k+1}^{j} - \boldsymbol{p}_{k} \tag{1.8}$$

In which j represents the iterate counter and k represents the increment counter. For simplicity, $\boldsymbol{p}_k$ may be chosen as the first iterate for $\boldsymbol{p}^j_{k+1}$.

The Riks-Wempner Arc Length Method, in one dimensional space, is illustrated below in Figure 1.1 (Crisfield, 1991). After converging to an equilibrium point ($\boldsymbol{p}_0$, $\lambda_0\boldsymbol{q}_e$), to obtain the solution for the next increment a predictor (which is both incremental and tangential) is calculated ($\Delta\boldsymbol{p}_1$, $\Delta\lambda_1$) using Equations 1.9 and 1.10 (Crisfield, 1991).

$$\Delta\boldsymbol{p}_{predictor} = \Delta\lambda_{predictor}\boldsymbol{K}_T^{-1}\boldsymbol{q}_e = \Delta\lambda_{predictor}\delta\boldsymbol{p}_e \tag{1.9}$$

$$\Delta\lambda_{predictor} = \pm\frac{\Delta l}{\sqrt{\delta\boldsymbol{p}_e{}^T\delta\boldsymbol{p}_e}} = \boldsymbol{z}\frac{\Delta l}{\sqrt{\delta\boldsymbol{p}_e{}^T\delta\boldsymbol{p}_e}} \tag{1.10}$$

The constant z can either be +1 or -1 depending on whether $\boldsymbol{K}_T$ is positive definite or indefinite, respectively; $\boldsymbol{K}_T$ becomes indefinite at a critical point. The first increment is found by adding the predictor and the solved iterate (which for the first increment is equal to the last converged equilibrium point); the consecutive increments are computed using the procedure given in Equations 1.11 and 1.12 (Crisfield, 1991). The process outlined above is repeated until the user-defined convergence criterion is attained.

$$\Delta \boldsymbol{p}_2 = \Delta \boldsymbol{p}_1 + \delta \boldsymbol{p}_1 \tag{1.11}$$

$$\Delta \lambda_2 = \Delta \lambda_1 + \delta \lambda_1 \tag{1.12}$$

The equations shown above can be easily misunderstood. Crisfield's notations of the increments above are not the difference from the new converged iterate from the old converged iterate, but from the new iterate from the old converged iterate.

An important fact to note is that the augmented stiffness matrix shown in Equation 1.6 is neither symmetric nor banded and, more importantly, has entries which are incremental. The load scaling parameter ψ is introduced in the matrix so that, if the lower right diagonal is small without ψ, that with the addition of ψ, it will become large enough that the matrix will no longer be ill-conditioned (but otherwise has no rationale). The increments in the augmented stiffness matrix in the lower left and lower right positions present a problem because they affect the eigenvalues and the lower right increment will cause the matrix to be ill-conditioned in the absence of the scaling factor.

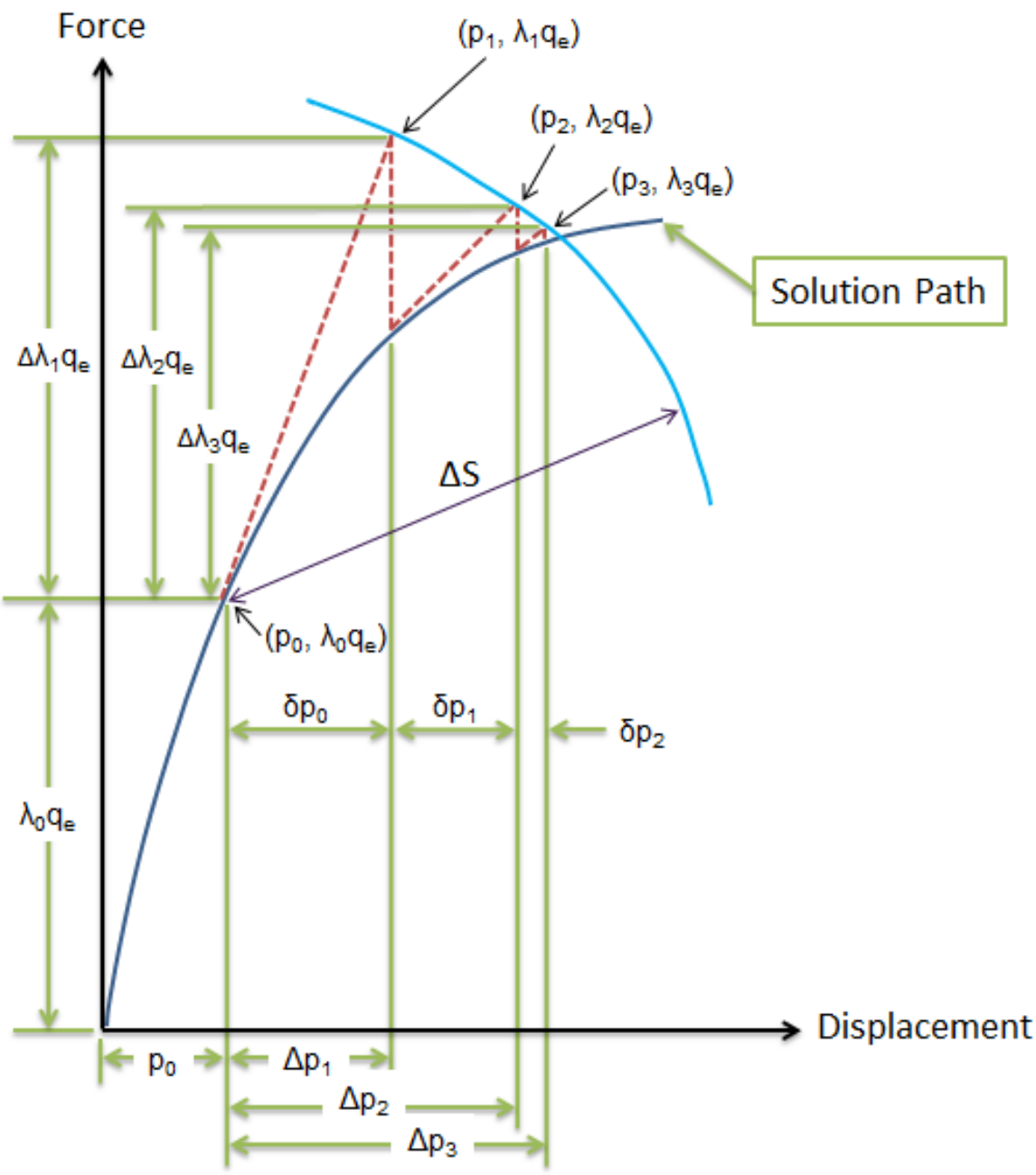

Figure 1.1: Graphical Representation of the Riks and Wempner Arc Length Method with $\psi = 1$

Although this augmented stiffness matrix is neither symmetric nor banded, we will later see that block triangularization may be used to compute the solution of Equation 1.6 by little more than conventional finite element procedures (Nicholson, 2008), as will be demonstrated in the later sections. Since this Arc Length Method makes use of Newton Iteration, it converges quadratically. Quadratic convergence is desirable because the error in the current iteration is proportional to the square of the error at the previous iterate, as shown in Equation 1.13 (Rao, 2002).

$$\in_{j+1} = -\frac{f''(x^*)}{2f'(x^*)} \in_j^2 \tag{1.13}$$

It should be noted that the solution can also diverge quadratically in an incorrect solution path, which usually results if the initial iterate is not in the *domain of attraction* for the correct solution. In fixed point iteration as opposed to Newton iteration, convergence is linear and relates the error between the current iteration and the previous iteration linearly, as shown in Equation 1.14 (Rao, 2002), and of course convergence in this case is usually much slower than for Newton Iteration.

$$\in_{j+1} = g'(\xi) \in_j \tag{1.14}$$

1.2.2 CRISFIELD ARC LENGTH METHODS

Early investigators such as Crisfield (Crisfield, 1991) considered this augmented stiffness matrix very unattractive due to its non-symmetric and non-banded characteristics, as well as the presence of incremental terms. Crisfield introduced several modifications to the Riks-Wempner ALM, the ensuing new method being

referred to throughout this study as the “Crisfield Spherical Arc Length Method” (CSALM). Later, instead of using Equation 1.6, Crisfield used Equations 1.4 and 1.5 and invoked the Batoz and Dhatt method for displacement control (Batoz and Dhatt, 1979) to obtain Equation 1.15 below; it separates the iterative displacement $\delta\boldsymbol{p}$ into two portions (Crisfield, 1991). The new load parameter is shown below as Equation 1.16 (Crisfield, 1991). In doing so Crisfield sought to avoid having an augmented stiffness matrix that is not banded and not symmetric.

$$\delta\boldsymbol{p} = -\boldsymbol{K}_T^{-1}\boldsymbol{\varphi}_{old} + \delta\lambda\boldsymbol{K}_T^{-1}\boldsymbol{q}_e = \delta\boldsymbol{p}^* + \delta\lambda\delta\boldsymbol{p}_e \tag{1.15}$$

$$\lambda_{new} = \lambda_{old} + \delta\lambda \tag{1.16}$$

Here $\delta\boldsymbol{p}^*$ denotes the iterative displacement change in Newton Iteration under load-control (conventional nonlinear FEA), and $\delta\boldsymbol{p}_e$ represents the displacement vector conjugate to the external load vector $\boldsymbol{q}_e$. This modification of the displacement makes the displacement increment proportional to the load increment. *In doing so, Crisfield’s version of the Arc Length Method abandons Newton Iteration, thus abandoning quadratic convergence,* and introduces a potentially complex quadratic root issue as well; the root issue has been addressed in several investigations (e.g. Memon and Su, 2004). This equation can be rewritten in incremental notation as shown below in Equation 1.17 (Crisfield, 1991), in which $\delta\lambda$ is now the only unknown yet to be found.

$$\Delta\boldsymbol{p}_{new} = \Delta\boldsymbol{p}_{old} + \delta\boldsymbol{p}^* + \delta\lambda\delta\boldsymbol{p}_e \tag{1.17}$$

Now the Riks-Wempner Arc Length Constraint equation, Equation 1.3, is rewritten as shown below in Equation 1.18 (Crisfield, 1991).

$$\Delta\boldsymbol{p}_{old}{}^T\Delta\boldsymbol{p}_{old} + \Delta\lambda_{old}^2\psi^2\boldsymbol{q}_e{}^T\boldsymbol{q}_e = \Delta\boldsymbol{p}_{new}{}^T\Delta\boldsymbol{p}_{new} + \Delta\lambda_{new}^2\psi^2\boldsymbol{q}_e{}^T\boldsymbol{q}_e = \Delta S^2 \tag{1.18}$$

Substituting Equation 1.17 into Equation 1.18 renders the quadratic equation shown below in Equation 1.19 (Crisfield, 1991).

$$a_1 \delta\lambda^2 + a_2 \delta\lambda + a_3 = 0 \tag{1.19}$$

In which scalars a_1, a_2, and a_3 are expressed in Equations 1.20 – 1.22 (Crisfield, 1991).

$$a_1 = \delta \boldsymbol{p}_e^T \delta \boldsymbol{p}_e + \psi^2 \boldsymbol{q}_e^T \boldsymbol{q}_e \tag{1.20}$$

$$a_2 = 2\delta \boldsymbol{p}_e (\Delta \boldsymbol{p}_{old} + \delta \boldsymbol{p}^*) + 2\Delta\lambda_{old} \psi^2 \boldsymbol{q}_e^T \boldsymbol{q}_e \tag{1.21}$$

$$a_3 = (\Delta \boldsymbol{p}_{old} + \delta \boldsymbol{p}^*)^T (\Delta \boldsymbol{p}_{old} + \delta \boldsymbol{p}^*) - \Delta S^2 + \Delta\lambda_{old}^2 \psi^2 \boldsymbol{q}_e^T \boldsymbol{q}_e \tag{1.22}$$

This quadratic equation is then solved for $\delta\lambda$, for two roots. The goal is to solve for both $\delta\lambda_1$ and $\delta\lambda_2$, which from Equation 1.17 leads to Equations 1.23 and 1.24. The next step is to determine which solution ($\Delta \boldsymbol{p}_{new1}$ or $\Delta \boldsymbol{p}_{new2}$) is nearest the previous incremental solution $\Delta \boldsymbol{p}_{old}$ (Crisfield, 1991).

$$\Delta \boldsymbol{p}_{new1} = \Delta \boldsymbol{p}_{old} + \delta \boldsymbol{p}^* + \delta\lambda_1 \delta \boldsymbol{p}_e \tag{1.23}$$

$$\Delta \boldsymbol{p}_{new2} = \Delta \boldsymbol{p}_{old} + \delta \boldsymbol{p}^* + \delta\lambda_2 \delta \boldsymbol{p}_e \tag{1.24}$$

The values $\delta\lambda_1$ and $\delta\lambda_2$ may be obtained using a quadratic solver algorithm, and the smallest angle between $\Delta \boldsymbol{p}_{old}$ and $\Delta \boldsymbol{p}_{new}$ is then determined by finding the larger cosine as expressed in Equation 1.25 (Crisfield, 1991).

$$\cos\theta = \frac{\Delta \boldsymbol{p}_{old}^T (\Delta \boldsymbol{p}_{old} + \delta \boldsymbol{p}^*)}{\Delta S^2} + \delta\lambda \frac{\Delta \boldsymbol{p}_{old}^T \delta \boldsymbol{p}_e}{\Delta s^2} = \frac{a_4 + a_5 \delta\lambda}{\Delta S^2} \tag{1.25}$$

The root selection process, with $\psi = 0$ (This is denoted as the Crisfield Cylindrical Arc Length Method; to be discussed later) is shown below in Figure 1.2 (Crisfield, 1991).

Crisfield noted that his ALM had an attractive benefit when compared to the Riks Wempner ALM because the only need is to solve a linear system using the tangent

stiffness matrix, which is symmetric and banded (Crisfield, 1991). However, it was also acknowledged that it will fail (Crisfield, 1991) if the method is used at the exact critical point (and presumably is ill-conditioned in the vicinity of the critical point). In our view this represents a severe deficiency: there certainly may be great interest in resolving the response at and near the critical point since the associated instability may be a precursor to structural failure. Furthermore, accuracy and stability will be *lost* as the arc length increment is reduced (refined) such that the applied load is near the critical load. Crisfield also made the statement that both Ramm (Ramm, 1981 and Ramm, 1982) and himself (Crisfield, 1981) individually determined that the load scaling parameter ψ had an insignificant effect on the solution, and advised setting it to zero (Crisfield 1991). In this event the Spherical ALM (same as the Cylindrical ALM but with $\Psi \neq 0$) reduces to what is called the Cylindrical ALM. Thereafter, Crisfield recommended the use of the Cylindrical rather than the Spherical ALM.

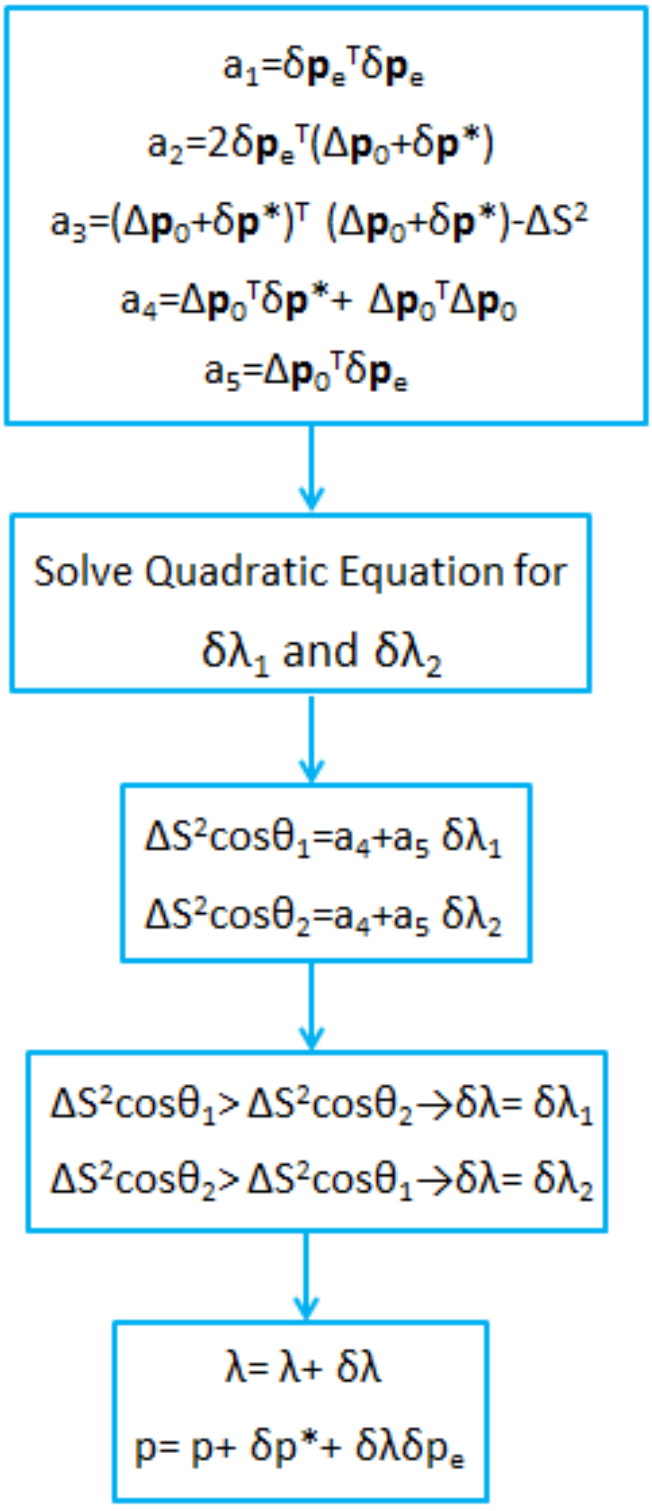

Figure 1.2: Flow Diagram of Crisfield's Root Selection Process

Solving the roots for $\delta\lambda$ in Equation 1.19 is outlined in Figure 1.2 for the Crisfield Cylindrical Arc Length Method and it may be observed that both Crisfield's Spherical and Cylindrical Arc Length Methods can yield two possible roots for $\delta\lambda$. Furthermore, the flow diagram illustrated in Figure 1.2 can be extended to solve the $\delta\lambda$ roots in Equation 1.19 for the Spherical ALM if the a_1, a_2 and a_3 equations in Figure 1.2 are expanded to include the ψ terms.

Other investigators introduced slightly different Arc Length Methods that are designated as a "Linearized Arc Length Method" throughout this paper. In particular Equation 1.5 can be rewritten as Equation 1.26, which is then rewritten again as Equation 1.27 (Crisfield, 1991).

$$\Delta \boldsymbol{p}_{old}{}^{T} \delta \boldsymbol{p} + \delta\lambda(\Delta\lambda_{old}\psi^2 \boldsymbol{q}_e{}^{T}\boldsymbol{q}_e) = -\frac{\xi_{old}}{2} \tag{1.26}$$

$$\delta\lambda(\Delta \boldsymbol{p}_{old}, \Delta\lambda_{old}) = \frac{-\frac{\xi_{old}}{2} - \Delta \boldsymbol{p}_{old}{}^{T}\delta \boldsymbol{p}^{*}}{(\Delta \boldsymbol{p}_{old}{}^{T}\delta \boldsymbol{p}_e + \Delta\lambda_{old}\psi^2 \boldsymbol{q}_e{}^{T}\boldsymbol{q}_e)} \tag{1.27}$$

Setting ξ_{old} equal to zero in Equation 1.26 yields Ramm's Linearized Arc Length Method (Ramm, 1981, Ramm, 1982) which renders the iterate orthogonal to the secant (rather than tangent) change (Crisfield, 1991). Setting ξ_{old} equal to zero and replacing the old increment ($\Delta \boldsymbol{p}_{old}$, $\Delta\lambda_{old}$) with the initial predictor ($\Delta \boldsymbol{p}_{new}$, $\Delta\lambda_{new}$) in Equations 1.26 and 1.27 yields the Riks and Wempner (Riks, 1972, Riks, 1979 and Wempner, 1971) Linearized Arc Length Method which renders the iterate orthogonal to the predictor (Crisfield, 1991)

Several more recent investigators have introduced modifications to the Riks-Wempner ALM (e.g. Geers,1999-a); a number of the modified versions are summarized in Crisfield (Crisfield, 1991), and Memon and Su (Memon and Su, 2004) publications. However it appears that the Crisfield ALMs are the most widely implemented, used and cited in current finite element practice, and therefore attention in the subsequent sections will be confined to their implementation and performance in several benchmark problems, for comparison with the Stiff Arc Length Method (Nicholson, 2004) to be presented next.

More recently, various authors (e.g. Geers, a-1999 and Verhoosel et al, 2008) have noted that the Crisfield methods appear to be effective in many buckling problems, but less so in problems involving material instabilities such as elastoplastic softening. The material instability of particular interest here will be presented at length in the subsequent sections. For now it suffices to say that the instability is associated with necking in elastoplastic materials and ensues from the fact that the stress-strain relations exhibit maxima in some materials at relatively small strains, and thereafter exhibit softening (negative stiffness). A major goal of the present investigation is to implement both the Crisfield methods and the Stiff ALM (presented below) in benchmark problems formulated to incorporate unstable elastoplastic behavior, and to compare their performance in continuing accurate computation at and beyond critical points.

1.2.3 STIFF ARC LENGTH METHOD

The final ALM to be discussed is the more recently developed arc length method termed as the “Stiff Arc Length Method” (Nicholson, 2004). The Stiff ALM introduces an Arc Length Constraint Equation with a vector which is chose to rigorously maximize stiffness, measured by the determinant, of the augmented stiffness matrix at the critical point. This method has the fundamental advantages that (i) the arc length vector is readily computed directly from the original (unaugmented) stiffness matrix, (ii) the augmented stiffness matrix does not incorporate any incremental terms or scale factors, (iii) the augmented stiffness matrix is 'stiff' (i.e. with maximized determinant) at the critical point, in contrast to singularity in the Riks-Wempner and Crisfield methods, and (iv) the iteration scheme consists of Newton Iteration and rigorously preserves quadratic convergence. The augmented stiffness matrix that is used is neither symmetric nor banded. However its *n by n* upper left hand block is symmetric and banded, with the consequence that the solution procedure may be reduced to little more than conventional finite element operations using block triangularization, forward substitution, and back substitution (Nicholson, 2004).

The equilibrium equation for the Stiff ALM is the same as Equation 1.1, but the Arc Length Constraint equation is different and is illustrated in Equation 1.28 (Nicholson, 2004).

$$\xi(\boldsymbol{p}_{k+1}^{j}, \lambda_{k+1}^{j}) = \boldsymbol{zt}^{T}(\boldsymbol{p}_{k+1}^{j} - \boldsymbol{p}_{k}) - zo(\lambda_{k+1}^{j} - \lambda_{k}) - \Delta S = 0 \qquad (1.28)$$

In which $\boldsymbol{zt}^{T}$ is an arc length vector, zo is a constant, and ΔS is the small positive arc length parameter representing the length of the increment in the load-displacement

space (Nicholson 2004) (i.e. the length of the path followed by the solution point at the current increment.) For this equation, the solution can be visualized as a diamond-shaped constraint domain intersecting the equilibrium curve, in which the initial iterate typically (but not necessarily) starts in the center of the constraint domain (Nicholson, 2004). This domain intersects the equilibrium curve at two points and thus the solution path can either converge in the forward or backward direction. Prior to reaching the critical point, the solution path strongly tends toward the forward direction; however near the critical point, the solution may well 'backtrack' unless coerced into converging forward. As will be seen in the subsequent sections, in the current benchmarks this difficulty may be avoided by slightly displacing the center of the arc length constraint domain to lie in the 'domain of attraction' of the forward solution. Doing so has no effect on the augmented stiffness matrix!

Using the arc length constraint equation (Equation 1.28) and Newton Iteration gives rise to Equation 1.29 (Nicholson, 2004).

$$\begin{bmatrix} \boldsymbol{p}_{k+1}^{j+1} \\ \lambda_{k+1}^{j+1} \end{bmatrix} = \begin{bmatrix} \boldsymbol{p}_{k+1}^{j} \\ \lambda_{k+1}^{j} \end{bmatrix} - \boldsymbol{K}_{T}^{*-1} \begin{bmatrix} \boldsymbol{\varphi}(\boldsymbol{p}_{k+1}^{j}, \lambda_{k+1}^{j}) \\ \xi(\boldsymbol{p}_{k+1}^{j}, \lambda_{k+1}^{j}) \end{bmatrix} = 0 \tag{1.29}$$

in which $\boldsymbol{K}_T^*$ is the augmented stiffness matrix, which is further shown as Equation 1.30 (Nicholson, 2004)

$$\boldsymbol{K}_T^* = \begin{bmatrix} \boldsymbol{K}_T & -\boldsymbol{q}_e \\ \boldsymbol{z}\boldsymbol{t}^T & zo \end{bmatrix} \tag{1.30}$$

$\boldsymbol{K}_T$ is the (unaugmented) stiffness matrix. Assuming $\boldsymbol{K}_T$ has unit rank deficiency at the critical point, it may be rewritten as in Equation 1.31 (Nicholson, 2004).The $\boldsymbol{q}_e$ term, as

introduced earlier, is the prescribed external load. The two terms $\boldsymbol{zt}^T$ and *zo* are a vector and a scalar respectively, to be identified later.

$$\boldsymbol{K}_T = \begin{bmatrix} \boldsymbol{K}_T^{n-1} & \boldsymbol{\kappa s}_{n-1} \\ \boldsymbol{\kappa s}_{n-1}{}^T & \kappa s_n \end{bmatrix} \tag{1.31}$$

Since this matrix has a unit rank deficiency at the critical point, any one of the rows within $\boldsymbol{K}_T$ is a linear combination of the others and can be expressed in terms of them using linear operations. The columns and rows of $\boldsymbol{K}_T$ can also be manipulated so that the matrix is nonsingular in the upper (n x 1) by (n x 1) block (Nicholson, 2004). Thus, except in very unusual circumstances (Nicholson 2004), $\boldsymbol{K}_T^{n-1}$ is a nonsingular block matrix, the vector denoted $\mathbf{ks}_{n-1}^T$ is linearly related to the (n-1) rows of $\boldsymbol{K}_T^{n-1}$ and κs_n is a scalar (Nicholson, 2004). The augmented stiffness matrix $\boldsymbol{K}_T^*$ may be rewritten as Equation 1.32 (Nicholson, 2004).

$$\boldsymbol{K}_T^* = \begin{bmatrix} \boldsymbol{K}_T^{n-1} & \boldsymbol{\kappa s}_{n-1} & -\boldsymbol{q}_{e_{n-1}} \\ \boldsymbol{\kappa s}_{n-1}{}^T & \kappa s_n & -q_e \\ \boldsymbol{zt}_{n-1}{}^T & zt_n & zo \end{bmatrix} \tag{1.32}$$

The determinant is now sought to measure how $\boldsymbol{zt}^T$ and *zo* affect the stiffness of the augmented stiffness matrix. To this end, an attractive transformation property is utilized; the orthogonal matrix $\boldsymbol{Q}$, which diagonalizes the matrix, while preserving the determinant ($\boldsymbol{Q}$ may include a permutation matrix to move the rows and columns to different positions).The transformed matrix is shown below in Equation 1.33 (Nicholson, 2004).

$$\boldsymbol{K}^{\#} = \begin{bmatrix} \boldsymbol{Q} & \boldsymbol{0} \\ \boldsymbol{0}^T & 1 \end{bmatrix} \begin{bmatrix} \boldsymbol{K}_T & -\boldsymbol{q}_e \\ \boldsymbol{zt}^T & zo \end{bmatrix} \begin{bmatrix} \boldsymbol{Q}^T & \boldsymbol{0} \\ \boldsymbol{0}^T & 1 \end{bmatrix} = \begin{bmatrix} \boldsymbol{\Lambda}_n & -\boldsymbol{q}_e{}^* \\ \boldsymbol{zt}^{*T} & zo^* \end{bmatrix} \tag{1.33}$$

The four quantities $\boldsymbol{\Lambda}_n$, $\boldsymbol{q}_e{}^*$, $\boldsymbol{zt}^*$ and zo^* are obtained as shown in Equation 1.34 (Nicholson, 2004).

$$\boldsymbol{\Lambda}_n = \boldsymbol{Q}(\boldsymbol{K}_T)\boldsymbol{Q}^T, \quad \boldsymbol{q}_e{}^* = \boldsymbol{Q}(\boldsymbol{q}_e)\boldsymbol{Q}^T, \quad \boldsymbol{zt}^* = \boldsymbol{Q}(\boldsymbol{zt})\boldsymbol{Q}^T, \quad zo^* = zo \tag{1.34}$$

The transformed matrix $\boldsymbol{K}^{\#}$ is expanded to show the eigenvalues along the diagonal, in matrix form, in Equation 1.35 (Nicholson, 2004). Generally speaking, the matrix will only contain one eigenvalue that is zero at the critical point and it may be permuted to the bottom right location of the unaugmented matrix.

$$\boldsymbol{K}^{\#} = \begin{bmatrix} \lambda e_1(\boldsymbol{K}_T) & 0 & 0 & . & . & . & . & 0 & -q_{e_1}{}^* \\ 0 & \lambda e_2(\boldsymbol{K}_T) & 0 & . & . & . & . & 0 & -q_{e_2}{}^* \\ 0 & 0 & \lambda e_3(\boldsymbol{K}_T) & . & . & . & . & 0 & -q_{e_3}{}^* \\ . & . & . & . & . & . & . & . & . \\ . & . & . & . & . & . & . & . & . \\ . & . & . & . & . & . & . & . & . \\ . & . & . & . & . & . & \lambda e_{n-1}(\boldsymbol{K}_T) & . & -q_{e_{n-1}}{}^* \\ 0 & 0 & 0 & . & . & . & . & 0 & -q_{e_n}{}^* \\ zt_1{}^* & zt_2{}^* & zt_3{}^* & . & . & . & zt_{n-1}{}^* & zt_n{}^* & zo^* \end{bmatrix} \tag{1.35}$$

The determinant of this transformed augmented stiffness matrix is the same as that of the augmented stiffness matrix and is shown below in Equation 1.36 (Nicholson, 2004).

$$det(\boldsymbol{K}^{\#}) = det(\boldsymbol{K}_T^*) = \boldsymbol{zt}_n{}^* \, \boldsymbol{q}_{e_n}{}^* \prod_{j=1}^{n-1} \lambda e_j(\boldsymbol{K}_T) \tag{1.36}$$

Observe that the determinant is independent of *zo*.

The vector $\boldsymbol{zt}$ which maximizes the determinant is orthogonal to all the $n-1$ rows of $\boldsymbol{K}_T$. The magnitude of the vector $\boldsymbol{zt}$ was normalized to unity in the derivation of the

Stiff Arc Length Method. In fact ***zt*** proves to be the null eigenvector of the (unaugmented) stiffness matrix at the critical point (Nicholson 2004).

The null eigenvector ***zt*** of the unaugmented stiffness matrix may be readily computed using Gram-Schmidt orthogonalization (Dahlquist and Björck, 1974). Doing so requires the use of trial vectors, which in this case are chosen to be the first $n-1$ rows of $\boldsymbol{K}_T$ (Nicholson, 2004). The first step in the procedure is to set $\boldsymbol{ags}_1^T$ equal to the first row of $\boldsymbol{K}_T$ and compute $\boldsymbol{ags}_1'$ using Equation 1.37 (Nicholson, 2004).

$$\boldsymbol{ags}_1' = \frac{\boldsymbol{ags}_1}{\sqrt{\boldsymbol{ags}_1^T \boldsymbol{ags}_1}} \tag{1.37}$$

All the subsequent steps are outlined in Equations 1.38 – 1.42 for the $n \times n$ $\boldsymbol{K}_T$ matrix (Nicholson, 2004).

$$\boldsymbol{ags}_j = j^{th} \ \ row \ \ of \ \ \boldsymbol{K}_T \tag{1.38}$$

$$\boldsymbol{ags}_j'' = \boldsymbol{ags}_j - \sum_{i=1}^{j-1} (\boldsymbol{ags}_j^T \boldsymbol{ags}_i')\boldsymbol{ags}_i' \tag{1.39}$$

$$\boldsymbol{ags}_j' = \frac{\boldsymbol{ags}_j''}{\sqrt{\boldsymbol{ags}_j''^T \boldsymbol{ags}_j''}} \tag{1.40}$$

$$\boldsymbol{zt}_j'' = \boldsymbol{q}_e - \sum_{i=1}^{n-1} (\boldsymbol{q}_e^T \boldsymbol{ags}_i')\boldsymbol{ags}_i' \tag{1.41}$$

$$\boldsymbol{zt}_j = \frac{\boldsymbol{zt}_j''}{\sqrt{\boldsymbol{zt}_j''^T \boldsymbol{zt}_j''}} \tag{1.42}$$

In which *j* equals 2 thru n-1, for the $n \times n$ matrix $\boldsymbol{K}_T$. An example illustrating this procedure is shown in Figure 1.3.

Lastly, it is also essential when passing through a critical point that both $\boldsymbol{zt}^T(\boldsymbol{p}^j_{k+1} - \boldsymbol{p}_k)$ and $zo(\lambda^j_{k+1} - \lambda_k)$ remain positive on either side of the critical point, to avoid a runaway solution. Accordingly it is necessary to change the sign of *zo* to –1 when the determinant of the unaugmented stiffness matrix $\boldsymbol{K}_T$ is less than or equal to zero to ensure that the successive load values will be smaller than their predecessors (Nicholson, 2004).

Given Parameters:

$$K_t = \begin{pmatrix} 1 & 3 & 7 \\ 4 & 1 & 9 \\ 5 & 8 & 2 \end{pmatrix} \qquad q_e = \begin{pmatrix} 1 \\ 2 \\ 3 \end{pmatrix}$$

Set:

$$a_1 = \begin{pmatrix} 1 \\ 3 \\ 7 \end{pmatrix} \qquad at_1 = \frac{1}{\sqrt{59}} \cdot \begin{pmatrix} 1 \\ 3 \\ 7 \end{pmatrix}$$

$$a_2 = \begin{pmatrix} 4 \\ 1 \\ 9 \end{pmatrix} \qquad att_2 = \begin{pmatrix} 4 \\ 1 \\ 9 \end{pmatrix} - \begin{pmatrix} 1.186 \\ 3.559 \\ 8.305 \end{pmatrix} \qquad at_2 = \frac{1}{\sqrt{14.949}} \cdot \begin{pmatrix} 2.814 \\ -2.559 \\ 0.695 \end{pmatrix}$$

$$ztt_3 = \begin{pmatrix} 1 \\ 2 \\ 3 \end{pmatrix} - \left[\begin{pmatrix} 0.475 \\ 1.424 \\ 3.322 \end{pmatrix} + \begin{pmatrix} -0.041 \\ 0.038 \\ -0.01 \end{pmatrix} \right] \qquad zt_3 = \frac{1}{\sqrt{0.709}} \cdot \begin{pmatrix} 0.567 \\ 0.539 \\ -0.312 \end{pmatrix}$$

Figure 1.3: Gram-Schmidt Orthogonalization Example

Chapter Two : ONE DEGREE-OF-FREEDOM COMPARISONS

2.1 SIMPLE ONE DIMENSIONAL SINE WAVE COMPARISON

A straightforward, not necessarily realistic, example is first sought to ensure that the MATHCAD implementations of the ALMs are correct and perform well in an unchallenging situation. A sine wave, shown below in Equation 2.1, is used for this purpose: it exhibits a maximum but the function is not flat in an extensive interval around the maxima. Of course, this equation is nowhere near representative of a nonlinear force-displacement curve for a metal experiencing elastoplasticity.

$$y = \sin(5x) \tag{2.1}$$

The sine wave equation, Equation 2.1, has a rapidly increasing slope before the critical point and a rapidly decreasing slope thereafter. The critical point (maximum) thus does not occur in a flat region; we believe this makes it relatively easy for a computational procedure to pass through the critical point without accumulating significant error and potentially diverging. The Crisfield Cylindrical and Spherical methods were coded in MATHCAD for the sine wave equation and their respective computational results have been compared with the exact equation. The results of the computations are illustrated below as Figure 2.1; the key parameters used are noted in Table 1.

Referring to Table 1, all three methods were evaluated using the same arc length parameter and the same convergence criteria. Upon examining Figure 2.1, the Cylindrical, Spherical and Stiff ALMs all follow the curve, but the Cylindrical and Spherical Arc Length Methods are somewhat less accurate.

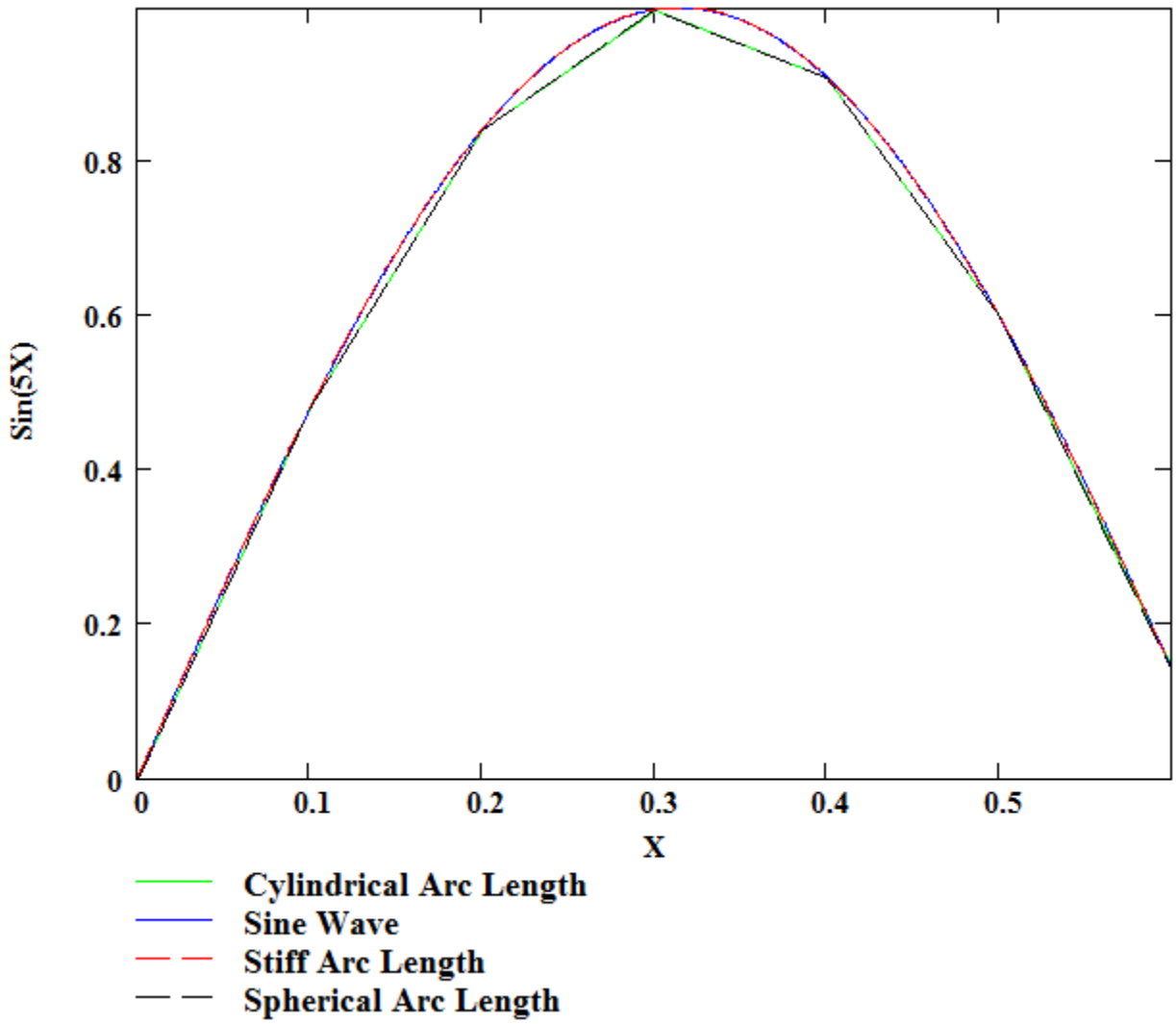

Figure 2.1: Simple One Degree-of-Freedom Arc Length Comparisons

The Stiff Arc Length Method follows the sine wave curve very closely using the same parameters as the other two methods, but it takes more iterates to converge and requires more increments to reach the end of the curve. A summary of varying some of the parameters for the three methods is given below in Tables 2-4.

Table 1: Figure 2.1 Key Parameters

Parameter	Cylindrical Arc Length Method	Spherical Arc Length Method	Stiff Arc Length Method
Arc Length	.01	.01	.01
Load Scaling Factor	N/A	.01	N/A
Convergence Criteria	$\|qi - \lambda_{k+1}qe\| \leq 10^{-7}$	$\|qi - \lambda_{k+1}qe\| \leq 10^{-7}$	$\|qi - \lambda_{k+1}qe\| \leq 10^{-7}$

Table 2: Simple One Degree-of-Freedom Stiff Arc Length Method Varying Parameter Summary

Arc Length Method (Parameter)	Highest Number of Iterates to Converge	Total Increments	Accuracy	General Comment
Stiff ($\Delta S = 1$)	5	4	Poor	Bypassed most of the curve, including critical point
Stiff ($\Delta S = .1$)	4	44	Accurate	Small amount of error around critical point
Stiff ($\Delta S = .01$)	3	432	Very Accurate	This was plotted in Figure 2.1
Stiff ($\Delta S = .001$)	2	4318	Very Accurate	Required many increments

Table 3: Simple One Degree-of-Freedom Cylindrical Arc Length Method Varying Parameter Summary

Arc Length Method (Parameter)	Highest Number of Iterates to Converge	Total Increments	Accuracy	General Comment
Cylindrical ($\Delta S^2 = .1$)	2	2	Poor	Bypassed almost the entire curve
Cylindrical($\Delta S^2 = .01$)	2	6	Good	This was plotted in Figure 2.1
Cylindrical($\Delta S^2 = .001$)	2	19	Very Accurate	Required very little increments

Table 4: Simple One Degree-of-Freedom Spherical Arc Length Method Varying Parameter Summary

Arc Length Method (Parameter)	Highest Number of Iterates to Converge	Total Increments	Accuracy	General Comment
Spherical(ΔS^2 = .01, Ψ=1)	N/A	N/A	N/A	Solution wouldn't converge
Spherical(ΔS^2 = .01, Ψ=.1)	6	7	Medium	Bypassed critical point
Spherical(ΔS^2 = .01, Ψ=.01)	3	7	Good	This was plotted in Figure 2.1
Spherical(ΔS^2 = .01, Ψ=.001)	3	7	Good	Results didn't really improve much from one above

Using Tables 2 thru 4 for comparison it may be noted that the Stiff ALM shows good accuracy using a large arc length parameter (step size) of 0.1 although it requires 44 increments. The Cylindrical ALM requires an arc length parameter of 0.01 or less in order to track the curve with good accuracy; although the Cylindrical ALM required only 6 iterates; its accuracy was not as good as in the Stiff ALM using an arc length parameter of 0.1. The Spherical ALM was analyzed by varying the load scaling parameter only while keeping the arc length parameter constant as shown in Table 4. It can be noted that choosing to large a Ψ value reduce the accuracy of the method or caused the procedure to fail.

In this investigation a primary concern is for accuracy at moderate increment sizes, and consistent improvement as the increment size is reduced. There is a benign explanation for the relatively high number of increments shown for SALM in Tables 3 and 4. The Crisfield methods use a *line search* (Crisfield, 1991) which in essence sets the initial iterate relatively close to the converged solution. But, in the current implementation of the Stiff ALM, the initial iterate is simply the solution at the previous

load step, which is further away from the solution if the increment size is relatively large. In fact an extrapolation procedure using the solutions at the previous several load steps could easily be incorporated in the Stiff ALM to make the initial iterate much closer to the converged solution, and thereby accelerate computation.

Choosing a small value of the load scaling factor has little effect on the Spherical ALM in that it then reduces to the Cylindrical ALM. It may be concluded that for a simple one dimensional problem (1 DOF) containing a rapidly changing slope before and after the critical point, such as a sine wave function, the Spherical ALM offers no advantage compared to the Cylindrical ALM, which is consistent with what Crisfield reported (Crisfield, 1991). Furthermore the Stiff ALM gives superior performance in that it does not require a very small arc length parameter in order to produce highly accurate results.

2.2 ONE DEGREE-OF-FREEDOM BENCHMARK

A one degree-of-freedom equation representative of elastoplastic behavior with an instability is now presented; it exhibits a gradual slope before and after the critical point (maximum load), and also exhibits a discontinuous stiffness change after elastic yield is reached. It will be seen that the model agrees closely with experimental data reported in the Atlas of Stress Strain Curves (ASM International, 2002). A force f depending on the displacement p is now formulated. The functional relation between the force and the displacement is implicit in a stiffness function as shown below in Equation 2.2.

$$\frac{df}{dp}=K_T(p) \tag{2.2}$$

The stiffness K_T must be selected such that it models elastoplastic behavior with instability and contains a critical point in a flat load-deflection region. This is accomplished in Equation 2.3.

$$\frac{df}{dp}=\begin{Bmatrix} K_e, & elastic \\ K_o-\frac{2}{\pi}K_1(\kappa op^{\#})tan^{-1}(\kappa op^{\#}), & plastic \end{Bmatrix} \tag{2.3}$$

Here K_e is the initial stiffness during elastic deformation, K_o is the matrix at the onset of plastic deformation (immediately after yield), and at large deformations the stiffness approaches the negative value K_o–K_1, in which $K_1>K_o$. The modified displacement $p^{\#}$ is equal to the total displacement p minus the displacement when plastic deformation is initiated p_y. The scalar κo is chosen to be a constant α, to be identified shortly, divided by the length of the member L. The initial critical point occurs at pc satisfying the equation shown below in Equation 2.4, which will be used to determine the value of α.

$$det\left[K_o-\frac{2}{\pi}K_1(\kappa opc)tan^{-1}(\kappa opc)\right]=0 \tag{2.4}$$

The function $f(p)$ is now determined that gives rise to the forgoing expression for $K_T(p)$. Equation 2.2 can be rewritten using the Chain Rule as shown below in Equation 2.5.

$$\frac{df}{dp}=\frac{df}{d(\kappa op^{\#})}\frac{d(\kappa op^{\#})}{dp^{\#}}\frac{dp^{\#}}{dp}=\frac{df}{d(\kappa op^{\#})}\kappa o \tag{2.5}$$

It is immediately recognized that Equation 2.5 can be rewritten as Equation 2.6.

$$\frac{df}{d(\kappa op^{\#})}\kappa o=K_o-\frac{2}{\pi}K_1(\kappa op^{\#})tan^{-1}(\kappa op^{\#}) \tag{2.6}$$

The force f can be inserted into two parts f_1 and f_2, whose sum equals f. The stiffness associated with f_1 and f_2 are shown in Equations 2.7 and 2.8 respectively.

$$\frac{df_1}{d(kop^{\#})}ko = K_o \tag{2.7}$$

$$\frac{df_2}{d(\kappa op^{\#})}\kappa o = -\frac{2}{\pi}K_1(\kappa op^{\#})tan^{-1}(\kappa op^{\#}) \tag{2.8}$$

Equation 2.7 can easily be integrated to yield Equation 2.9 shown below.

$$f_1 = K_o p^{\#} \tag{2.9}$$

Equation 2.8 can be submitted to integration by parts using Equation 2.10 (Zill, 2001).

$$\int x\,tan^{-1}(x)dx = \frac{1}{2}x^2\,tan^{-1}(x) - \frac{1}{2}x + \frac{1}{2}tan^{-1}(x) + C \tag{2.10}$$

Using Equation 2.10, Equation 2.8 is now integrated as shown in Equation 2.11.

$$f_2 = -\frac{2}{\pi}K_1\frac{1}{\kappa o}\left[\frac{1}{2}(\kappa op^{\#})^2\,tan^{-1}(\kappa op^{\#}) - \frac{1}{2}(\kappa op^{\#}) + \frac{1}{2}tan^{-1}(\kappa op^{\#}) + C\right] \tag{2.11}$$

Omitting the details, the constant coefficient C can be found by setting f_2 equal to f_y (at initial yield) and setting $p^{\#}$ equal to zero. After performing elementary mathematical operations the value of C is obtained as shown in Equation 2.12.

$$C = -\frac{\pi}{2}\frac{(\kappa of_y)}{K_1} \tag{2.12}$$

The force f is now found by adding Equations 2.9 and 2.11 to furnish Equation 2.13.

$$f = K_o p^{\#} - \frac{2}{\pi}K_1\frac{1}{\kappa o}\left[\frac{1}{2}(\kappa op^{\#})^2\,tan^{-1}(\kappa op^{\#}) - \frac{1}{2}(\kappa op^{\#}) + \frac{1}{2}tan^{-1}(\kappa op^{\#})\right] + f_y \tag{2.13}$$

2.3 ONE DEGREE-OF-FREEDOM BENCHMARK COMPARISON

The derived force as a function of displacement is now illustrated in Figure 2.2 shown below. The plot contains a maximum at about 1.049 x 10^5 lbs at a displacement of 0.5” with a gradually changing slope near the critical point. Table 5 summarizes the key parameters used to generate the plot shown in Figure 2.2. In particular the convergence criterion compares the summed magnitudes of the equilibrium error "unbalanced force" and the arc length error to a 'tolerance'.

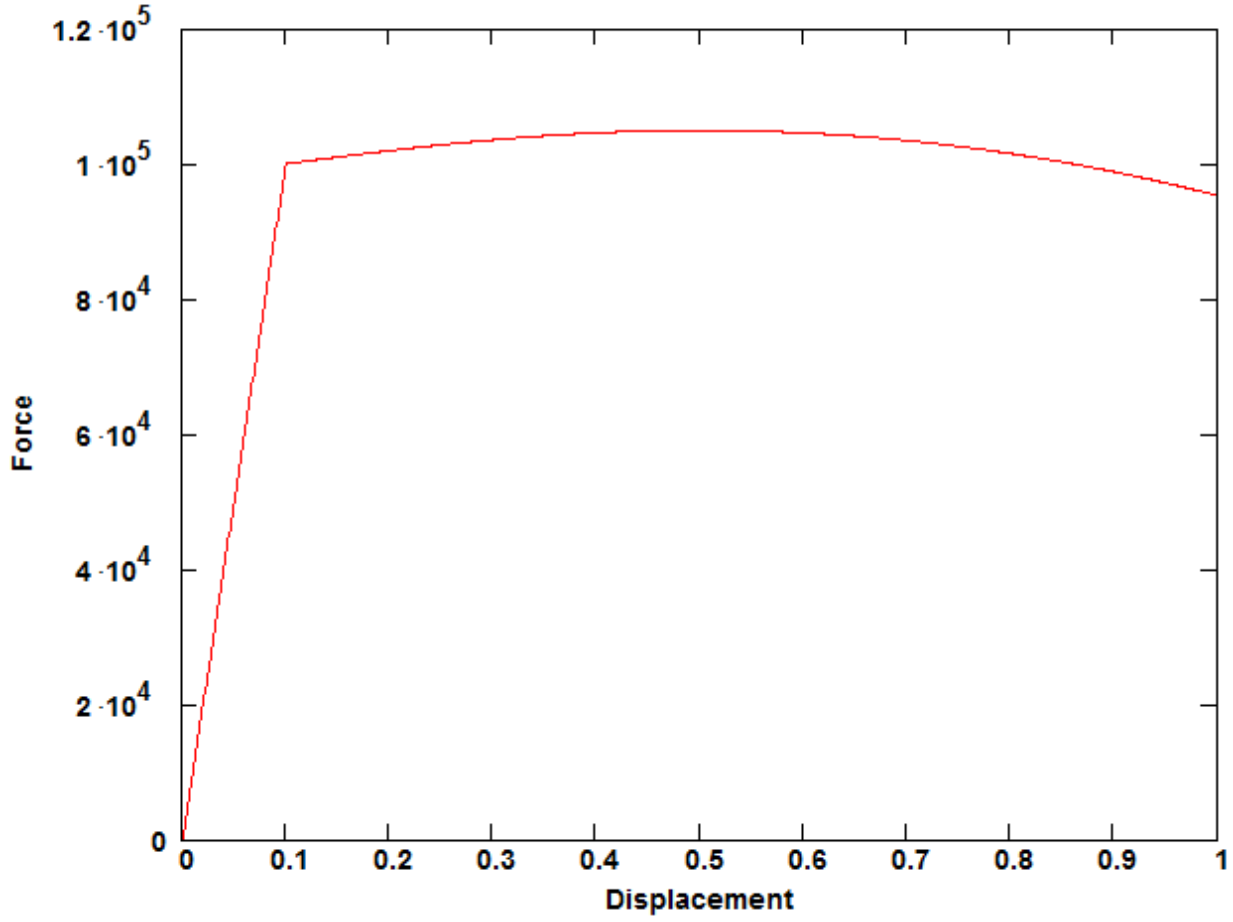

Figure 2.2: One Degree-of-Freedom Benchmark Plot

Table 5: Figure 2.2 Key Parameters

Parameter	E_e (psi)	E_{po} (psi)	E_{p1} (psi)	A (in^2)	L (in)	p_y (in)	α
Value	10^7	2×10^5	2.2×10^5	1	10	.1	36.699

The Stiff, Cylindrical and Spherical ALMs were coded in MATHCAD for the one degree-of-freedom benchmark equation. The MATHCAD codes for the Stiff ALM and the Spherical ALM may be found in Appendix A and B respectively. The resulting illustration is presented below as Figure 2.3. Some of the key parameters used in order to create Figure 2.3 are noted in Table 6

Table 6: Figure 2.3 Key Parameters

Parameter	Cylindrical Arc Length Method	Spherical Arc Length Method	Stiff Arc Length Method
Arc Length	.1	.1	.1
Load Scaling Factor	N/A	.00001	N/A
Convergence Criteria	$\lvert qi - \lambda_{k+1} qe \rvert \leq 10^{-7}$	$\lvert qi - \lambda_{k+1} qe \rvert \leq 10^{-7}$	$\lvert qi - \lambda_{k+1} qe \rvert \leq 10^{-7}$

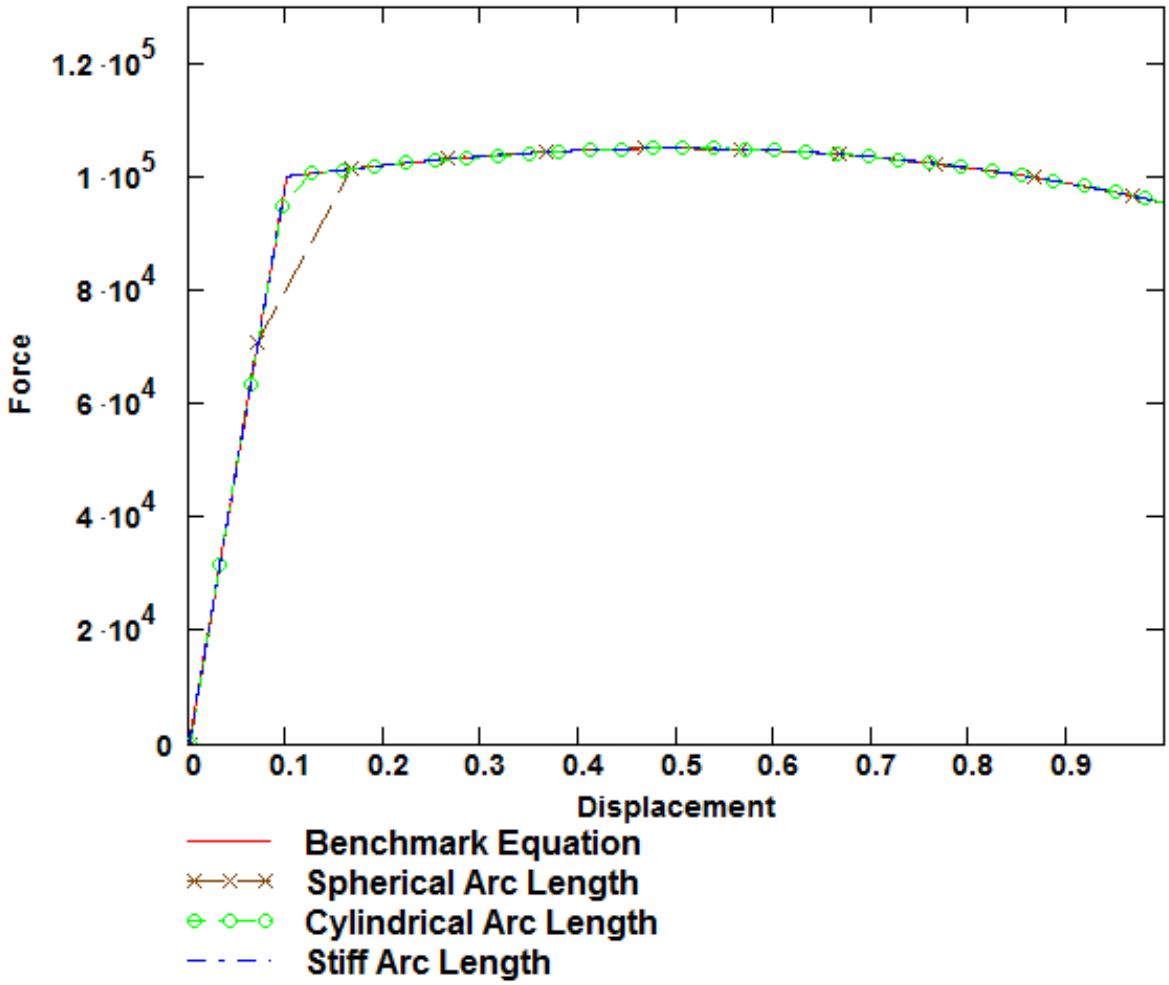

Figure 2.3: One Degree-of-Freedom Benchmark Arc Length Comparisons

Examining Figure 2.3 above, which is for a very large arc length parameter value (0.1), it is evident that the Stiff Arc Length Method follows the one degree-of-freedom curve very closely, while the Spherical ALM follows the curve fairly well, the Cylindrical ALM bypasses the entire elastic region and the discontinuity point. At this stage, in terms of accuracy the Spherical ALM appears to be a good competitor to the Stiff ALM using the parameters shown in Table 6. But further evaluation shows that the load parameter must be smaller than a certain critical value for it to perform accurately, at the price of a

high number of increments. Tables 7 thru 9 show the results of each of the three methods when their arc length and load scaling parameters are varied.

Table 7: One Degree-of-Freedom Stiff Arc Length Method Varying Parameter Summary

Arc Length Method (Parameter)	Highest Number of Iterates to Converge	Total Increments	Accuracy	General Comment
Stiff ($\Delta S = 1$)	6	3	Poor	Bypassed most of the curve, including critical point
Stiff ($\Delta S = .1$)	4	32	Very Accurate	This was plotted in Figure 2.3
Stiff ($\Delta S = .01$)	3	319	Very Accurate	Required many increments
Stiff ($\Delta S = .001$)	3	3185	Very Accurate	Required many increments

Table 8: One Degree-of-Freedom Cylindrical Arc Length Method Varying Parameter Summary

Arc Length Method (Parameter)	Highest Number of Iterates to Converge	Total Increments	Accuracy	General Comment
Cylindrical ($\Delta S^2 = 1$)	3	1	Poor	Bypassed the entire curve
Cylindrical($\Delta S^2 = .1$)	3	4	Poor	This was plotted in Figure 2.3
Cylindrical($\Delta S^2 = .01$)	4	12	Very Accurate	Performance was very accurate
Cylindrical($\Delta l^2 = .001$)	3	32	Good	Bypassed discontinuity

Referring to Table 7, the Stiff ALM performs with great accuracy with an arc length parameter of 0.1. Using arc length parameters smaller than 0.1 provides even more accuracy but has computational cost of requiring several more increments.

Table 8 analyzes the Cylindrical ALM as it varies with the arc length parameter. Using an arc length parameter of 1 and 0.1, the accuracy suffers significantly; however using an arc length parameter of 0.01 provides excellent accuracy with only 12 increments. Another interesting thing to note is that when the arc length parameter was decreased from 0.01 to 0.001 *the performance actually deteriorated*. Finally, Crisfield's Spherical ALM was investigated as shown in Table 9. Selecting an arc length parameter of 0.1 and a load scaling parameter of .0001 does not allow the solution to converge beyond the elastic region. A similar observation holds using an arc length parameter of 0.01, while keeping the load scaling parameter of 0.0001. Selecting the arc length parameter as 0.1 and choosing a load scaling parameter of 0.00001 allows the solution to follow the entire curve but with some inaccuracies at the discontinuity. However further decreasing the load scaling parameter increases the error because this case is very close to the Cylindrical ALM, and accordingly contains large error near the slope discontinuity. Decreasing the arc length parameter while varying the load parameter decreases the error; however the results follow the same pattern as above, namely the load parameter actually increases the error if it becomes sufficiently small. The Spherical ALM works well when the optimal value of the load and arc length parameter are chosen but it takes trial and error (user intervention) to identify what the optimal values are.

The erratic behavior of the Cylindrical and Spherical ALMs indicates that their effectiveness requires skillful "user intervention". We believe this poses a serious risk of

unreliability when implemented in a widely used nonlinear Finite Element code used by analysts with varying skill levels.

Table 9: One Degree-of-Freedom Spherical Arc Length Method Varying Parameter Summary

Arc Length Method (Parameter)	Highest Number of Iterates to Converge	Total Increments	Accuracy	General Comment
Spherical(ΔS^2 = .1, Ψ=.0001)	N/A	N/A	Poor	Solution wouldn't converge beyond elastic region
Spherical(ΔS^2 = .1, Ψ=.00001)	10	7	Good	This was plotted in Figure 2.3
Spherical(ΔS^2 = .1, Ψ=.000001)	7	4	Poor	Bypassed elastic region and discontinuity
Spherical(ΔS^2 = .01, Ψ=.0001)	N/A	N/A	Poor	Solution wouldn't converge beyond elastic region
Spherical(ΔS^2 = .01, Ψ=.00001)	8	20	Excellent	Small amount of error around discontinuity
Spherical(ΔS^2 = .01, Ψ=.000001)	6	11	Good	Bypassed some of the elastic region and discontinuity

2.4 ONE DEGREE-OF-FREEDOM COMPARISONS USING REAL STRESS-STRAIN DATA

Next, several empirical stress-strain curves are used to demonstrate the realism of the one degree-of-freedom equation discussed in Section 2.2. Figures 2.4 and 2.5 below are material stress-strain curves obtained from Atlas of Stress-Strain Curves (ASM International, 2002); they exhibit a gradually decreasing slope until a critical point is reached well into the plastic region of the material, after which the slope is negative.

Figure 2.4 depicts the behavior of aluminum alloy AL 3033, while aluminum alloy AL 7075 is depicted in Figure 2.5. The published curves were digitized using the software program Datathief (Tummers, 2006), and the figures below have been drawn from the resulting spreadsheet.

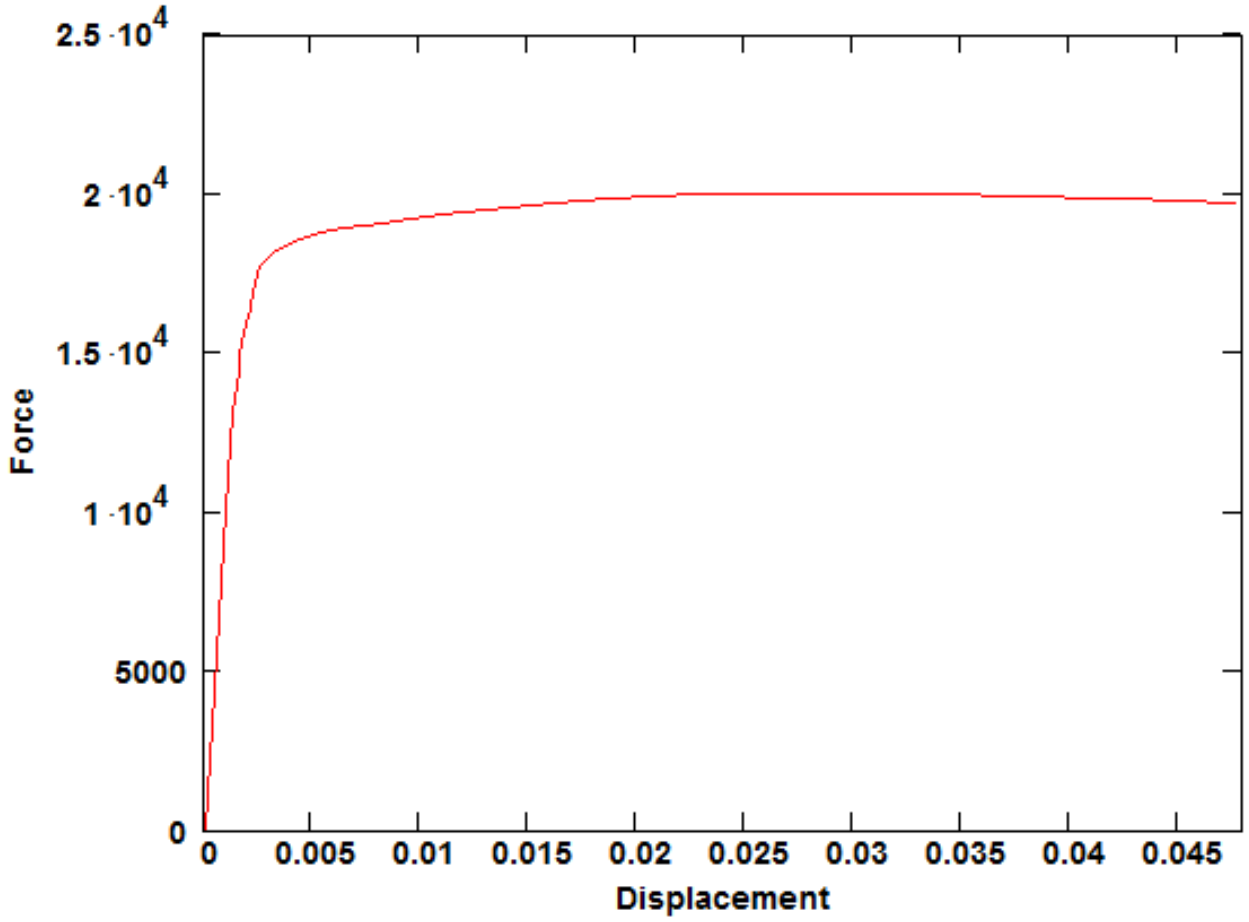

Figure 2.4: Al 3003 Stress-Strain Curve Replicated using Datathief

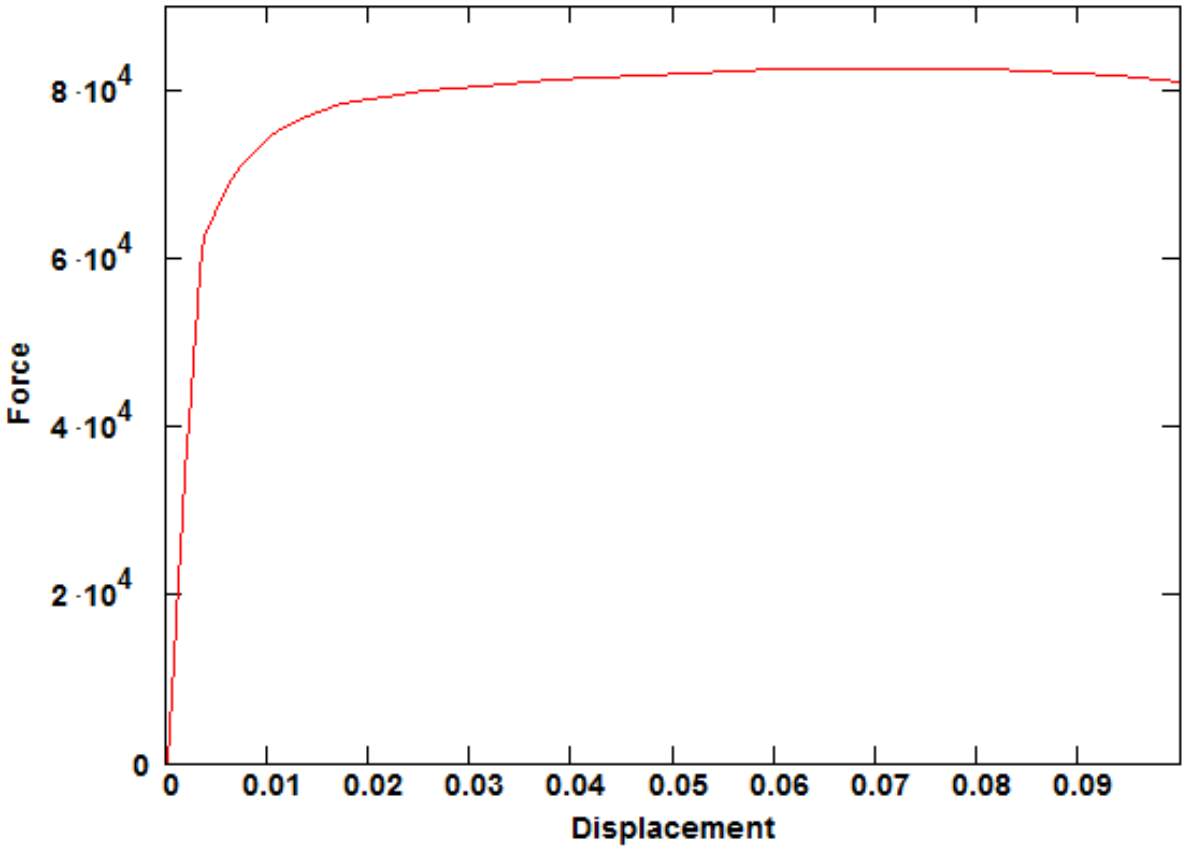

Figure 2.5: Al 7075 True Stress-Strain Curve Replicated using Datathief

The performance of the ALMs with respect to following a curve that exhibits similar elastoplastic behavior has already been demonstrated in Section 2.2; of course the coefficients in the one degree-of-freedom equation in Section 2.2 have been modified to accommodate the material proprieties shown in Figures 2.4 and 2.5.

Next the new material data sets are used to evaluate the performance of the three ALMs. The two stress-strain curves were digitized using the program Datathief, enabling data points from the actual curves to be into MATHCAD. Figures 2.6 and 2.7

show the comparisons of the three ALMs to the modified benchmark one degree-of-freedom equation and the actual material curves for Al 3003 and Al 7075.

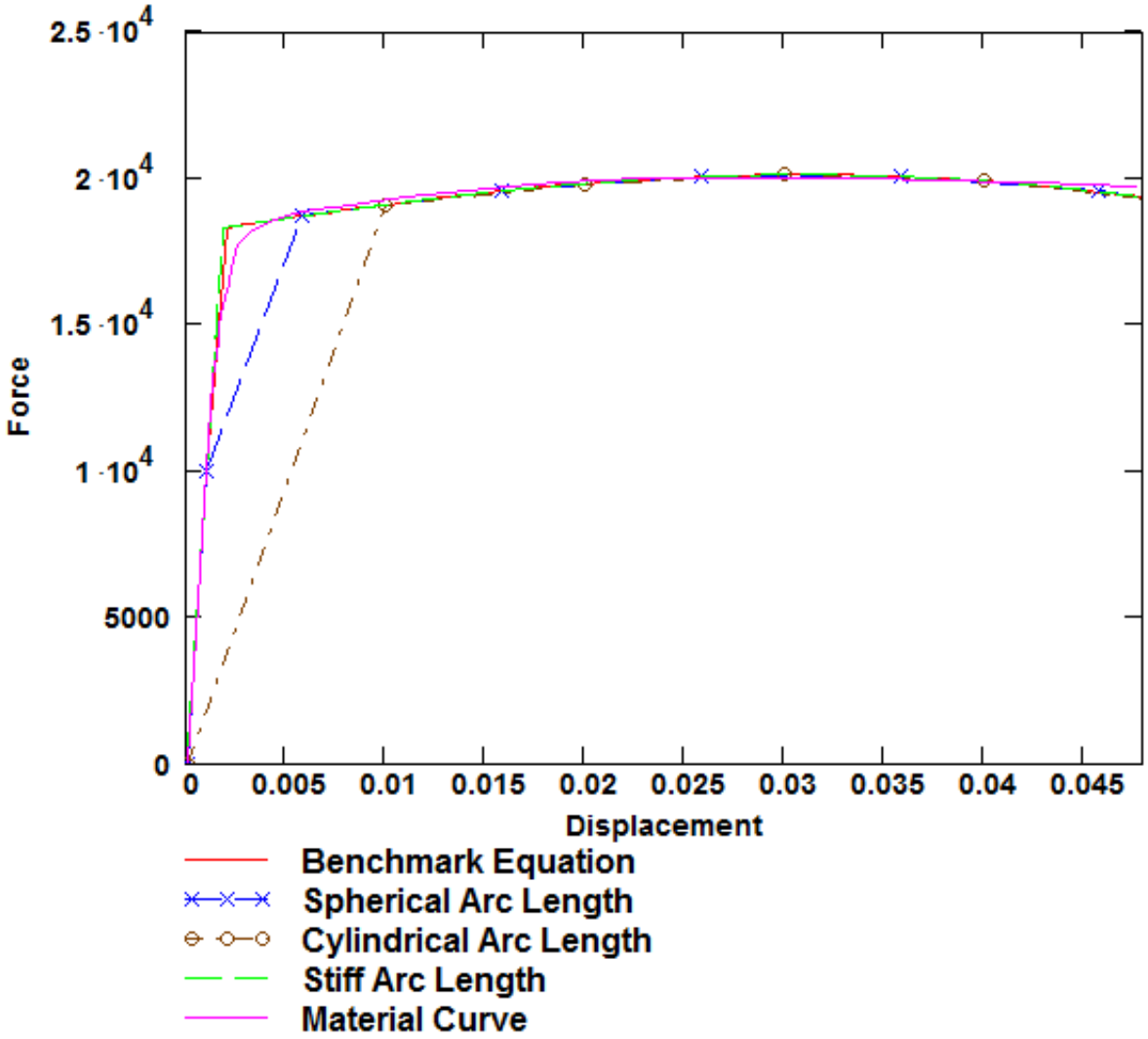

Figure 2.6: Al 3003 Stress-Strain Curve Comparisons

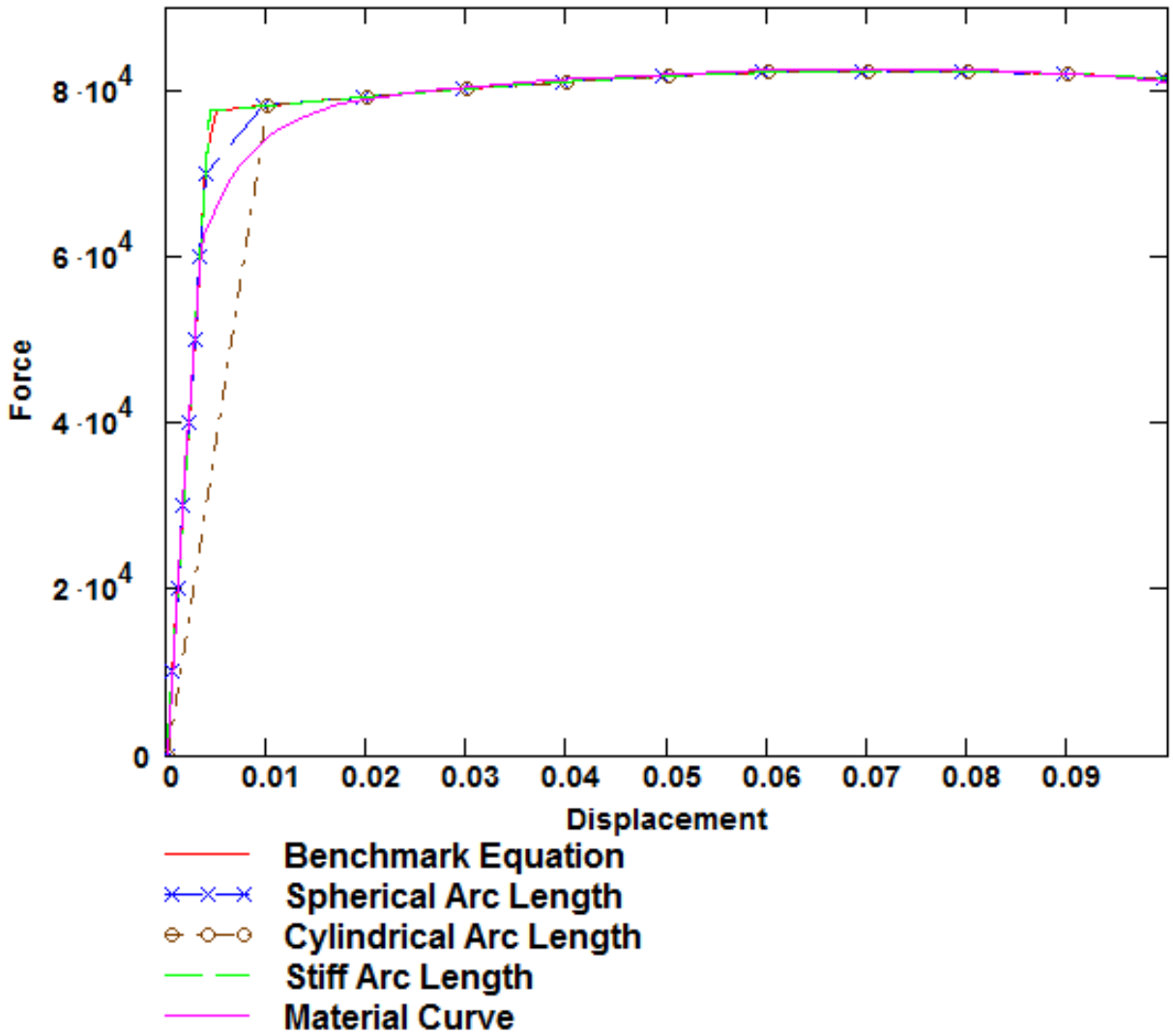

Figure 2.7: Al 7075 Stress-Strain Curve Comparisons

The actual material stress-strain plot is shown in magenta in both figures. The graphs are both plotted using force versus displacement with the cross-sectional area and overall length, both being equal to unity so that this directly correlates to the stress-strain curve data in the two material curves. Both the Aluminum 3003 and Aluminum 7075 stress-strain curves have a smooth but rapid transition region between the elastic and plastic region of the material. The one degree-of-freedom equation was derived

using the assumption that there is a sharp transition, and thus there is a slope discontinuity present directly at initial yield. The benchmark equation could have been easily modified with a transition function to eliminate the slope discontinuity. But this was not of interest in the present investigation due to the facts that (1) it is more demanding on the arc length methods to follow an abrupt change in stiffness, (2) certain materials actually do approximate abrupt transitions such as the model equation incorporated, and (3) classical 3D material models in elastoplasticity incorporate abrupt transitions.

The three ALMs have been applied to the one degree-of-freedom equation, using the material properties of the Al 3003 and Al 7075 material curves, as illustrated in Figures 2.6 and 2.7. The parameters for the three ALMs are shown in Table 10.

Table 10: Figures 2.6 and 2.7 Key Parameters

Parameter	Cylindrical Arc Length Method	Spherical Arc Length Method	Stiff Arc Length Method
Arc Length	.0001	.0001	.001
Load Scaling Factor	N/A	.000001	N/A
Convergence Criteria	$\|qi - \lambda_{k+1}qe\| \leq 10^{-7}$	$\|qi - \lambda_{k+1}qe\| \leq 10^{-7}$	$\|qi - \lambda_{k+1}qe\| \leq 10^{-7}$

As shown in Figures 2.6 and 2.7 the Stiff ALM followed the model equation very accurately using a larger arc length parameter than the Cylindrical and Spherical methods. However, using an arc length parameter an order of magnitude smaller than what was used for the Stiff Arc Length method, the Cylindrical and Spherical ALMs

experience a significant error around the discontinuity, possibly due to the initial predictor that Crisfield invokes in his arc length methods. The Spherical ALM performs better than the Cylindrical ALM; however it takes some 'tweaking" of the load scaling parameter ψ to induce the arc length method to perform accurately.

Chapter Three : THREE DEGREE-OF-FREEDOM COMPARISONS

3.1 THREE DEGREE-OF-FREEDOM BENCHMARK

A three DOF benchmark problem is now formulated. The eight bar truss shown below in Figure 3.1 contains three independent degrees-of-freedom; horizontal displacement at node 2 (p2x), vertical displacement at node 3 (p3y), and a vertical displacement at node 4 (p4y). The nodes of interest have the initial coordinates (x20, y20), (x30, y30) and (x40, y40), relative to the origin at the bottom middle node.

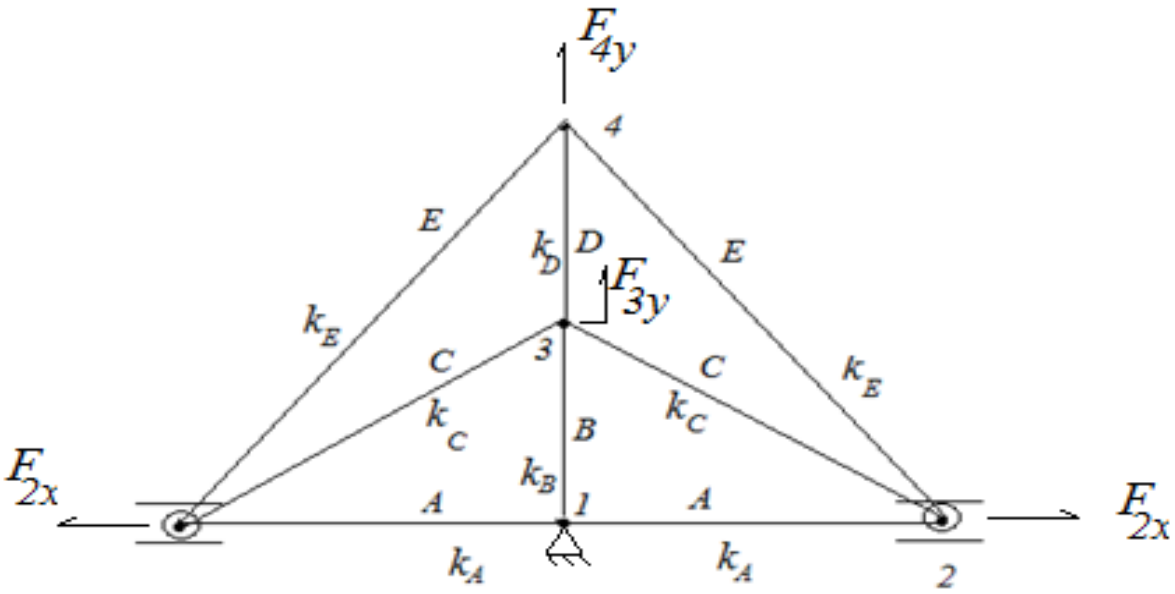

Figure 3.1: Benchmark 3 DOF Truss

The truss members have lengths L_A, L_B, L_C, L_D and L_E. All truss members are connected by frictionless pin joints and are assumed to experience uniaxial tension under monotonically increasing loads whose maximum values are consistent with small strain kinematics. All the truss members have the same cross-sectional area A, and contain

elastic-plastic material behavior that is represented by the stiffness relations shown in Equations 3.1 and 3.2.

$$\boldsymbol{ke}(\boldsymbol{\varepsilon}) = A\boldsymbol{E}_e \quad \boldsymbol{\varepsilon} \le \boldsymbol{\varepsilon}_y \tag{3.1}$$

$$\boldsymbol{ke}(\boldsymbol{\varepsilon}) = A\left[\boldsymbol{E}_{po} - \frac{2}{\pi}\boldsymbol{E}_{p1}\tan^{-1}\left\{\alpha(\boldsymbol{\varepsilon} - \boldsymbol{\varepsilon}_y)\right\}\right] \quad \boldsymbol{\varepsilon} > \boldsymbol{\varepsilon}_y \tag{3.2}$$

In which $\boldsymbol{\varepsilon}$ denotes the strain and $\boldsymbol{\varepsilon}_y$ is the strain at initial yield. Of course this relation is the same as was used for the 1 DOF benchmark calculations. The parameter $\boldsymbol{E}_{po}$ is the stiffness just after initial yield, and the stiffness at large strain is $\boldsymbol{E}_{po}$-$\boldsymbol{E}_{p1}$ which is chosen to be negative to model instability. After performing some elementary manipulations, the strain in each member can be approximated as shown in Equations 3.3 thru 3.7.

$$\varepsilon_A = \frac{p2x}{L_A} \tag{3.3}$$

$$\varepsilon_B = \frac{p3y}{L_B} \tag{3.4}$$

$$\varepsilon_C \sim \frac{x20p2x + y30p3y}{L_C{}^2} \tag{3.5}$$

$$\varepsilon_D = \frac{p4y - p3y}{L_D} \tag{3.6}$$

$$\varepsilon_E \sim \frac{x20p2x + y40p4y}{L_E{}^2} \tag{3.7}$$

The incremental stain-displacement relationship is shown below as Equation 3.8.

$$d\boldsymbol{E} = \boldsymbol{G}d\boldsymbol{D} \tag{3.8}$$

In which $d\boldsymbol{E}$ is the incremental strain vector, $d\boldsymbol{D}$ is the incremental displacement vector, and $\boldsymbol{G}$ is a geometry matrix; each of these quantities are shown below in Equations 3.9 thru 3.11 respectively.

$$d\boldsymbol{E} = \begin{pmatrix} d\varepsilon_A \\ d\varepsilon_B \\ d\varepsilon_C \\ d\varepsilon_D \\ d\varepsilon_E \end{pmatrix} \tag{3.9}$$

$$d\boldsymbol{D} = \begin{pmatrix} dp2x \\ dp3y \\ dp4y \end{pmatrix} \tag{3.10}$$

$$\boldsymbol{G} = \begin{bmatrix} \frac{1}{L_A} & 0 & 0 \\ 0 & \frac{1}{L_B} & 0 \\ \frac{L_A}{L_C^{\,2}} & \frac{L_B}{L_C^{\,2}} & 0 \\ 0 & -\frac{1}{L_D} & \frac{1}{L_D} \\ \frac{L_A}{L_E^{\,2}} & 0 & \frac{(L_B + L_D)}{L_E^{\,2}} \end{bmatrix} \tag{3.11}$$

The forces in the members can be found by integrating the stiffness relations with respect to strain. The resulting force relations are shown in Equations 3.12 and 3.13.

$$\mathbf{f}(\boldsymbol{\varepsilon}) = A(\mathbf{E}_e\boldsymbol{\varepsilon}) \quad \boldsymbol{\varepsilon} \le \boldsymbol{\varepsilon}_y \tag{3.12}$$

$$\boldsymbol{f}(\boldsymbol{\varepsilon}) = A\left[\boldsymbol{E}_e\boldsymbol{\varepsilon}_y + \boldsymbol{E}_{po}(\boldsymbol{\varepsilon}-\boldsymbol{\varepsilon}_y) - \frac{2}{\pi\alpha}\boldsymbol{E}_{p1}\left\{\alpha(\boldsymbol{\varepsilon}-\boldsymbol{\varepsilon}_y)tan^{-1}(\alpha(\boldsymbol{\varepsilon}-\boldsymbol{\varepsilon}_y))\right\}\right]$$

$$+A\left[\frac{1}{\pi\alpha}\boldsymbol{E}_{p1}\,ln(1+(\alpha(\boldsymbol{\varepsilon}-\boldsymbol{\varepsilon}_y))^2)\right] \quad \boldsymbol{\varepsilon} > \boldsymbol{\varepsilon}_y \tag{3.13}$$

The forces in the truss can be consolidated into a vector (array) as a function of strain, which in turn is a function of displacement; this is shown in Equation 3.14.

$$\boldsymbol{f}(\boldsymbol{E}(\boldsymbol{D})) = \begin{pmatrix} f_A \\ f_B \\ f_C \\ f_D \\ f_E \end{pmatrix} \tag{3.14}$$

A kernal of the stiffness matrix to be presented may now be expressed using the individual member stiffness values, with the rest of the matrix containing zeros. Equation 3.15 shows the kernal stiffness matrix.

$$\boldsymbol{\Gamma}(\boldsymbol{E}(\boldsymbol{D})) = \frac{d\boldsymbol{f}}{d\boldsymbol{E}} = \begin{bmatrix} ke_A & 0 & 0 & 0 & 0 \\ 0 & ke_B & 0 & 0 & 0 \\ 0 & 0 & ke_C & 0 & 0 \\ 0 & 0 & 0 & ke_D & 0 \\ 0 & 0 & 0 & 0 & ke_E \end{bmatrix} \tag{3.15}$$

The individual lengths of the members can be represented in matrix form as shown in Equation 3.16.

$$\boldsymbol{\Omega} = \begin{bmatrix} L_A & 0 & 0 & 0 & 0 \\ 0 & L_B & 0 & 0 & 0 \\ 0 & 0 & L_C & 0 & 0 \\ 0 & 0 & 0 & L_D & 0 \\ 0 & 0 & 0 & 0 & L_E \end{bmatrix} \tag{3.16}$$

Applied to a finite element model with n displacement degrees-of-freedom, the Principle of Virtual Work is stated in Equation 3.17.

$$\int \delta \boldsymbol{e}^T \boldsymbol{s} dV = \delta \boldsymbol{p}^T \boldsymbol{F} \tag{3.17}$$

Where δ is the variational operator, $\boldsymbol{e}$ is the 9x1 strain vector, $\boldsymbol{s}$ is the 9x1 stress vector, $\boldsymbol{p}$ is the nx1 (global) displacement vector and $\boldsymbol{F}$ is the nx1 (global) external force vector. In the current example, we have the correspondences shown in Equation 3.18.

$$\boldsymbol{p} \to \boldsymbol{D}, \ \boldsymbol{e} \to \boldsymbol{E}, \ \boldsymbol{s} \to \boldsymbol{f}/A, \ \delta \boldsymbol{e}^T \to \delta \boldsymbol{D}^T \boldsymbol{G}^T \tag{3.18}$$

The Principle of Virtual Work may now be applied to write the equilibrium unbalance force vector $\boldsymbol{\varphi}$ as shown in Equation 3.19

$$\delta \boldsymbol{D}^T \boldsymbol{\varphi} = \delta \boldsymbol{D}^T \left(\frac{1}{A} \int \boldsymbol{G}^T \boldsymbol{f} dV - \boldsymbol{F} \right) \tag{3.19}$$

Integrating Equation 3.19 and rearranging leads to Equation 3.20.

$$\begin{aligned} \boldsymbol{\varphi}(\boldsymbol{E}(\boldsymbol{D})) &= \frac{1}{A} \int \boldsymbol{G}^T \boldsymbol{f}(\boldsymbol{E}) dV - \boldsymbol{F} \\ &= \frac{1}{A} \boldsymbol{G}^T \begin{pmatrix} L_A f_A \\ L_B f_B \\ L_C f_C \\ L_D f_D \\ L_E f_E \end{pmatrix} - \boldsymbol{F} \\ &= \boldsymbol{G}^T \boldsymbol{\Omega} \boldsymbol{f}(\boldsymbol{E}) - \boldsymbol{F} \end{aligned} \tag{3.20}$$

Of course, at equilibrium the unbalanced force vector $\boldsymbol{\varphi}$ vanishes. To employ Newton Iteration, $\boldsymbol{\varphi}(\boldsymbol{E}(\boldsymbol{D})) = 0$ needs to be solved. Differentiation is used to derive the Jacobian matrix as shown in Equation 3.21.

$$
\begin{aligned}
d\boldsymbol{\varphi} &= \boldsymbol{J} d\boldsymbol{D}, \\
\boldsymbol{J}(\boldsymbol{E}(\boldsymbol{D})) &= \boldsymbol{G}^T \left(\int \frac{1}{A} \boldsymbol{\Gamma} dV \right) \boldsymbol{G} \\
&= \boldsymbol{G}^T \boldsymbol{\Omega}^{1/2} \left[\boldsymbol{\Gamma}(\boldsymbol{E}(\boldsymbol{D})) \right] \boldsymbol{\Omega}^{1/2} \boldsymbol{G}
\end{aligned}
\tag{3.21}
$$

Here **J**(**E**(**D**)) is the *same as the Finite Element tangent stiffness matrix*, usually denoted as $\boldsymbol{K}_T$ in the Finite Element Method (Nicholson, 2004). The solution of $\boldsymbol{\varphi}(\boldsymbol{E}(\boldsymbol{D})) = 0$ using Newton Iteration gives rise to the scheme shown in Equation 3.22.

$$
\boldsymbol{J}(\boldsymbol{D}_{k+1}^{j})(\boldsymbol{D}_{k+1}^{j+1} - \boldsymbol{D}_{k+1}^{j}) = -\boldsymbol{\varphi}(\boldsymbol{D}_{k+1}^{j+1}) \tag{3.22}
$$

Shown below in Figure 3.2 is a plot of this benchmark equation. As noted in Figure 3.2 is the maximum forces for node 2, 3, and 4 are 2.29 x 10^5, 6.85 x 10^4 and 1.91 x 10^5 respectively. Figure 3.2 is a plot of three curves; each curve consists of the force and displacement path for one particular node. Accordingly, for a give set of forces the exact displacements may be computed from the foregoing relations. The goal is to use the ALMs to integrate the Finite Element equation, Equation 3.21.

3.2 THREE DEGREE-OF-FREEDOM COMPARISONS

If the results for three ALMs were shown on one illustration, as in the in previous chapter, the figure would get too cluttered and not helpful for comparing performance. Accordingly, each ALM is presented with its own subset of graphs. Table 11 shows the key parameters used for each of the three Arc Length Methods.

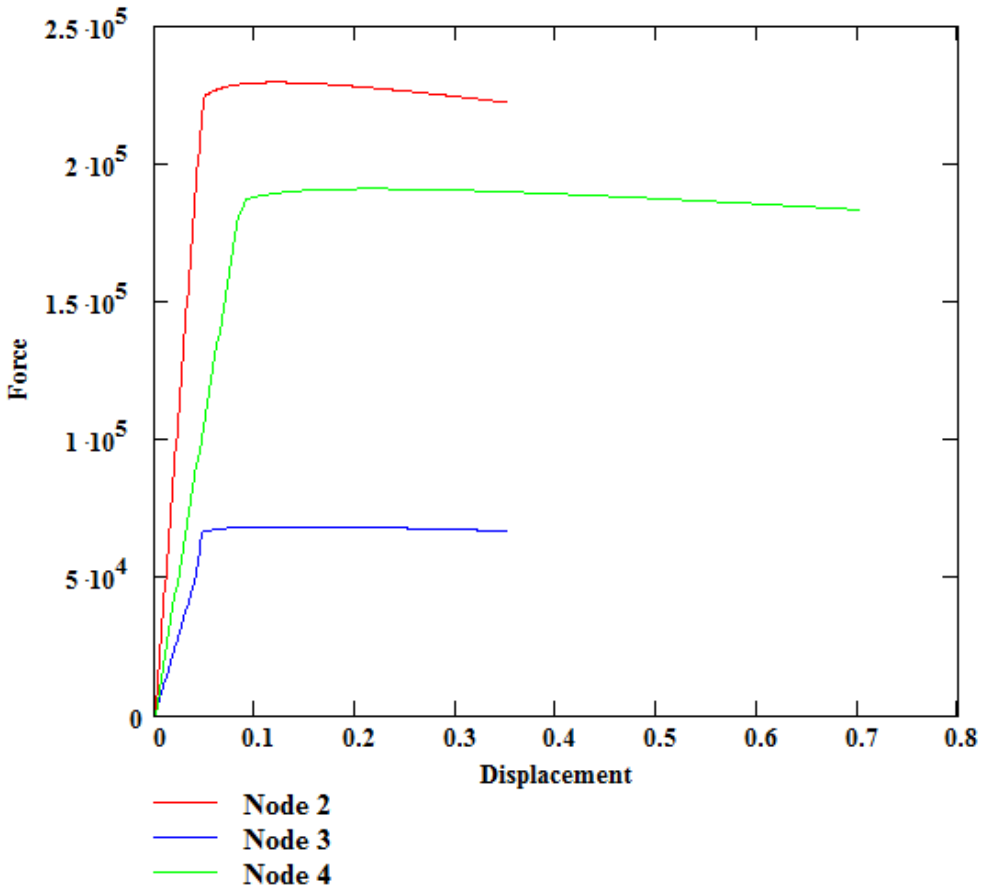

Figure 3.2: Three Degree-of-Freedom Benchmark Plot

Table 11: Key Parameters for 3 DOF Curves

Parameter	E_e (psi)	E_{po} (psi)	E_{p1} (psi)	A (in^2)	s_y (psi)	ε_y (in/in)	εmax (in/in)
Value	10^7	5×10^5	6.25×10^5	1	10^5	.01	.025
Parameter	**α**	**L_A (in)**	**L_B (in)**	**L_C (in)**	**L_D (in)**	**L_E (in)**	
Value	205.179	5	4.5	6.727	4.160	10	

For all three methods, there is an inherent difference between the model equation and the ALM results because the loading paths to reach the final prescribed load are slightly different. In plasticity, the deflections at a given load are affected by the history of how the loads were applied. The reference curves from the model equation (Figure 3.2) have been generated by increasing the displacement at a node at a constant incremental value, and then solving for the corresponding force at each increment until the final displacement is reached. The computational results ensue from incrementing the arc length, meaning that the loads and displacement increments are applied simultaneously subject to the arc length constraint. The curves should be very close and, in particular, agree exactly at the maximum loads since the maximum loads in the reference curves were used as the input external force in the arc length methods. The ALM procedures are 'self-validating' in that ALM converges only if the unbalanced force vector vanishes. However, if convergence does not occur in 20 iterations, the last iterate is taken to be the solution and then would appear on the associated figure. One reason for continuing to the next increment after twenty iterates is to determine whether the solution process thereafter regains the correct path.

Shown below in Figure 3.3, is the Stiff Arc Length Method plotted against the three degree-of-freedom benchmark equation. Referring to Figure 3.3, the SALM (1) gives very close values along the curves, (2) agrees exactly at the maximum load and (3) continues computation accurately at and beyond the critical point.

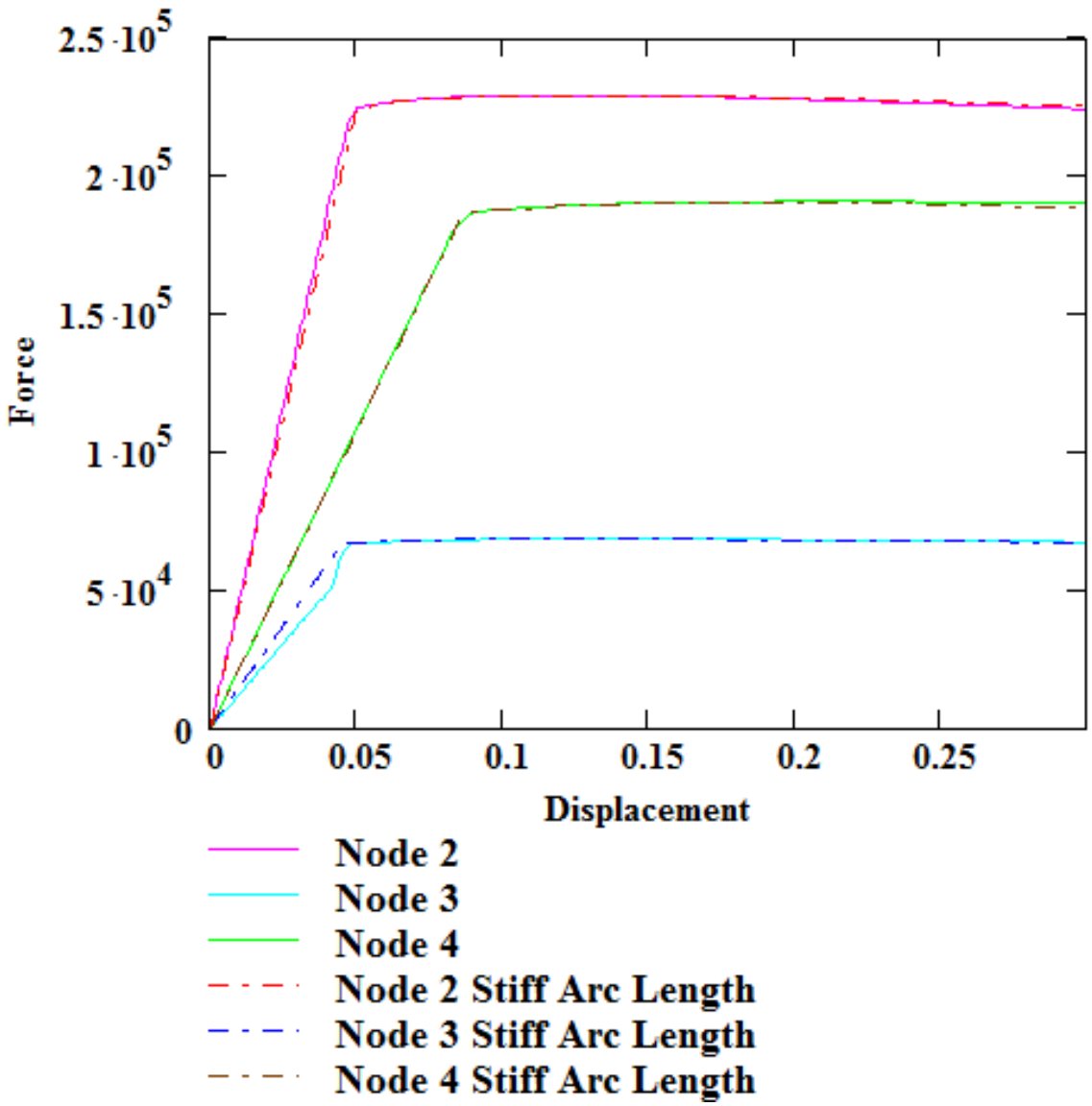

Figure 3.3: Three Degree-of-Freedom Benchmark Comparison to the Stiff Arc Length Method

As previously mentioned, the maximum loads observed in the model equation were input into the ALM benchmark calculations, so the model equation and the ALMs should all have the same maximum prescribed load.

It was discovered that a multiplier change from 1.0 to 1.11 is needed on the load at the center of the stiff arc length constraint equation, to shift this region slightly downwards. Doing so allowed the solution path emanating from the critical point to converge in the forward direction and not backtrack. As previously mentioned two potential solutions, a forward solution and a backtracking solution, exist at the critical point since the loads decreases for both directions; i.e. the critical point may become a bifurcation point. This modification is interpreted as shifting the "zone of attraction" for the forward solution to include the initial iterate; the notion of a zone of attraction is a common issue in Newton Iteration. If the initial iterate is in the “domain of attraction" of the backtracking solution, the solution will in fact backtrack. Note an important fact: the multiplier modification has no effect on the augmented tangent stiffness matrix nor on the equilibrium relation Furthermore the multiplier modification is only needed at the critical point and thereafter the process reverts to the 1.0 factor This last observation supports the “domain of attraction” interpretation of the modification.

More specifically, the multiplier is applied to the previous converged load in the arc length constraint equation as shown in Equation 3.23.

$$\xi(\boldsymbol{p}_{k+1}^{j}, \lambda_{k+1}^{j}) = \boldsymbol{zt}^{T}(\boldsymbol{p}_{k+1}^{j} - \boldsymbol{p}_{k}) - zo(\lambda_{k+1}^{j} - 1.11\lambda_{k}) - \Delta S = 0 \qquad (3.23)$$

The 1.11 multiplier was employed in several different cases for which the material parameters that control the solution path and the increment sizes were significantly altered, and yet the 1.11 multiplier worked in all cases. The 1.11 multiplier allows the solution path to continue accurately beyond the critical point, although after further examination, it was found that the maximum computed load differs very slightly from the

prescribed maximum load. The error between the prescribed load and the maximum loads experienced for all three nodes at the critical point was less than 0.04%, making this error at the critical point of little consequence.

Furthermore, it must be acknowledged that a general method for making the modification has not yet been established, and that further study on the modification is recommended for future work.

Figure 3.4 is a plot of the number of iterations for convergence at each increment for the Stiff Arc Length Method. Referring to Figure 3.4, the highest number of iterates was 15 (and hence there was convergence), and this occurred at increment 121 corresponding to the critical point.

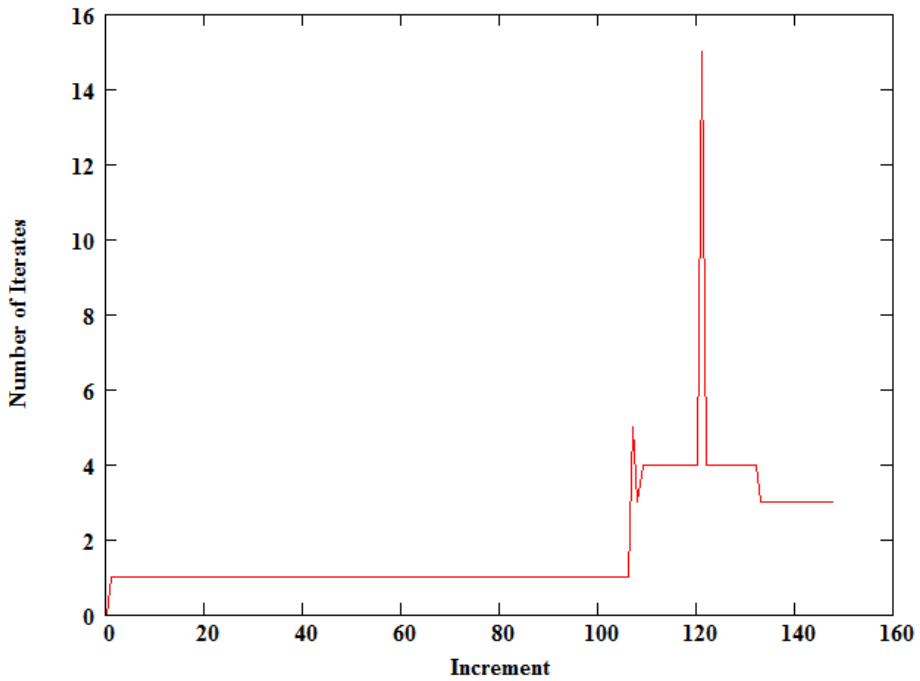

Figure 3.4: Stiff Arc Length Method Number of Iterations Plot

The determinant of the Jacobian matrix at each converged increment is shown in Figure 3.5. Observe that the converged determinant is never equal to or smaller than zero. The iterative determinate does become near zero and negative near the critical point; however those several iterates don't converge until after the critical point is surpassed, where the determinate is no longer zero or negative. As expected, the determinant is largest, and constant, in the elastic region and then significantly drops when entering into the plastic region of the material. (The determinant in the lower plateau on the right is actually of the order of 10^{13}.)

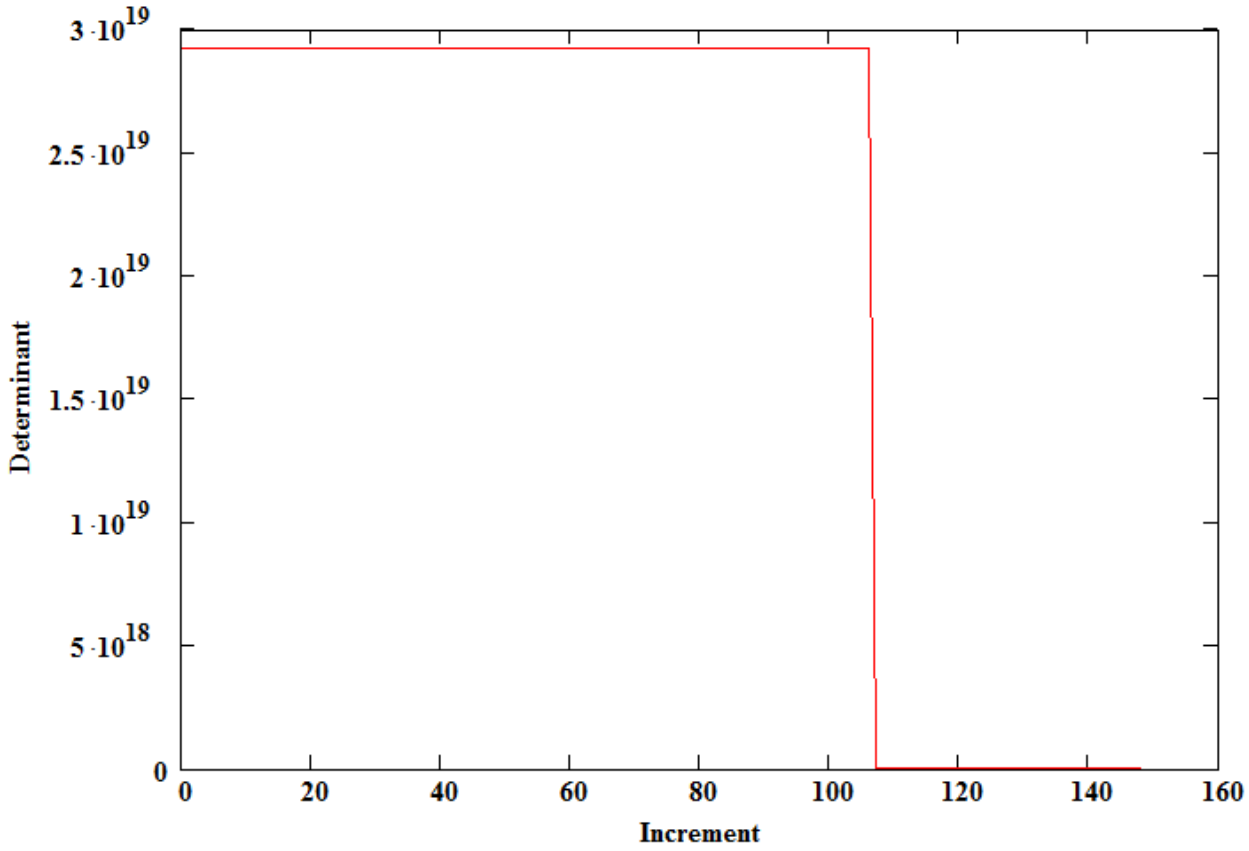

Figure 3.5: Stiff Arc Length Method Converged Determinants

Figure 3.6 shows the residuals at each node of the truss member. The residual is the magnitude difference between the internal and external forces and is vanishes at equilibrium. Figure 3.7 shows the variation of the displacement and load products in the Arc Length Constraint Equation (1.28) with respect to each other at each increment. The displacement product is nothing more than $\boldsymbol{zt}^T(\boldsymbol{p}^j_{k+1} - \boldsymbol{p}_k)$ while the load product is $zo(\lambda^j_{k+1} - \lambda_k)$.Clearly, as one product increases the other decreases. The plot shows that the load product dominates most of the arc length constraint equation in the elastic region; then the displacement product dominates in the plastic region. At the critical point the displacement product shows an upward spike, while the load product shows a downward spike.

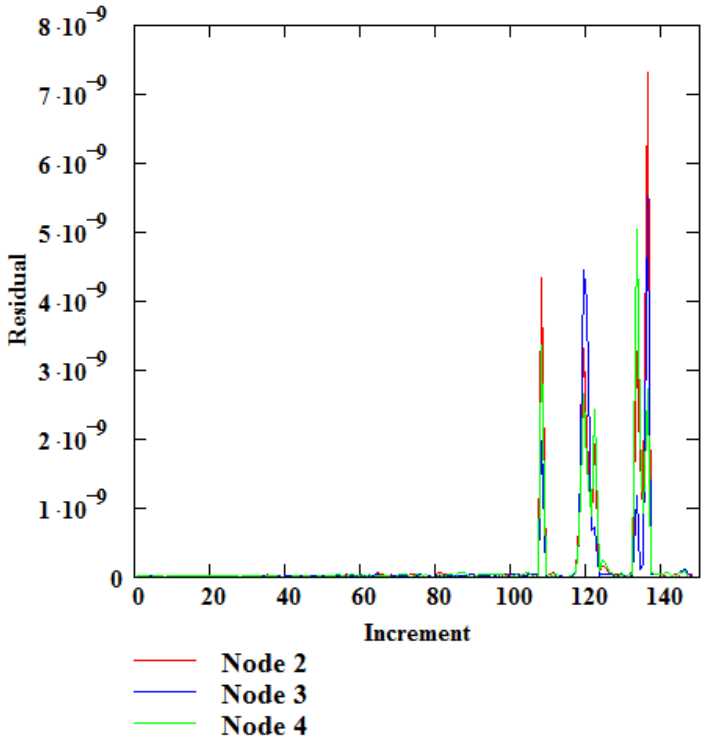

Figure 3.6: Stiff Arc Length Method Residuals at Each Degree-of-Freedom

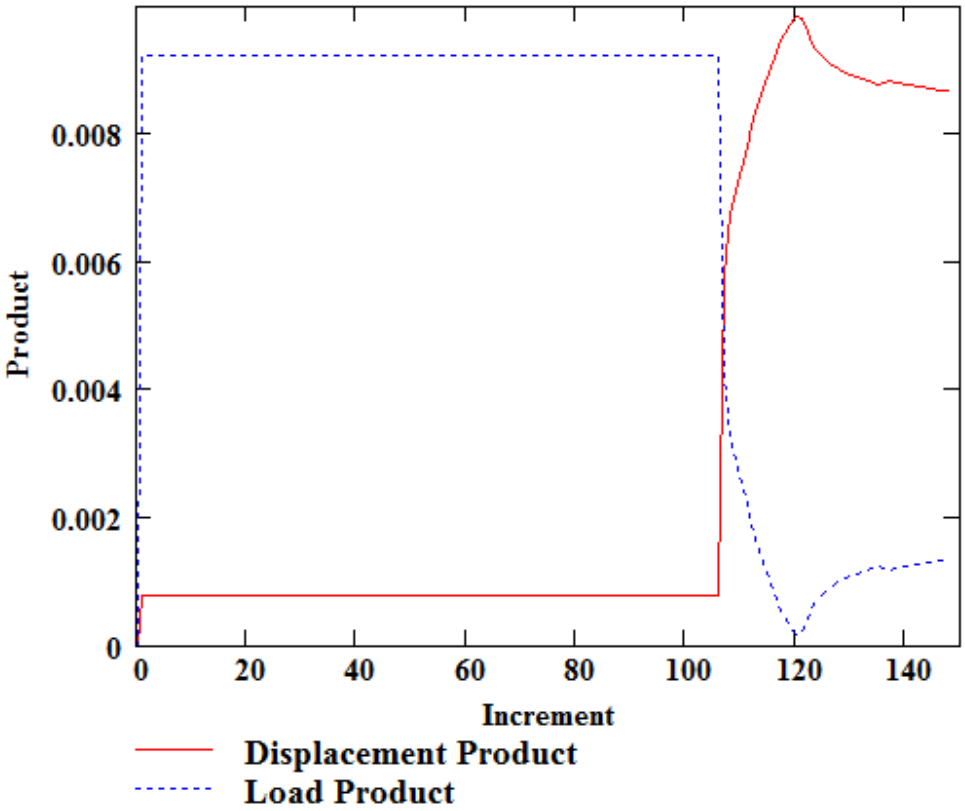

Figure 3.7: Stiff Arc Length Method Displacement and Load Product

Shown below in Figure 3.8 are the forces and displacements at each node *at each iterate*, showing the path that the solution took to attain the converged solution. It can be noted that the solution path oscillated for several iterations about the critical point. This agrees with Table 12 and Figure 3.4 showing that at the critical point the Stiff Arc Length Method took 15 iterates to converge back onto the solution path. The MATHCAD code for this problem can be found in Appendix C. The Stiff ALM method has been applied several times with different arc length parameters to investigate the differences in performance and accuracy. The results are summarized in Table 12.

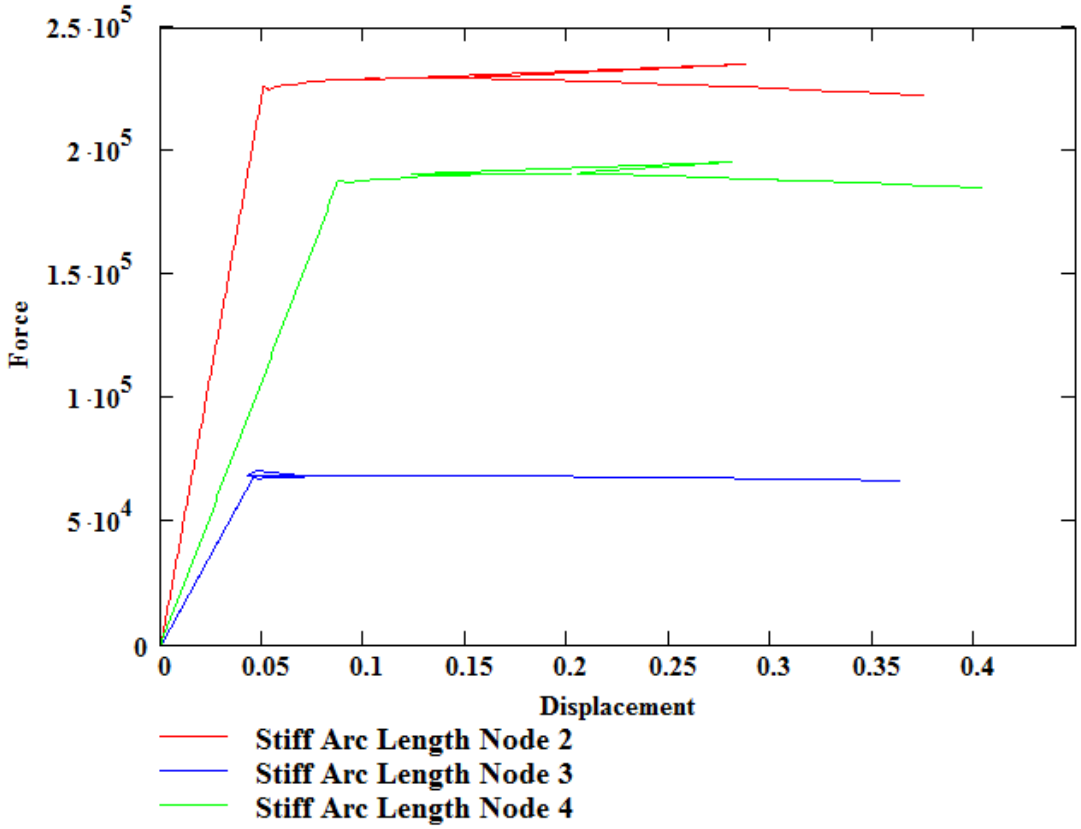

Figure 3.8: Stiff Arc Length Method Force and Displacement Iterates

Table 12: Three Degree-of-Freedom Stiff Arc Length Method Varying Parameter Summary

Arc Length Method (Parameter)	Highest Number of Iterates to Converge	Total Increments	Accuracy	General Comment
Stiff (ΔS = .1)	N/A	N/A	Poor	Bypasses discontinuities and doesn't reach critical point
Stiff (ΔS = .01)	15	148	Very Accurate	This was plotted in Figure 3.3
Stiff (ΔS = .001)	13	1476	Very Accurate	Excellent performance
Stiff (ΔS = .0001)	13	14757	Very Accurate	No significant increase in performance

Next the Crisfield Cylindrical ALM has been assessed as shown in Figure 3.9, for which the arc length parameter equals 0.1. This ALM was able to continue beyond the critical point; however the solution path only had 6 converged values and the actual curve was not followed closely, we believe due to the initial predictor bypassing the discontinuity and the critical point. This method appears to have only worked because the predictor allowed the solution path to jump over major features of the curve, including the critical point. Most importantly in our view, further evaluation revealed an important difficulty: when a smaller arc length parameter is chosen, the converged increments follow the solution path more accurately up to the critical point; but thereafter the method backtracks. Figure 3.10 is a plot of the number of iterations it took to converge at each increment for the Cylindrical ALM. Referring to Figure 3.10 the highest number of iterates was 5 and the Arc Length Method converged generated only 6 increments.

The determinant of the Jacobian matrix at each converged increment is shown in Figure 3.11. The determinant becomes negative after proceeding beyond the critical point as shown in Figure 3.11.

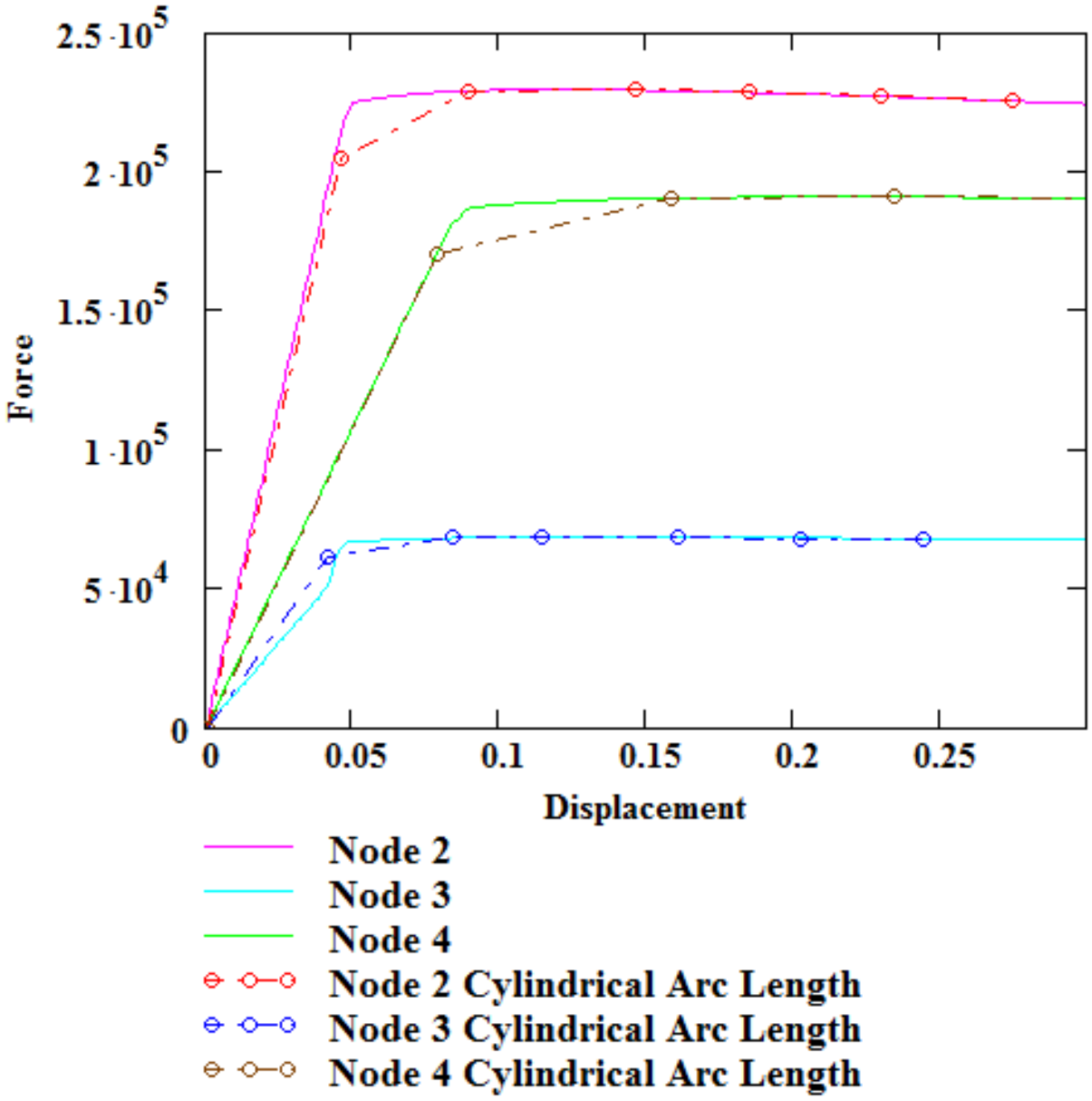

Figure 3.9: Three Degree-of-Freedom Benchmark Comparison to the Cylindrical Arc Length Method

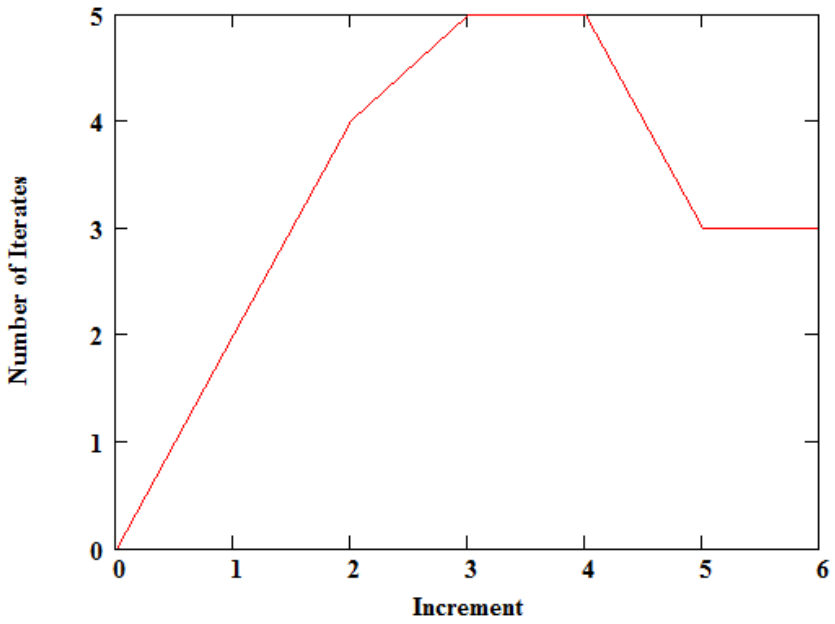

Figure 3.10: Cylindrical Arc Length Method Number of Iterations Plot

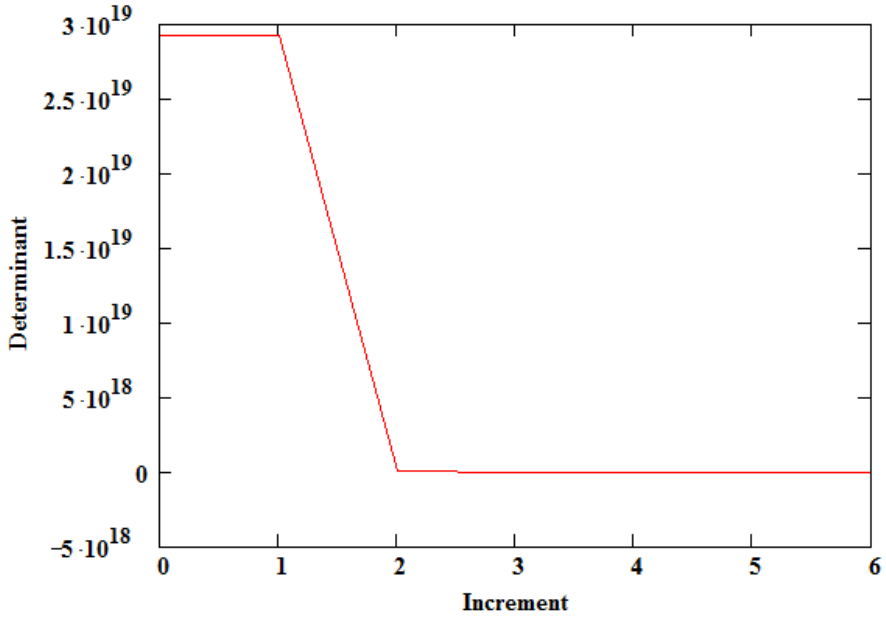

Figure 3.11: Cylindrical Arc Length Method Converged Determinants

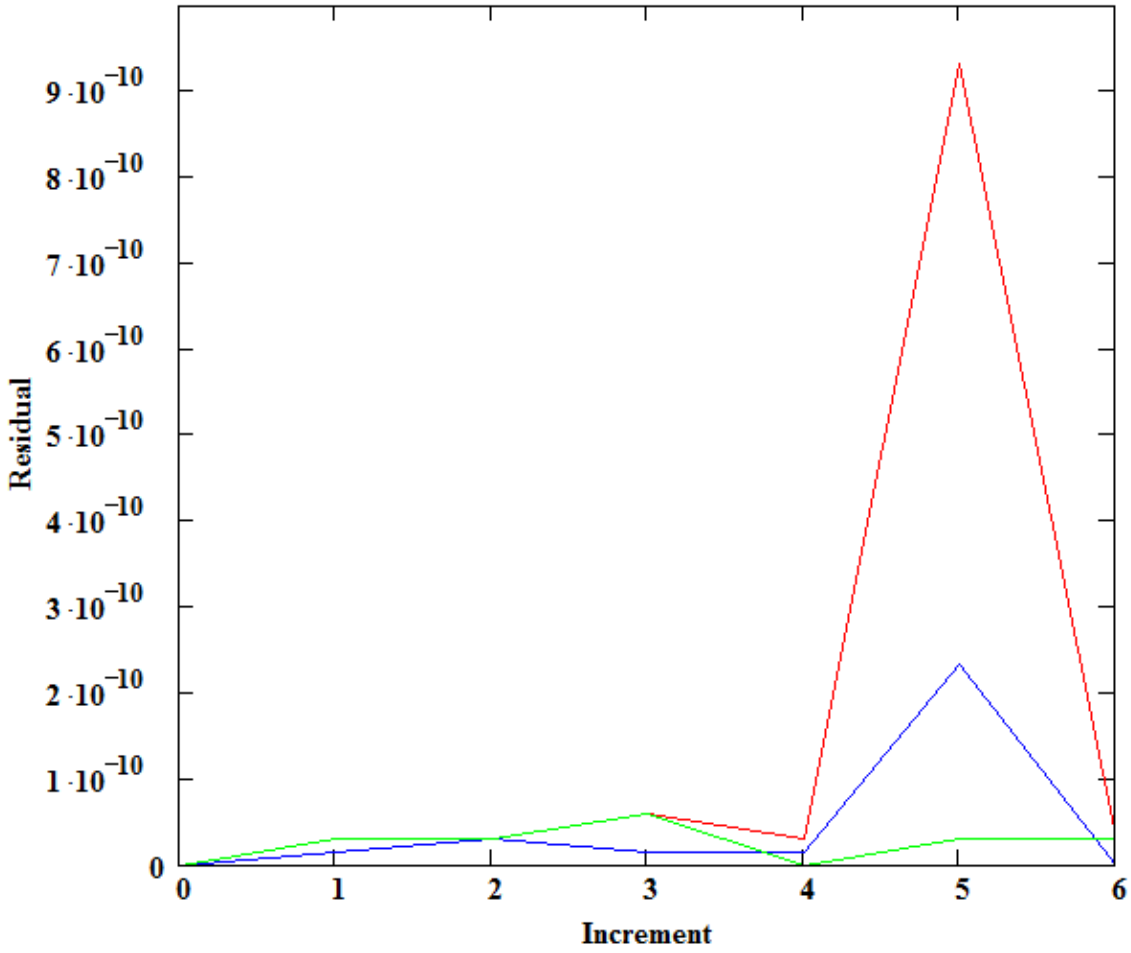

Figure 3.12: Cylindrical Arc Length Method Residuals at Each Degree-of-Freedom

Figure 3.12 above shows the residuals at each node of the truss member. The process of having an initial predictor for the first iterate is shown in Figure 3.13, where it is seen that the initial predictor jumps over the discontinuity after which the Arc Length Method must correct itself back to the solution path curve. The Cylindrical ALM was then executed several times with different arc length parameters to note the difference in accuracy and performance, this summary is shown in Table 13.

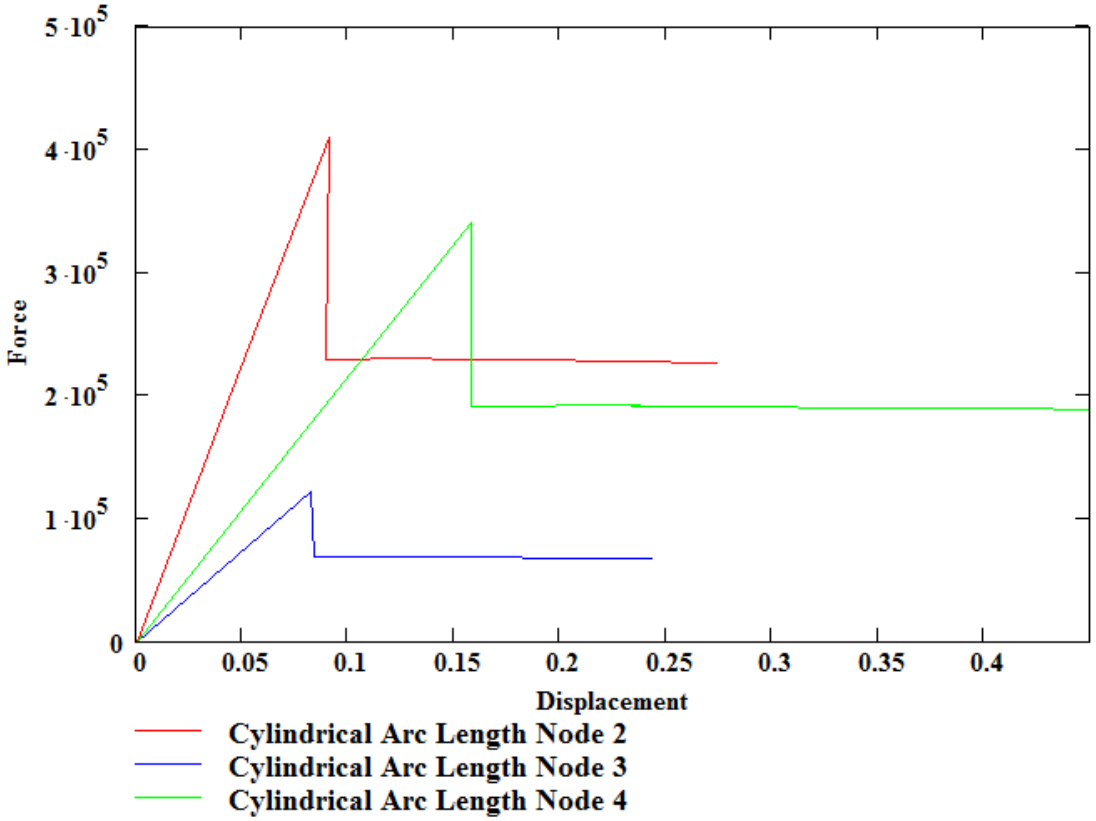

Figure 3.13: Cylindrical Arc Length Method Force and Displacement Iterates

Table 13: Three Degree-of-Freedom Cylindrical Arc Length Method Varying Parameter Summary

Arc Length Method (Parameter)	Highest Number of Iterates to Converge	Total Increments	Accuracy	General Comment
Cylindrical ($\Delta S^2 = .1$)	4	2	Poor	Bypassed almost the entire curve
Cylindrical($\Delta S^2 = .01$)	5	6	Medium	This was plotted in Figure 3.9
Cylindrical($\Delta S^2 = .001$)	N/A	N/A	Poor	Solution failed at critical point and started converging backwards
Cylindrical($\Delta S^2 = .0001$)	N/A	N/A	Poor	Solution failed at critical point and started converging backwards

In our view, most importantly Table 13 indicates that using a smaller arc length parameter *causes the Cylindrical Arc Length Method to backtrack from the critical point*. Shown below in Figure 3.14 is a plot of the Cylindrical ALM using an arc length parameter of .001 which causes the solution to backtrack after approaching the critical point.

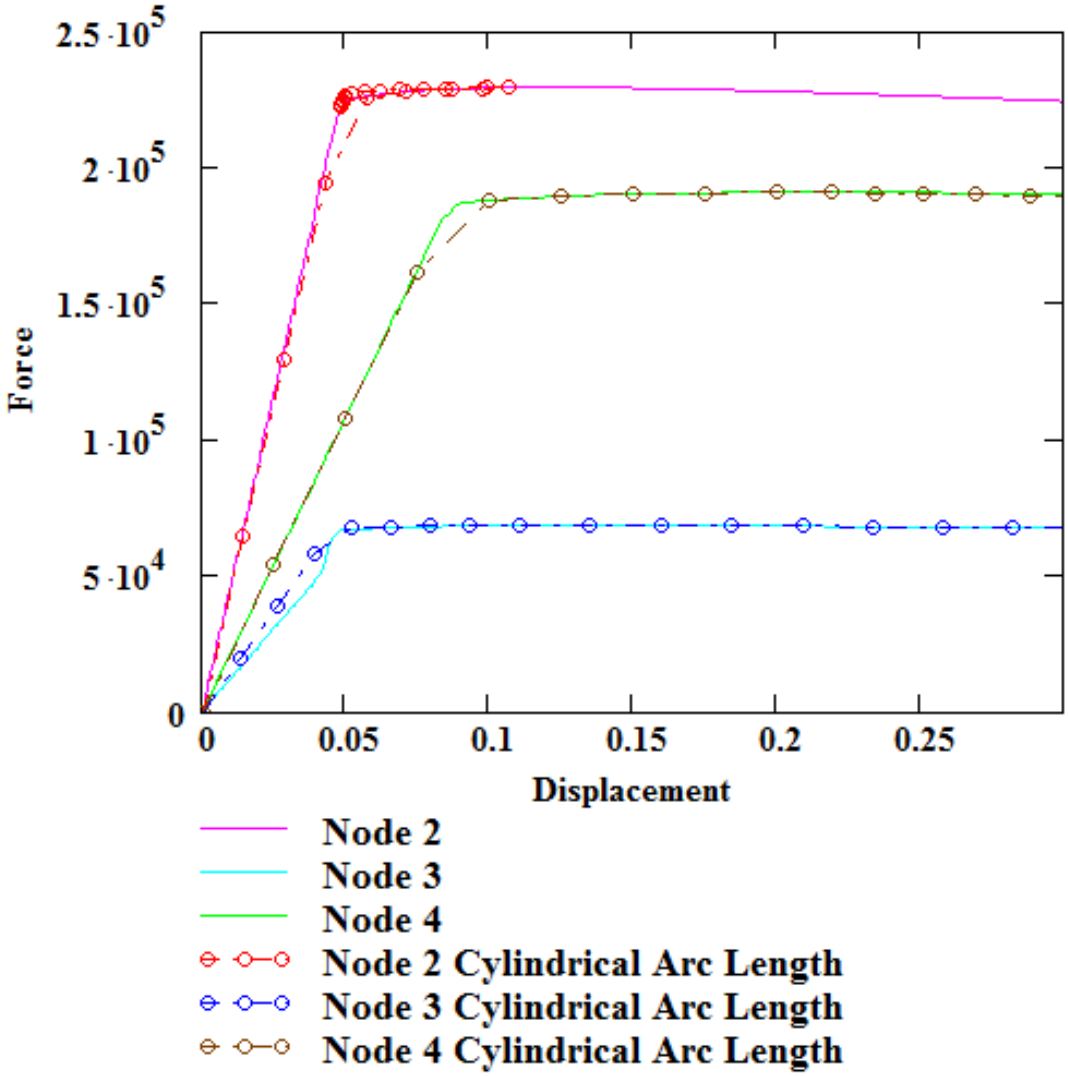

Figure 3.14: Cylindrical Arc Length Method Backtracking Plot

Finally, Crisfield's Spherical Arc Length Method was investigated, as shown in Figure 3.15. This graph looks very similar to the one in Figure 3.9 because only a small load scaling parameter value works. Recall that when the load parameter becomes zero or significantly near zero, the Spherical and Cylindrical ALMs become very similar.

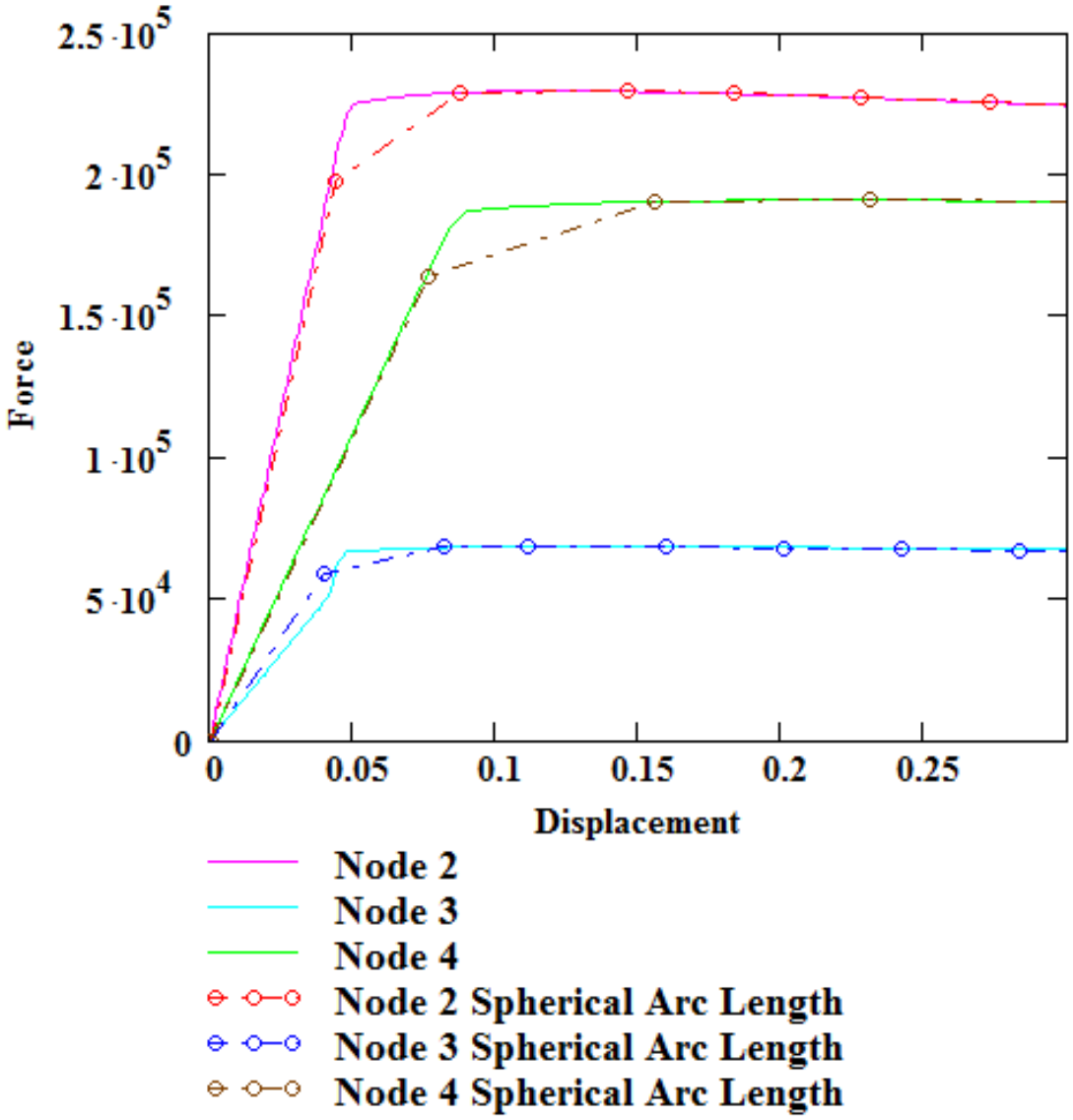

Figure 3.15: Three Degree-of-Freedom Benchmark Comparison to the Spherical Arc Length Method

Just like the Cylindrical ALM, the solution path had very few increments, but the path fluctuated around the reference curve, bypassed the discontinuity and likely bypassed the critical point. Figures 3.16 and 3.17 are the number of iterations required for convergence and the determinant at each convergence, respectively.

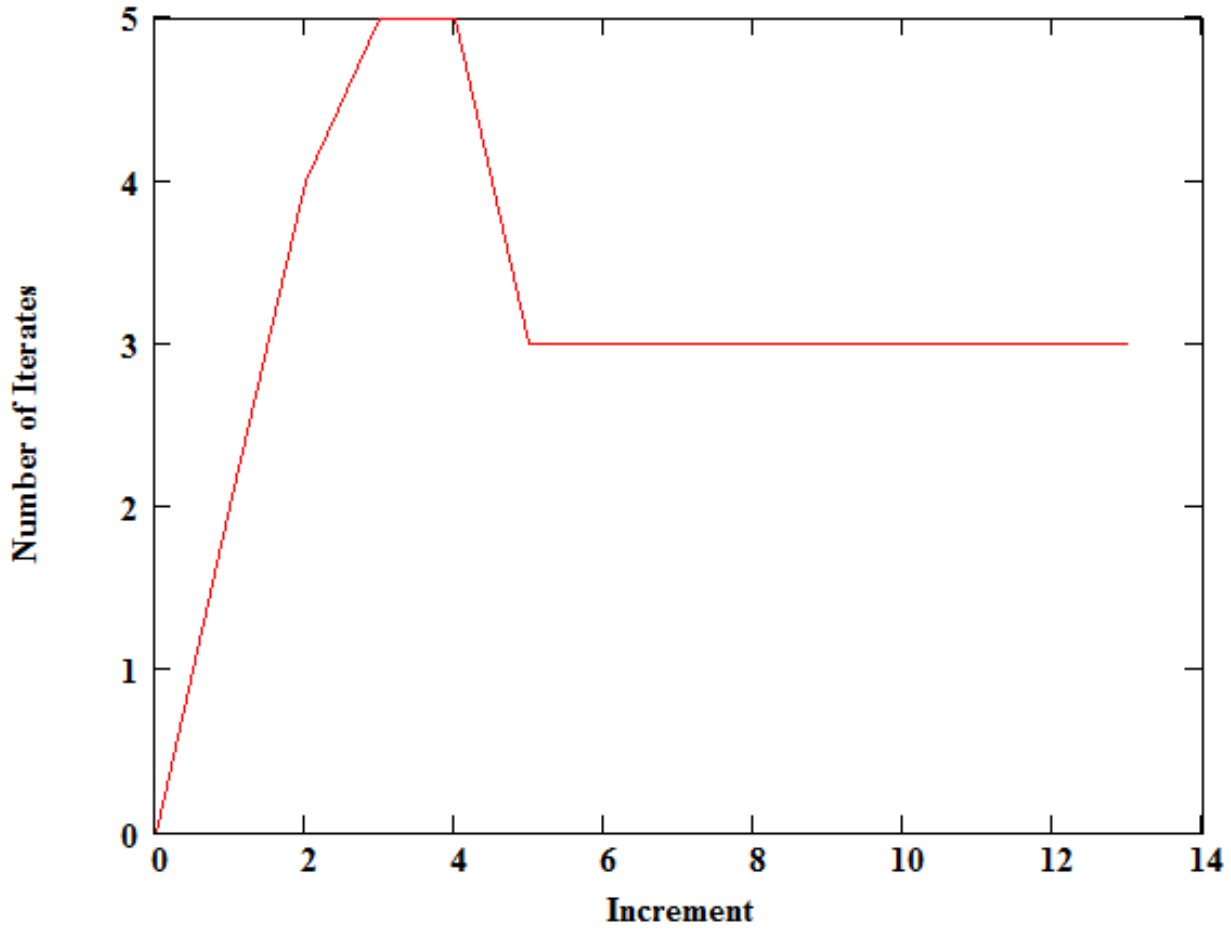

Figure 3.16: Spherical Arc Length Method Number of Iterations Plot

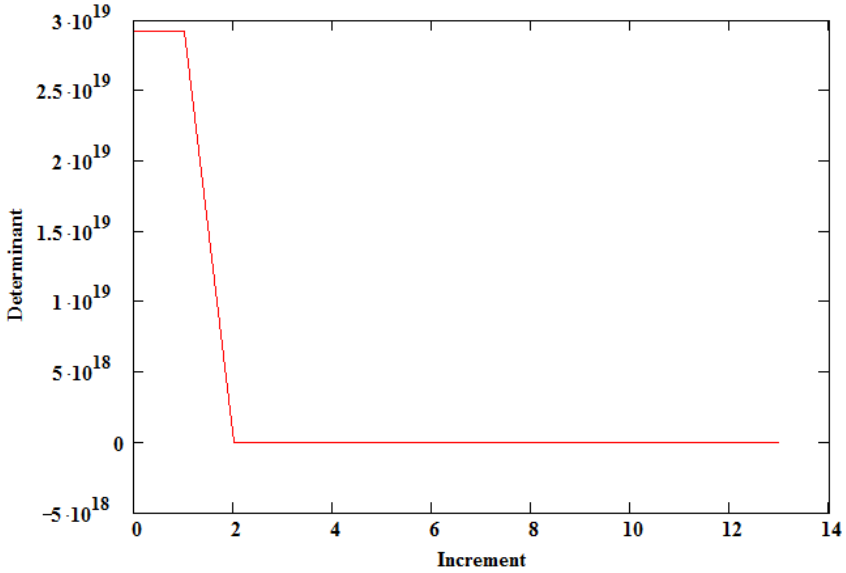

Figure 3.17: Spherical Arc Length Method Converged Determinants

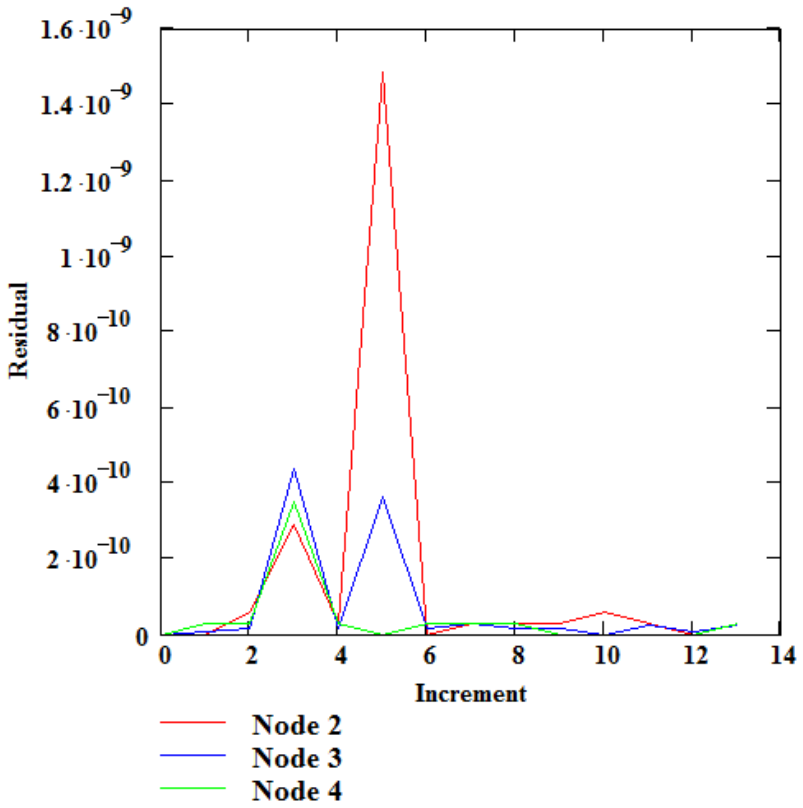

Figure 3.18: Spherical Arc Length Method Residuals at Each Degree-of-Freedom

The residuals for the Spherical ALM at each node are shown in Figure 3.18. The iterative process for the Spherical ALM is similar to that of the Cylindrical ALM, and is shown below in Figure 3.19.

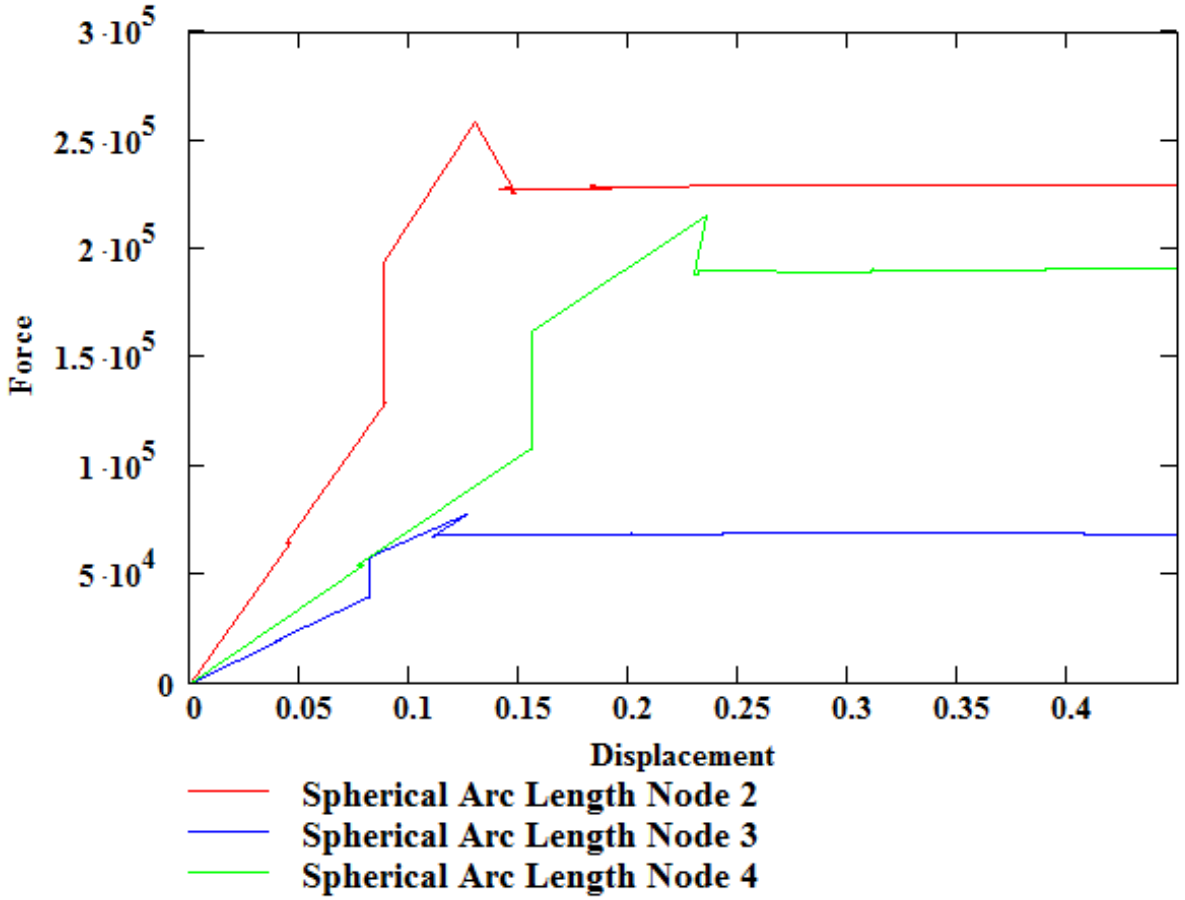

Figure 3.19: Spherical Arc Length Method Force and Displacement Iterates

The Spherical ALM was further examined by manipulating the arc length and load parameter. The results are shown in Table 14. A very small load parameter was needed to enable the method to converge without encountering complex numbers, essentially rendering this Spherical ALM results similar to the results of the Cylindrical ALM. This code can be found in Appendix D.

Table 14: Three Degree-of-Freedom Spherical Arc Length Method Varying Parameter Summary

Arc Length Method (Parameter)	Highest Number of Iterates to Converge	Total Increments	Accuracy	General Comment
Spherical($\Delta S^2 = .1$, $\Psi = .000001$)	N/A	N/A	N/A	Solution wouldn't converge, ran into complex numbers
Spherical($\Delta S^2 = .1$, $\Psi = .0000001$)	4	5	Poor	Bypassed almost the entire curve
Spherical($\Delta S^2 = .01$, $\Psi = .000001$)	N/A	N/A	N/A	Solution wouldn't converge, ran into complex numbers
Spherical($\Delta S^2 = .01$, $\Psi = .0000001$)	5	13	Medium	This was plotted in Figure 3.14
Spherical($\Delta S^2 = .001$, $\Psi = .000001$)	N/A	N/A	N/A	Solution wouldn't converge, ran into complex numbers
Spherical($\Delta S^2 = .001$, $\Psi = .0000001$)	N/A	N/A	Poor	Solution failed at critical point and started converging backwards

Chapter Four : CONCLUSIONS

Accurate computations at and beyond the critical point in a solution path are important because instabilities associated with critical points are precursors to damage events. Arc Length Methods have been introduced to predict structural behavior approaching or at failure events and to offer insight into the associated damage and failure mechanisms. Modeling behavior at and beyond weak instabilities such as elastoplastic softening is of greater interest in the current investigation, rather than behavior at strong instabilities. Two reasons for this interest are the fact that (1) weak instabilities are more challenging computationally since the tangent stiffness matrix is nearly singular for an extensive solution path interval encompassing the critical point, and (2) the fact that weak instabilities have received comparatively little attention in the FEA community.

Several investigators have commented that the widely used Crisfield and other current ALMs sometimes fail at the critical point associated with (weak) material instabilities even though they are thought to be reliable when applied to buckling (strong instability) problems. The more recent Stiff ALM has features which expected to offer better performance than current methods at and near critical points. Most importantly, instead of the singular augmented stiffness matrix of the Crisfield and other current methods, the Stiff ALM selects an arc length vector which maximizes the stiffness of the augmented tangent stiffness matrix.

The overall goals of the present investigation include implementing the ALMs, demonstrating that the Stiff ALM is valid, and demonstrating that its attractive

mathematical features result in superior computational performance. Accordingly, the present investigation has formulated two simple but demanding benchmark problems, implemented the Crisfield and Stiff ALMs for the benchmarks, to compare the performance of the Stiff and Crisfield ALMs.

In the one degree-of-freedom case, the Stiff ALM showed high accuracy and stability even when using large arc length parameter values (increment sizes). While the Cylindrical ALM only required a few increments to follow the entire solution path, the accuracy suffered. Also, apparently because of the type of predictor used, in some cases it jumped over the critical point.

As for the Spherical ALM, it shows marginally better performance than the Cylindrical ALM but only if a particular load scaling parameter value is chosen, whose identification requires user intervention in the form of trial and error.

In the three degree-of-freedom case, the Stiff ALM converged very accurately along the solution path but took several iterations and a slight shift of the center of the arc length constraint domain to allow computations to continue beyond the critical point. The shift involves the factor 1.11 which seems to be a problem-insensitive value. For example, after modifying the material properties to severely flatten the material curve, and after using a wide range of arc length parameter values, and the Stiff Arc Length still converged at and beyond the critical point.

The Cylindrical ALM in the three degree-of-freedom case was able to continue beyond the critical point, but only in the case when a large arc length parameter value was chosen. This had to do with the method incorporating a predictor which 'jumped

over' the critical point region. When using decreased arc length parameter values the accuracy of the Cylindrical ALM should have improved but instead failed at the critical point. Deteriorating performance with decreasing increment sizes is considered very problematic in FEA. A likely explanation of this outcome is as follows: as the arc length parameter value decreased the solution process generated iterates close to the critical point and thereby failed owing to near-singularity of the augmented tangent stiffness matrix in the vicinity of the critical point.

The Spherical ALM performed very poorly in the three degree-of-freedom case. It succeeded only when certain values of the load parameter and large values of the arc length parameter were used, whose identification required user intervention in the form of trial and error. It likewise showed failure as the arc length parameter value decreased.

As expected, the Stiff ALM was shown to be a strong contender to the widely accepted Crisfield ALMs.

In summary the Crisfield Arc Length Methods have the following main disadvantages:

1. They abandon Newton Iteration by making the displacement increment proportional to the load increment. Therefore this method can at most attain linear convergence rather than the attractive quadratic convergence characteristic of Newton Iteration; in addition the method introduces a potential quadratic root issue.

2. The arc length constraint does not reflect the properties of the (unaugmented) tangent stiffness matrix; nor is there a rationale in terms of the stiffness of the augmented tangent stiffness matrix.
3. Inherent in the relations in this Arc Length Method, at the exact location of the critical point the augmented tangent stiffness matrix is singular and solution process fails and the augmented tangent stiffness matrix is near-singular in an extensive interval encompassing the critical point.
4. The augmented stiffness matrix includes incremental terms.

The Stiff Arc Length Method chooses the arc length vector to maximize the determinant of the augmented stiffness matrix at the critical point. To maximize the determinant, the optimal arc length vector is simply the null eigenvector of the unaugmented stiffness matrix. The null eigenvector may be readily computed using Gram-Schmidt orthogonalization to find a vector orthogonal to the first *n-1* rows of $\boldsymbol{K}_T$.

In summary the Stiff Arc Length Method offers the following advantages:

1. It fully implements Newton Iteration, thus benefitting from its quadratic convergence property.
2. The arc length vector is not incremental and requires no ad hoc scale factor to prevent ill-conditioning in the augmented tangent stiffness matrix.
3. The arc length vector is derived from the unaugmented stiffness matrix, and is strictly obtained by maximizing the determinant of the augmented stiffness matrix at the critical point. This of course justifies

the expectation that the augmented stiffness matrix is not singular or near-singular at the critical point.

Chapter Five : FUTURE WORK

The Stiff Arc Length Method has many advantages over the current widely used Crisfield methods, as noted above. Here suggestions are offered for further improvements. Crisfield's Cylindrical and Spherical Arc Length Methods make use of initial predictors to help accelerate the process of convergence; it also appears these predictors are linear. The Stiff Arc Length Method currently requires many more iterations and increments than the Crisfield methods, because the iteration process starts with the previous converged solution. The Stiff Arc Length Method could benefit from using initial predictors, such as the linear predictors shown in Equations 5.1 and 5.2.

$$\boldsymbol{p}_{k+1}^{0} = \boldsymbol{p}_k + \varsigma(\boldsymbol{p}_k - \boldsymbol{p}_{k-1}) \tag{5.1}$$

$$\lambda_{k+1}^{0} = \lambda_k + \varsigma(\lambda_k - \lambda_{k-1}) \tag{5.2}$$

In which the superscript "0" denotes the starting iterate. However using initial predictors has a downside as noted in both Chapters 2 and 3: if there is a slope discontinuity in the curve the predictor may overshoot significantly and bypass part of the solution path.

Several investigators have advocated the use of an interval halving method near the critical point or wherever convergence is not attained within a prescribed number of iterations. The use of an interval reducing algorithm based off of previous determinant increments may increase the performance of the ALM in the vicinity of the critical point. For example using three consecutive converged values of the determinant, of the unaugmented stiffness matrix, the total arc length increase at which the critical point is

reached can be predicted, and the arc length parameter value can then be changed to equal half of the increase. This notion is based off of the assumption the determinant vanishes at the critical point.

As illustration, suppose the values $\boldsymbol{ke}(x_n)$, $\boldsymbol{ke}(x_{n-1})$, and $\boldsymbol{ke}(x_{n-2})$ have been computed. A quadratic model may be introduced in the form of Equation 5.3.

$$\boldsymbol{ke}(x - x_{n-2}) = \boldsymbol{ke}_{n-2} + \boldsymbol{q}(x - x_{n-2}) + \boldsymbol{r}(x - x_{n-2})^2 \tag{5.3}$$

The values for $\boldsymbol{q}$ and $\boldsymbol{r}$ are now sought to fit the computed curve using three values. Considering the two relations listed below in Equation 5.4, a matrix can be formed to solve for the two unknowns as shown in Equation 5.5.

$$\begin{aligned} \boldsymbol{ke}_n - \boldsymbol{ke}_{n-2} &= \boldsymbol{q}\Delta_2 x + \boldsymbol{r}\Delta_2 x^2, \Delta_2 x = x_n - x_{n-2} \\ \boldsymbol{ke}_n - \boldsymbol{ke}_{n-1} &= \boldsymbol{q}\Delta_1 x + \boldsymbol{r}\Delta_1 x^2, \Delta_1 x = x_n - x_{n-1} \end{aligned} \tag{5.4}$$

$$\begin{bmatrix} \Delta_1 x & \Delta_1 x^2 \\ \Delta_2 x & \Delta_2 x^2 \end{bmatrix} \begin{Bmatrix} \boldsymbol{q} \\ \boldsymbol{r} \end{Bmatrix} = \begin{Bmatrix} \boldsymbol{ke}_n - \boldsymbol{ke}_{n-1} \\ \boldsymbol{ke}_n - \boldsymbol{ke}_{n-2} \end{Bmatrix} \rightarrow \begin{Bmatrix} \boldsymbol{q} \\ \boldsymbol{r} \end{Bmatrix} = \frac{1}{\Delta_1 x \Delta_2 x(\Delta_2 x - \Delta_1 x)} \begin{bmatrix} \Delta_2 x^2 & -\Delta_1 x^2 \\ -\Delta_2 x & \Delta_1 x \end{bmatrix} \begin{Bmatrix} \boldsymbol{ke}_n - \boldsymbol{ke}_{n-1} \\ \boldsymbol{ke}_n - \boldsymbol{ke}_{n-2} \end{Bmatrix} \tag{5.5}$$

Introducing the predictor x_p such that $\boldsymbol{ke}_p = 0$ at x_p, the quadratic model may be rewritten as Equation 5.6.

$$\boldsymbol{ke}_{n-2} + \boldsymbol{q}(x_p - x_{n-2}) + \boldsymbol{r}(x_p - x_{n-2})^2 = 0 \tag{5.6}$$

Where the predictor x_p can now expressed in the form of Equation 5.7.

$$x_p = x_{n-2} + \frac{\left[-\boldsymbol{q} \pm \sqrt{\boldsymbol{q}^2 - 4\boldsymbol{ke}_{n-2}\boldsymbol{r}}\right]}{2\boldsymbol{r}} \tag{5.7}$$

Of course the value under the square root must be positive. Equation 5.7 will have two roots, but only the lower root is of interest. After using the previous converged increments to determine the value of the predicted increment $x_p - x_n$, if this quantity is

less than current increment, then replace the current increment with $\left(x_p - x_n\right)/2$. The predicted increment should be evaluated at each iterate to see if it should be reduced again using the algorithm, and a lower bound tolerance should be chosen to prevent the increment from being reducing indefinitely. In the truss problem, the determinant of the Jacobian matrix would replace ***ke*** in Equations 5.3 thru 5.7, and the total arc length ΔS_T would replace *x*. (Since the determinant may be difficult to calculate in large-scale FEA problems, an alternative quantity may be used based on Gram-Schmidt orthogonalization.) The total arc length is nothing other than $\Delta S_T = \sum_j \Delta S_j$. This suggested algorithm in essence predicts where the critical point is and reduces the increment only on approach to the critical point. Doing so offers an attractive potential for good performance at considerably less effort, by allowing relatively large increments away from the critical point along with high resolution near the critical point. After the critical point is reached and surpassed, the previous increment (arc length parameter) may be restored.

Both the Stiff ALM and Crisfield's Spherical and Cylindrical ALMs may encounter convergence issues at slope discontinuities, although none were observed in the Stiff ALM. Crisfield's methods appear to be more prone to failure near slope discontinuities. In particular, the predictor may cause the solution process to set the iterate well away from the correct (equilibrium) relation, with the consequence that the solution process is not able to converge to the correct relation. This is a problem worth noting because classical plasticity models such as linear isotropic hardening with a Von Mises yield

surface are inherently discontinuous; also observed stress strain curves generated from experimental data often show a sharp slope change at initial yield. Difficulties at slope discontinuities did not appear to be an issue for the Stiff Arc Length Method as formulated here, since the last converged solution is used as the initial iterate. If a predictor is used to generate the initial iterate, a problem may arise, although it appears that the Stiff ALM is performs well in regaining the correct equilibrium curve. However, if problems do occur there are a few options to circumvent this issue. The material model may be modified in advance to 'smooth out' the slope discontinuity. Alternatively, if at some point in the solution process, the residuals after one iterate are suddenly large compared to previous steps, the solution process may then backtrack to use progressively smaller increments until the residuals meet a tolerance.

Since the Stiff Arc Length Method performs so well in elastoplastic problems at the critical point, it would be attractive to apply it to necking and other strain localization applications. Specifically, this method might be used to further understanding the phenomenon of necking and predicting its development to the point of failure. Several necking experiments could easily be performed in conjunction with the modeling. Agreement between experiment and computation would likely provide a strong impetus to adoption of the method widely in the FEA community.

Additional investigation is needed as to why the 1.11 multiplier in the load product of the arc length constraint equation works at the critical point. Fortunately, the 1.11 multiplier seems to be problem-insensitive in that it is effective for several different material curves as the material properties are varied significantly. The multiplier is only

required at the critical point and nowhere else in the solution path. Nor does it have any effect on the augmented tangent stiffness matrix. It is very desirable to avoid requiring the user to intervene to allow the Arc Length Method to continue computation at and through critical points.

The view has been expressed that the multiplier shifts the constraint region such that the initial iterate is in the 'domain of attraction' of the correct solution. Investigation is needed to examine the iteration process at the critical point and to consider the effect of starting to the near right and to the near left. Recall that the sign in the arc length constraint load term changes at the critical point. However the solution process does not necessarily yield values exactly on the critical point, but instead the associated increment straddles it. Perhaps a value between +1 and -1 should be introduced which is proportionate to the fraction of the increment to the left and to the right of the critical point. Investigation is also needed on the benefits of increment size reduction near the critical point, since the increment will typically straddle the critical point.

Of course it is desirable to demonstrate how the Stiff ALM can be implemented in a large scale finite element code, rather than in simple benchmarks. Usually solvers in commercial codes such as ANSYS are not accessible through the user interface. However there are several publically available codes which may be modified to incorporate the Stiff ALM in the solver. One code is of particular interest. The text Finite Element Plasticity and Metalforming Analysis (Rowe et al, 1990) gives the source code for a simple elastic-plastic code using plane strain, plane stress and axisymmetric triangular elements and linear kinematics (Rowe et al, 1990). Since the code uses a

constant plastic modulus, it would be necessary to modify it by creating a loop inside the code to compute the plastic modulus as a function of strain. The intent would be to implement the elastoplastic softening material model in the current investigation. The solver would of course need to be rewritten and highlighted. The thereby modified code would be applicable to simple necking simulations.

Finally, in order for the Stiff Arc Length Method to gain more visibility, especially now that the performance has been verified through several examples, this investigation should be incorporated into an article for submission to a journal. Publishing the results, as well as the MATHCAD codes, will afford interested investigators an opportunity to familiarize themselves with the Stiff ALM and its performance compared to previous methods, and perhaps even to conduct further research or performance assessment, or implement it in state-of-the-art finite element codes.

APPENDIX A:
STIFF ARC LENGTH 1 DOF MATHCAD CODE

Parameters

$Ee := 10^7$ $Epo := 2 \times 10^5$ $Ep1 := 1.1 \cdot Epo$ $Sy := 10^5$ $A := 1$ $L := 10$ $dmax := .5$ $dy := \frac{Sy \cdot L}{Ee}$ $fy := \frac{Ee \cdot A \cdot dy}{L}$

$dy = 0.1$ $fy = 1 \times 10^5$

Solve for α

Guess Value $\alpha := 1$

Given

$$0 = \frac{Epo \cdot A}{L} - \left[\frac{2}{\pi} \cdot \frac{Ep1 \cdot Ao}{L} \cdot \left[\frac{\alpha}{L} \cdot (dmax - dy)\right] \cdot \operatorname{atan}\left[\frac{\alpha}{L} \cdot (dmax - dy)\right]\right]$$

$\alpha := \text{Find}(\alpha)$

$\alpha = 36.699$

$\kappa := \frac{\alpha}{L}$

Governing Equations

$fe(x) := \frac{Ee \cdot Ao}{L} \cdot x$ $ge(x) := \frac{d}{dx} fe(x)$

$fp1(x) := \left[\frac{Epo \cdot Ao}{L} \cdot (x - dy)\right]$

$$fp2(x) := -\left[\frac{2}{\pi}\cdot\frac{Ep1\cdot Ao}{L}\cdot\frac{1}{\kappa}\cdot\left[\left[\frac{1}{2}\cdot[\kappa\cdot(x-dy)]^2\cdot\operatorname{atan}[\kappa\cdot(x-dy)]\right]-\frac{1}{2}\cdot[\kappa\cdot(x-dy)]+\frac{1}{2}\cdot\operatorname{atan}[\kappa\cdot(x-dy)]\right]\right]+fy$$

$$fp(x) := fp1(x) + fp2(x) \qquad gp(x) := \frac{Epo\cdot Ao}{L} - \left[\frac{2}{\pi}\cdot\frac{Ep1\cdot Ao}{L}\cdot[\kappa\cdot(x-dy)]\cdot\operatorname{atan}[\kappa\cdot(x-dy)]\right]$$

$$qe := fp(dmax) \qquad qe = 1.049\times 10^5$$

Stiff_Arc_Length :=
- $t \leftarrow 1$
- $\Delta S \leftarrow .001$
- $zo \leftarrow 2$
- $zt \leftarrow 1$
- $Pc \leftarrow 0$
- $\lambda c \leftarrow 0$
- $n \leftarrow 0$
- $k \leftarrow 0$
- $P_0 \leftarrow 0$
- $\lambda_0 \leftarrow 0$
- $z \leftarrow 0$
- for $m \in 0..100000$
  - while $t = 1$
    - if $P_k > dy$
      - $\begin{pmatrix} P_{k+1} \\ \lambda_{k+1} \end{pmatrix} \leftarrow \begin{pmatrix} P_k \\ \lambda_k \end{pmatrix} - \begin{pmatrix} gp(P_k) & -qe \\ zt & zo \end{pmatrix}^{-1} \cdot \begin{bmatrix} fp(P_k) - qe\cdot\lambda_k \\ zt\cdot(P_k - Pc) + zo\cdot(\lambda_k - \lambda c) - \Delta S \end{bmatrix}$ if $gp(P_k) \geq 0$

$$\begin{pmatrix} P_{k+1} \\ \lambda_{k+1} \end{pmatrix} \leftarrow \begin{pmatrix} P_k \\ \lambda_k \end{pmatrix} - \begin{pmatrix} gp(P_k) & -qe \\ zt & -1 \cdot zo \end{pmatrix}^{-1} \cdot \begin{bmatrix} fp(P_k) - qe \cdot \lambda_k \\ zt \cdot (P_k - Pc) + (-1) \cdot zo \cdot (\lambda_k - \lambda c) - \Delta S \end{bmatrix} \quad \text{if} \quad gp(P_k) < 0$$

$n \leftarrow n + 1$

if $P_k \leq dy$

$$\begin{pmatrix} P_{k+1} \\ \lambda_{k+1} \end{pmatrix} \leftarrow \begin{pmatrix} P_k \\ \lambda_k \end{pmatrix} - \begin{pmatrix} ge(P_k) & -qe \\ zt & zo \end{pmatrix}^{-1} \cdot \begin{bmatrix} fe(P_k) - qe \cdot \lambda_k \\ zt \cdot (P_k - Pc) + zo \cdot (\lambda_k - \lambda c) - \Delta S \end{bmatrix}$$

$n \leftarrow n + 1$

$qi \leftarrow fp(P_{k+1})$ if $P_{k+1} > dy$

$qi \leftarrow fe(P_{k+1})$ if $P_{k+1} \leq dy$

if $|qi - \lambda_{k+1} \cdot qe| < \rho$

$t \leftarrow 2$

$Pc \leftarrow P_{k+1}$

$\lambda c \leftarrow \lambda_{k+1}$

$Nc \leftarrow n$

break if $t = 2$

break if $n \geq 10$

$k \leftarrow k + 1$

$z \leftarrow z + 1$

$Pconv_z \leftarrow Pc$

$\lambda conv_z \leftarrow \lambda c$

$Nconv_z \leftarrow Nc$

$Fconv_z \leftarrow qe \cdot \lambda conv_z$

$Inc_z \leftarrow z$

$$
\left|\begin{array}{l}
\left|\begin{array}{l} t \leftarrow 1 \\ n \leftarrow 0 \\ \text{break if } Pc \geq 1.0 \end{array}\right| \\
\begin{pmatrix} Pconv \\ \lambda conv \\ Nconv \\ Inc \\ Fconv \end{pmatrix}
\end{array}\right|
$$

SA := Stiff_Arc_Length

Displacement Values

$SA_0 =$

	0
0	0.0000000
1	$4.9856350 \cdot 10^{-5}$
2	$9.9712701 \cdot 10^{-5}$
3	$1.4956905 \cdot 10^{-4}$
4	$1.9942540 \cdot 10^{-4}$
5	$2.4928175 \cdot 10^{-4}$
6	$2.9913810 \cdot 10^{-4}$
7	$3.4899445 \cdot 10^{-4}$
8	$3.9885080 \cdot 10^{-4}$
9	$4.4870715 \cdot 10^{-4}$
10	$4.9856350 \cdot 10^{-4}$
11	$5.4841985 \cdot 10^{-4}$
12	$5.9827620 \cdot 10^{-4}$
13	$6.4813255 \cdot 10^{-4}$

Load Values

$SA_4 =$

	0
0	0
1	49.8563503
2	99.7127006
3	149.5690509
4	199.4254012
5	249.2817515
6	299.1381018
7	348.9944521
8	398.8508024
9	448.7071526
10	498.5635029
11	548.4198532
12	598.2762035
13	648.1325538

Number of Iterations

$SA_2 =$

	0
0	0
1	1
2	1
3	1
4	1
5	1
6	1
7	1
8	1
9	1
10	1
11	1
12	1
13	1

$SAN := SA_2$

$SAI := SA_3$

$SAy := SA_4$

$SAx := SA_0$

APPENDIX B:
SPHERICAL ARC LENGTH 1 DOF MATHCAD CODE

Parameters

$Ee := 10^7$ $Epo := 2 \times 10^5$ $Ep1 := 1.1 \cdot Epo$ $Sy := 10^5$ $A := 1$ $L := 10$ $dmax := .5$ $dy := \frac{Sy \cdot L}{Ee}$ $fy := \frac{Ee \cdot A \cdot dy}{L}$

$dy = 0.1$ $fy = 1 \times 10^5$

Solve for α

Guess Value $\alpha := 1$

Given

$$0 = \frac{Epo \cdot A}{L} - \left[\frac{2}{\pi} \cdot \frac{Ep1 \cdot Ao}{L} \cdot \left[\frac{\alpha}{L} \cdot (dmax - dy)\right] \cdot \operatorname{atan}\left[\frac{\alpha}{L} \cdot (dmax - dy)\right]\right]$$

$\alpha := \text{Find}(\alpha)$

$\alpha = 36.699$

$$\kappa := \frac{\alpha}{L}$$

Governing Equations

$$fe(x) := \frac{Ee \cdot Ao}{L} \cdot x \qquad ge(x) := \frac{d}{dx} fe(x)$$

$$fp1(x) := \left[\frac{Epo \cdot Ao}{L} \cdot (x - dy)\right]$$

$$fp2(x) := -\left[\frac{2}{\pi}\cdot\frac{Ep1\cdot Ao}{L}\cdot\frac{1}{\kappa}\cdot\left[\left[\frac{1}{2}\cdot\lfloor\kappa\cdot(x-dy)\rfloor^2\cdot\operatorname{atan}\lfloor\kappa\cdot(x-dy)\rfloor\right]-\frac{1}{2}\cdot\lfloor\kappa\cdot(x-dy)\rfloor+\frac{1}{2}\cdot\operatorname{atan}\lfloor\kappa\cdot(x-dy)\rfloor\right]\right]+fy$$

$$fp(x) := fp1(x) + fp2(x) \qquad gp(x) := \frac{Epo\cdot Ao}{L}-\left[\frac{2}{\pi}\cdot\frac{Ep1\cdot Ao}{L}\cdot\lfloor\kappa\cdot(x-dy)\rfloor\cdot\operatorname{atan}\lfloor\kappa\cdot(x-dy)\rfloor\right]$$

$$qe := fp(dmax) \qquad qe = 1.049\times 10^5$$

Spherical_Arc_Length :=

$t \leftarrow 1$

$\Delta l \leftarrow \sqrt{.001}$

$Pc \leftarrow 0$

$\psi \leftarrow 0.00001$

$\lambda c \leftarrow 0$

$n \leftarrow 0$

$k \leftarrow 0$

$P_0 \leftarrow 0$

$\lambda_0 \leftarrow 0$

$z \leftarrow 0$

for $m \in 0..10000$

  while $t = 1$

    if $P_k > dy$

      if $n = 0$

        $\Delta\lambda_{k+1} \leftarrow 1\cdot\dfrac{\Delta l}{(gp(Pc))^{-1}\cdot qe}$

$\Delta P_{k+1} \leftarrow \Delta\lambda_{k+1} \cdot \left(gp(Pc)^{-1}\right) \cdot qe$

$n \leftarrow n + 1$

$P_{k+1} \leftarrow \Delta P_{k+1} + Pc$

$\lambda_{k+1} \leftarrow \Delta\lambda_{k+1} + \lambda c$

$k \leftarrow k + 1$

$\delta pe \leftarrow gp(Pc)^{-1} \cdot qe$

$a1 \leftarrow (\delta pe)^2 + \psi^2 (qe)^2$

$\delta p \leftarrow -1 \cdot gp(Pc)^{-1} \cdot \left(fp(P_k) - qe\,\lambda_k\right)$

$a2 \leftarrow \left[2 \cdot \delta pe \cdot \left[(\Delta P_k) + \delta p\right]\right] + \left[2 \cdot (\Delta\lambda_k) \cdot \psi^2 (qe)^2\right]$

$a3 \leftarrow \left[(\Delta P_k) + \delta p\right]^2 - \Delta l^2 + \left|(\Delta\lambda_k)^2 \cdot \psi^2 \cdot (qe)^2\right|$

$\delta\lambda \leftarrow polyroots\begin{pmatrix} a3 \\ a2 \\ a1 \end{pmatrix}$

$a4 \leftarrow (\Delta P_k) \cdot \delta p + (\Delta P_k)^2$

$a5 \leftarrow (\Delta P_k) \cdot (\delta pe)$

$cos1 \leftarrow a4 + (a5 \cdot \delta\lambda_0)$

$cos2 \leftarrow a4 + (a5 \cdot \delta\lambda_1)$

$root1 \leftarrow \delta\lambda_0$

$root2 \leftarrow \delta\lambda_1$

if $Im(\delta\lambda_0) = 0 \wedge Im(\delta\lambda_1) = 0$

$\delta\lambda\lambda \leftarrow \delta\lambda_0$

$\delta\lambda\lambda \leftarrow \delta\lambda_1$ if $\cos 2 \geq \cos 1$

$\Delta P_{k+1} \leftarrow \Delta P_k + [\delta p + (\delta\lambda\lambda \cdot \delta pe)]$

$\Delta\lambda_{k+1} \leftarrow \Delta\lambda_k + \delta\lambda\lambda$

$P_{k+1} \leftarrow \Delta P_{k+1} + Pc$

$\lambda_{k+1} \leftarrow \Delta\lambda_{k+1} + \lambda c$

break if $\mathrm{Im}(\delta\lambda_0) \neq 0 \vee \mathrm{Im}(\delta\lambda_1) \neq 0$

if $P_k \leq dy$

if $n = 0$

$$\Delta\lambda_{k+1} \leftarrow 1 \cdot \frac{\Delta l}{(ge(Pc))^{-1} \cdot qe}$$

$\Delta P_{k+1} \leftarrow \Delta\lambda_{k+1} \cdot \left(ge(Pc)^{-1}\right) \cdot qe$

$n \leftarrow n + 1$

$P_{k+1} \leftarrow \Delta P_{k+1} + Pc$

$\lambda_{k+1} \leftarrow \Delta\lambda_{k+1} + \lambda c$

$k \leftarrow k + 1$

$\delta pe \leftarrow ge(Pc)^{-1} \cdot qe$

$a1 \leftarrow (\delta pe)^2 + \psi^2 (qe)^2$

$\delta p \leftarrow -1 \cdot ge(Pc)^{-1} \cdot (fe(P_k) - qe\,\lambda_k)$

$a2 \leftarrow [2 \cdot \delta pe \cdot [(\Delta P_k) + \delta p]] + [2 \cdot (\Delta\lambda_k) \cdot \psi^2 (qe)^2]$

$$a3 \leftarrow \left[\left(\Delta P_k\right) + \delta p\right]^2 - \Delta l^2 + \left[\left(\Delta\lambda_k\right)^2 \cdot \psi^2 \cdot \left(qe\right)^2\right]$$

$$\delta\lambda \leftarrow \text{polyroots}\begin{pmatrix} a3 \\ a2 \\ a1 \end{pmatrix}$$

$$a4 \leftarrow \left(\Delta P_k\right) \cdot \delta p + \left(\Delta P_k\right)^2$$

$$a5 \leftarrow \left(\Delta P_k\right) \cdot \left(\delta pe\right)$$

$$cos1 \leftarrow a4 + \left(a5 \cdot \delta\lambda_0\right)$$

$$cos2 \leftarrow a4 + \left(a5 \cdot \delta\lambda_1\right)$$

$$\delta\lambda\lambda \leftarrow \delta\lambda_0$$

$$\delta\lambda\lambda \leftarrow \delta\lambda_1 \quad \text{if} \quad cos2 > cos1$$

$$\Delta P_{k+1} \leftarrow \Delta P_k + \left[\delta p + \left(\delta\lambda\lambda \cdot \delta pe\right)\right]$$

$$\Delta\lambda_{k+1} \leftarrow \Delta\lambda_k + \delta\lambda\lambda$$

$$P_{k+1} \leftarrow \Delta P_{k+1} + Pc$$

$$\lambda_{k+1} \leftarrow \Delta\lambda_{k+1} + \lambda c$$

$$root1 \leftarrow \delta\lambda_0$$

$$root2 \leftarrow \delta\lambda_1$$

break if $\text{Im}\left(\delta\lambda_0\right) \neq 0 \vee \text{Im}\left(\delta\lambda_1\right) \neq 0$

$$qi \leftarrow fp\left(P_{k+1}\right) \quad \text{if} \quad P_{k+1} > dy$$

$$qi \leftarrow fe\left(P_{k+1}\right) \quad \text{if} \quad P_{k+1} \leq dy$$

$$n \leftarrow n + 1$$

if $\left|qi - \lambda_{k+1} \cdot qe\right| \leq \rho$

$$t \leftarrow 2$$

$Pc \leftarrow P_{k+1}$

$\lambda c \leftarrow \lambda_{k+1}$

$Nc \leftarrow n$

$k \leftarrow k + 1$

break if $t = 2$

break if $n \geq 10$

break if $\mathrm{Im}(\delta\lambda_0) \neq 0 \vee \mathrm{Im}(\delta\lambda_1) \neq 0$

$z \leftarrow z + 1$

$Pconv_z \leftarrow Pc$

$\lambda conv_z \leftarrow \lambda c$

$Nconv_z \leftarrow Nc$

$Fconv_z \leftarrow qe \cdot \lambda conv_z$

$Inc_z \leftarrow z$

$t \leftarrow 1$

$n \leftarrow 0$

break if $Pc \geq 1.0$

$$\begin{pmatrix} Pconv \\ \lambda conv \\ Nconv \\ Fconv \\ Inc \\ root1 \\ root2 \end{pmatrix}$$

CSA := Spherical_Arc_Length

Displacement Values

$CSA_0 =$

	0
0	$0.000000000000000 \cdot 10^{0}$
1	$3.146583877637780 \cdot 10^{-3}$
2	$6.293167755275480 \cdot 10^{-3}$
3	$9.439751632913200 \cdot 10^{-3}$
4	$1.258633551055100 \cdot 10^{-2}$
5	$1.573291938818870 \cdot 10^{-2}$
6	$1.887950326582640 \cdot 10^{-2}$
7	$2.202608714346410 \cdot 10^{-2}$
8	$2.517267102110190 \cdot 10^{-2}$
9	$2.831925489873960 \cdot 10^{-2}$
10	$3.146583877637730 \cdot 10^{-2}$
11	$3.461242265401500 \cdot 10^{-2}$
12	$3.775900653165280 \cdot 10^{-2}$
13	$4.090559040929060 \cdot 10^{-2}$
14	$4.405217428692830 \cdot 10^{-2}$
15	$4.719875816456600 \cdot 10^{-2}$

Load Values

$CSA_3 =$

	0
0	0
1	$3.1466 \cdot 10^{3}$
2	$6.2932 \cdot 10^{3}$
3	$9.4398 \cdot 10^{3}$
4	$1.2586 \cdot 10^{4}$
5	$1.5733 \cdot 10^{4}$
6	$1.888 \cdot 10^{4}$
7	$2.2026 \cdot 10^{4}$
8	$2.5173 \cdot 10^{4}$
9	$2.8319 \cdot 10^{4}$
10	$3.1466 \cdot 10^{4}$
11	$3.4612 \cdot 10^{4}$
12	$3.7759 \cdot 10^{4}$
13	$4.0906 \cdot 10^{4}$
14	$4.4052 \cdot 10^{4}$
15	$4.7199 \cdot 10^{4}$

Number of Iterations

$CSA_2 =$

	0
0	0
1	2
2	2
3	2
4	2
5	2
6	2
7	2
8	2
9	2
10	2
11	2
12	2
13	2
14	2
15	2

$CSAN := CSA_2$

$CSAI := CSA_4$

$CSAy := CSA_3$

$CSAx := CSA_0$

APPENDIX C:
STIFF ARC LENGTH 3 DOF MATHCAD CODE

Parameters

$Ee := 10^7$ $\quad sy := 10^5$ $\quad fy := \frac{sy}{A}$

$Epo := 5 \times 10^5$ $\quad \varepsilon y := \frac{sy}{Ee}$ $\quad \varepsilon max := .025$

$Ep1 := 1.25 \cdot Epo$ $\quad A := 1$ $\quad \rho := 10^{-8}$

Geometry

$La := 5$ $\quad Le := 10$ $\quad x20 := La$

$Lb := 4.5$ $\quad h := \left(Le^2 - La^2\right)^{.5}$ $\quad y30 := Lb$

$Lc := \left(La^2 + Lb^2\right)^{.5}$ $\quad Ld := h - Lb$ $\quad y40 := h$

$Lc = 6.726812024$

$h = 8.660254038$

$Ld = 4.160254038$

Solve for α:

Guess Value

$\alpha := 10$

Given

$$0 = A \cdot \left[Epo - \frac{2}{\pi} \cdot Ep1 \cdot \operatorname{atan}\left[\alpha \cdot (\varepsilon max - \varepsilon y)\right] \right]$$

$\alpha := \text{Find}(\alpha)$ $\quad \alpha = 205.178902478$

Governing Equations

$$\text{ea}(d2x) := \frac{d2x}{La} \qquad \text{ec}(d2x, d3y) := \frac{x20 \cdot d2x + y30 \cdot d3y}{Lc^2} \qquad \text{ee}(d2x, d4y) := \frac{x20 \cdot d2x + y40 \cdot d4y}{Le^2}$$

$$\text{eb}(d3y) := \frac{d3y}{Lb} \qquad \text{ed}(d3y, d4y) := \frac{d4y - d3y}{Ld}$$

$$kelastic := A \cdot Ee$$

$$kplastic(\varepsilon) := A \cdot \left[Epo - \frac{2}{\pi} \cdot Ep1 \cdot \text{atan}[\alpha \cdot (\varepsilon - \text{ey})] \right]$$

$$K(ka, kb, kc, kd, ke) := \begin{pmatrix} ka & 0 & 0 & 0 & 0 \\ 0 & kb & 0 & 0 & 0 \\ 0 & 0 & kc & 0 & 0 \\ 0 & 0 & 0 & kd & 0 \\ 0 & 0 & 0 & 0 & ke \end{pmatrix} \qquad G := \begin{pmatrix} \frac{1}{La} & 0 & 0 \\ 0 & \frac{1}{Lb} & 0 \\ \frac{La}{Lc^2} & \frac{Lb}{Lc^2} & 0 \\ 0 & \frac{-1}{Ld} & \frac{1}{Ld} \\ \frac{La}{Le^2} & 0 & \frac{Lb + Ld}{Le^2} \end{pmatrix} \qquad \Lambda := \begin{pmatrix} La & 0 & 0 & 0 & 0 \\ 0 & Lb & 0 & 0 & 0 \\ 0 & 0 & Lc & 0 & 0 \\ 0 & 0 & 0 & Ld & 0 \\ 0 & 0 & 0 & 0 & Le \end{pmatrix} \qquad \Lambda sqrt := \begin{pmatrix} \sqrt{La} & 0 & 0 & 0 & 0 \\ 0 & \sqrt{Lb} & 0 & 0 & 0 \\ 0 & 0 & \sqrt{Lc} & 0 & 0 \\ 0 & 0 & 0 & \sqrt{Ld} & 0 \\ 0 & 0 & 0 & 0 & \sqrt{Le} \end{pmatrix}$$

$$J(ka, kb, kc, kd, ke) := G^T \cdot \Lambda sqrt \cdot K(ka, kb, kc, kd, ke) \cdot \Lambda sqrt \cdot G$$

$$Deti := \left| J(kelastic, kelastic, kelastic, kelastic, kelastic) \right|$$

$$Jinitial := J(kelastic, kelastic, kelastic, kelastic, kelastic)$$

$$felastic(\varepsilon) := A \cdot Ee \cdot \varepsilon$$

$$fplastic(\varepsilon) := A \cdot \left[Ee \cdot \varepsilon y + Epo \cdot (\varepsilon - \varepsilon y) - \frac{2}{\pi \cdot \alpha} \cdot Ep1 \left[\alpha \cdot (\varepsilon - \varepsilon y) \cdot \operatorname{atan}\left[\alpha \cdot (\varepsilon - \varepsilon y)\right] - \frac{1}{2} \cdot \ln\left[1 + \left[\alpha \cdot (\varepsilon - \varepsilon y)\right]^2\right] \right] \right]$$

Internal Force and Stiffness Algorithm

force_and_stiffness(d2, d3, d4) :=

- εa ← εa(d2)
- εb ← εb(d3)
- εc ← εc(d2, d3)
- εd ← εd(d3, d4)
- εe ← εe(d2, d4)
- ka ← kelastic
- fa ← felastic(εa)
- if εa > εy
  - ka ← kplastic(εa)
  - fa ← fplastic(εa)
- kb ← kelastic
- fb ← felastic(εb)
- if εb > εy
  - kb ← kplastic(εb)
  - fb ← fplastic(εb)
- kc ← kelastic
- fc ← felastic(εc)
- if εc > εy
  - kc ← kplastic(εc)
  - fc ← fplastic(εc)
- kd ← kelastic

```
fd ← felastic(εd)
if εd > εy
    kd ← kplastic(εd)
    fd ← fplastic(εd)
ke ← kelastic
fe ← felastic(εe)
if εe > εy
    ke ← kplastic(εe)
    fe ← fplastic(εe)
(fa
 fb
 fc
 fd
 fe
 ka
 kb
 kc
 kd
 ke)
```

Gram Schmidt Algorithm

$$\text{gram\_schmidt}(\text{Jacobian}, q2, q3, q4) := \left| \text{row1} \leftarrow \begin{pmatrix} \text{Jacobian}_{0,0} \\ \text{Jacobian}_{0,1} \\ \text{Jacobian}_{0,2} \end{pmatrix} \right.$$

$$
\begin{aligned}
&\alpha 1_{\iota} \leftarrow \frac{row1}{\sqrt{row1^{T} \cdot row1}} \\
&row2 \leftarrow \begin{pmatrix} Jacobian_{1,0} \\ Jacobian_{1,1} \\ Jacobian_{1,2} \end{pmatrix} \\
&\alpha 2_{tt} \leftarrow row2 - \left(row2^{T} \cdot \alpha 1_{\iota}\right) \cdot \alpha 1_{\iota} \\
&\alpha 2_{\iota} \leftarrow \frac{\alpha 2_{tt}}{\sqrt{\alpha 2_{tt}{}^{T} \cdot \alpha 2_{tt}}} \\
&g_{\iota} \leftarrow \begin{pmatrix} q2 \\ q3 \\ q4 \end{pmatrix} - \left(\left(\begin{pmatrix} q2 \\ q3 \\ q4 \end{pmatrix}^{T} \alpha 1_{\iota}\right) \cdot \alpha 1_{\iota} - \left(\left(\begin{pmatrix} q2 \\ q3 \\ q4 \end{pmatrix}^{T} \alpha 2_{\iota}\right) \cdot \alpha 2_{\iota}\right.\right. \\
&Answer \leftarrow \frac{g_{\iota}}{\sqrt{g_{\iota}{}^{T} \cdot g_{\iota}}} \\
&Answer
\end{aligned}
$$

Stiff Arc Length Method

$$
\begin{aligned}
&Stiff\_Arc\_Length(q2, q3, q4, num, s) := \\
&\quad t \leftarrow 1 \\
&\quad z \leftarrow 0 \\
&\quad k \leftarrow 0 \\
&\quad n \leftarrow 0 \\
&\quad \gamma \leftarrow 1 \\
&\quad \Delta S \leftarrow s \\
&\quad zo \leftarrow 1
\end{aligned}
$$

$$Pc_0 \leftarrow \begin{pmatrix} 0 \\ 0 \\ 0 \end{pmatrix}$$

$$P_0 \leftarrow \begin{pmatrix} 0 \\ 0 \\ 0 \end{pmatrix}$$

$$\lambda conv_0 \leftarrow 0$$

$$\lambda_0 \leftarrow 0$$

$$Jac \leftarrow Jinitial$$

$$qe \leftarrow \begin{pmatrix} q2 \\ q3 \\ q4 \end{pmatrix}$$

$$\omega \leftarrow \begin{pmatrix} 0 \\ 0 \\ 0 \end{pmatrix}$$

$$zt \leftarrow gram\_schmidt(Jinitial, q2, q3, q4)$$

$$ztt \leftarrow (zt)^T$$

$$Det_0 \leftarrow Deti$$

$$Dconv_0 \leftarrow Deti$$

$$P2_0 \leftarrow 0$$

$$P3_0 \leftarrow 0$$

$$P4_0 \leftarrow 0$$

for $m \in 0..num$

  while $t = 1$

$$\begin{pmatrix} P2_{k+1} \\ P3_{k+1} \\ P4_{k+1} \\ \lambda_{k+1} \end{pmatrix} \leftarrow \begin{pmatrix} P2_k \\ P3_k \\ P4_k \\ \lambda_k \end{pmatrix} - \begin{pmatrix} Jac_{0,0} & Jac_{0,1} & Jac_{0,2} & -1 \cdot qe_0 \\ Jac_{1,0} & Jac_{1,1} & Jac_{1,2} & -1 \cdot qe_1 \\ Jac_{2,0} & Jac_{2,1} & Jac_{2,2} & -1 \cdot qe_2 \\ ztt_{0,0} & ztt_{0,1} & ztt_{0,2} & \gamma \cdot zo \end{pmatrix}^{-1} \cdot \begin{bmatrix} \omega_0 - qe_0 \cdot \lambda_k \\ \omega_1 - qe_1 \cdot \lambda_k \\ \omega_2 - qe_2 \cdot \lambda_k \\ zt^T \cdot (P_k - Pc_z) + zo \cdot \gamma \cdot (\lambda_k - \lambda conv_z) - \Delta S \end{bmatrix}$$

if $\gamma = 1$

$KP \leftarrow force\_and\_stiffness(P2_{k+1}, P3_{k+1}, P4_{k+1})$

$JP \leftarrow J(KP_5, KP_6, KP_7, KP_8, KP_9)$

$DP \leftarrow |JP|$

if $DP \le 0$

$\gamma \leftarrow -1$

$$X \leftarrow \begin{bmatrix} \omega_0 - qe_0 \cdot \lambda_k \\ \omega_1 - qe_1 \cdot \lambda_k \\ \omega_2 - qe_2 \cdot \lambda_k \\ zt^T \cdot (P_k - Pc_z) + zo \cdot \gamma \cdot (\lambda_k - 1.11\,\lambda conv_z) - \Delta S \end{bmatrix}$$

$$\begin{pmatrix} P2_{k+1} \\ P3_{k+1} \\ P4_{k+1} \\ \lambda_{k+1} \end{pmatrix} \leftarrow \begin{pmatrix} P2_k \\ P3_k \\ P4_k \\ \lambda_k \end{pmatrix} - \begin{pmatrix} Jac_{0,0} & Jac_{0,1} & Jac_{0,2} & -1 \cdot qe_0 \\ Jac_{1,0} & Jac_{1,1} & Jac_{1,2} & -1 \cdot qe_1 \\ Jac_{2,0} & Jac_{2,1} & Jac_{2,2} & -1 \cdot qe_2 \\ ztt_{0,0} & ztt_{0,1} & ztt_{0,2} & \gamma \cdot zo \end{pmatrix}^{-1} \cdot X$$

$$P_{k+1} \leftarrow \begin{pmatrix} P2_{k+1} \\ P3_{k+1} \end{pmatrix}$$

$$\begin{pmatrix} P4_{k+1} \end{pmatrix}$$

$n \leftarrow n + 1$

$SF \leftarrow \text{force\_and\_stiffness}\left(P2_{k+1}, P3_{k+1}, P4_{k+1}\right)$

$Jac \leftarrow J\left(SF_5, SF_6, SF_7, SF_8, SF_9\right)$

$Det_{k+1} \leftarrow |Jac|$

$zt \leftarrow \text{gram\_schmidt}(Jac, q2, q3, q4)$

$ztt \leftarrow (zt)^T$

$$\omega \leftarrow (G)^T \cdot \Lambda \cdot \begin{pmatrix} SF_0 \\ SF_1 \\ SF_2 \\ SF_3 \\ SF_4 \end{pmatrix}$$

if $\left(\left|\omega_0 - qe_0 \cdot \lambda_{k+1}\right| \leq \rho\right) \wedge \left(\left|\omega_1 - qe_1 \cdot \lambda_{k+1}\right| \leq \rho\right) \wedge \left(\left|\omega_2 - qe_2 \cdot \lambda_{k+1}\right| \leq \rho\right)$

- $t \leftarrow 2$
- $Pconv \leftarrow P_{k+1}$
- $\lambda c \leftarrow \lambda_{k+1}$
- $Nc \leftarrow n$
- $res2 \leftarrow \left|\omega_0 - qe_0 \cdot \lambda_{k+1}\right|$
- $res3 \leftarrow \left|\omega_1 - qe_1 \cdot \lambda_{k+1}\right|$
- $res4 \leftarrow \left|\omega_2 - qe_2 \cdot \lambda_{k+1}\right|$
- $Detc \leftarrow Det_{k+1}$

$LPv \leftarrow zt^{T} \cdot \left(P_{k+1} - Pc_{z}\right)$

$RPv \leftarrow zo \cdot \gamma \cdot \left(\lambda_{k+1} - \lambda conv_{z}\right)$

$Iter_{k} \leftarrow k$

$k \leftarrow k + 1$

break if $t = 2$

break if $n > 20$

$z \leftarrow z + 1$

$P2conv_{z} \leftarrow Pconv_{0}$

$P3conv_{z} \leftarrow Pconv_{1}$

$P4conv_{z} \leftarrow Pconv_{2}$

$RP_{z} \leftarrow RPv$

$LP_{z} \leftarrow LPv$

$$Pc_{z} \leftarrow \begin{pmatrix} Pconv_{0} \\ Pconv_{1} \\ Pconv_{2} \end{pmatrix}$$

$\lambda conv_{z} \leftarrow \lambda c$

$Nconv_{z} \leftarrow Nc$

$F2conv_{z} \leftarrow qe_{0} \cdot \lambda conv_{z}$

$F3conv_{z} \leftarrow qe_{1} \cdot \lambda conv_{z}$

$F4conv_{z} \leftarrow qe_{2} \cdot \lambda conv_{z}$

$Res2_{z} \leftarrow res2$

$Res3_z \leftarrow res3$

$Res4_z \leftarrow res4$

$Dconv_z \leftarrow Detc$

$Inc_z \leftarrow z$

$t \leftarrow 1$

break if $n \geq 20$

$n \leftarrow 0$

break if $z \geq 500000$

break if $P4conv_z \geq .4$

$$\begin{pmatrix} P2conv \\ P3conv \\ P4conv \\ F2conv \\ F3conv \\ F4conv \\ Nconv \\ Inc \\ Iter \\ \lambda conv \\ Res2 \\ Res3 \\ Res4 \\ Dconv \\ RP \\ LP \\ P2 \end{pmatrix}$$

$$\begin{pmatrix} P3 \\ P4 \\ \lambda \end{pmatrix}$$

$ans := Stiff\_Arc\_Length(2.294283 \times 10^5, 6.848022 \times 10^4, 1.908459 \cdot 10^5, 16000, .01)$

$d2 := ans_0 \quad d3 := ans_1 \quad d4 := ans_2 \quad f2 := ans_3 \quad f3 := ans_4 \quad f4 := ans_5$

$N := ans_6 \quad Inc := ans_7 \quad Iter := ans_8 \quad \lambda c := ans_9 \quad Res2 := ans_{10}$

$Res3 := ans_{11} \quad Res4 := ans_{12} \quad Detc := ans_{13} \quad RP := ans_{14} \quad LP := ans_{15}$

$P2 := ans_{16} \quad P3 := ans_{17} \quad P4 := ans_{18} \quad \lambda := ans_{19}$

$F2 := 2.294283 \times 10^5 \cdot \lambda \quad F3 := 6.848022 \times 10^4 \cdot \lambda \quad F4 := 1.908459 \cdot 10^5 \cdot \lambda$

Model Equation Max Forces:

$\max(f2m) = 2.29428200 \times 10^5$

$\max(f3m) = 6.84802130 \times 10^4$

$\max(f4m) = 1.90845862 \times 10^5$

Critical Point Percent Difference Error:

$$\frac{2.294283 \cdot 10^5 - \max(f2)}{2.294283 \cdot 10^5} \cdot 100 = 0.034$$

$$\frac{6.848022 \times 10^4 - \max(f3)}{6.848022 \times 10^4} \cdot 100 = 0.034$$

$$\frac{1.908459 \cdot 10^5 - \max(f4)}{1.908459 \cdot 10^5} \cdot 100 = 0.034$$

APPENDIX D:
SPHERICAL ARC LENGTH 3 DOF MATHCAD CODE

Parameters

$Ee := 10^7$ $\quad sy := 10^5$ $\quad fy := \frac{sy}{A}$

$Epo := 5 \times 10^5$ $\quad \varepsilon y := \frac{sy}{Ee}$ $\quad \varepsilon max := .025$

$Ep1 := 1.25 \cdot Epo$ $\quad A := 1$ $\quad \rho := 10^{-8}$

Geometry

$La := 5$ $\quad Le := 10$ $\quad x20 := La$

$Lb := 4.5$ $\quad h := \left(Le^2 - La^2\right)^{.5}$ $\quad y30 := Lb$

$Lc := \left(La^2 + Lb^2\right)^{.5}$ $\quad Ld := h - Lb$ $\quad y40 := h$

$Lc = 6.726812024$

$h = 8.660254038$

$Ld = 4.160254038$

Solve for α:

Guess Value

$\alpha := 10$

Given

$$0 = A \cdot \left[Epo - \frac{2}{\pi} \cdot Ep1 \cdot \operatorname{atan}\left[\alpha \cdot (\varepsilon max - \varepsilon y)\right] \right]$$

$\alpha := \text{Find}(\alpha)$ $\quad \alpha = 205.178902478$

Governing Equations

$$\text{ea}(d2x) := \frac{d2x}{La} \qquad \text{ec}(d2x, d3y) := \frac{x20 \cdot d2x + y30 \cdot d3y}{Lc^2} \qquad \text{ee}(d2x, d4y) := \frac{x20 \cdot d2x + y40 \cdot d4y}{Le^2}$$

$$\text{eb}(d3y) := \frac{d3y}{Lb} \qquad \text{ed}(d3y, d4y) := \frac{d4y - d3y}{Ld}$$

$$kelastic := A \cdot Ee$$

$$kplastic(\varepsilon) := A \cdot \left[Epo - \frac{2}{\pi} \cdot Ep1 \cdot \text{atan}[\alpha \cdot (\varepsilon - \text{ey})] \right]$$

$$K(ka, kb, kc, kd, ke) := \begin{pmatrix} ka & 0 & 0 & 0 & 0 \\ 0 & kb & 0 & 0 & 0 \\ 0 & 0 & kc & 0 & 0 \\ 0 & 0 & 0 & kd & 0 \\ 0 & 0 & 0 & 0 & ke \end{pmatrix} \qquad G := \begin{pmatrix} \frac{1}{La} & 0 & 0 \\ 0 & \frac{1}{Lb} & 0 \\ \frac{La}{Lc^2} & \frac{Lb}{Lc^2} & 0 \\ 0 & \frac{-1}{Ld} & \frac{1}{Ld} \\ \frac{La}{Le^2} & 0 & \frac{Lb + Ld}{Le^2} \end{pmatrix}$$

$$\Lambda := \begin{pmatrix} La & 0 & 0 & 0 & 0 \\ 0 & Lb & 0 & 0 & 0 \\ 0 & 0 & Lc & 0 & 0 \\ 0 & 0 & 0 & Ld & 0 \\ 0 & 0 & 0 & 0 & Le \end{pmatrix} \qquad \Lambda sqrt := \begin{pmatrix} \sqrt{La} & 0 & 0 & 0 & 0 \\ 0 & \sqrt{Lb} & 0 & 0 & 0 \\ 0 & 0 & \sqrt{Lc} & 0 & 0 \\ 0 & 0 & 0 & \sqrt{Ld} & 0 \\ 0 & 0 & 0 & 0 & \sqrt{Le} \end{pmatrix}$$

$$J(ka, kb, kc, kd, ke) := G^T \cdot \Lambda sqrt \cdot K(ka, kb, kc, kd, ke) \cdot \Lambda sqrt \cdot G$$

$$Deti := \left| J(kelastic, kelastic, kelastic, kelastic, kelastic) \right|$$

$$Jinitial := J(kelastic, kelastic, kelastic, kelastic, kelastic)$$

$$felastic(\varepsilon) := A \cdot Ee \cdot \varepsilon$$

$$fplastic(\varepsilon) := A \cdot \left[Ee \cdot \varepsilon y + Epo \cdot (\varepsilon - \varepsilon y) - \frac{2}{\pi \cdot \alpha} \cdot Ep1 \left[\alpha \cdot (\varepsilon - \varepsilon y) \cdot \operatorname{atan}\left[\alpha \cdot (\varepsilon - \varepsilon y)\right] - \frac{1}{2} \cdot \ln\left[1 + \left[\alpha \cdot (\varepsilon - \varepsilon y)\right]^2\right] \right] \right]$$

Internal Force and Stiffness Algorithm

force_and_stiffness(d2, d3, d4) :=

- εa ← εa(d2)
- εb ← εb(d3)
- εc ← εc(d2, d3)
- εd ← εd(d3, d4)
- εe ← εe(d2, d4)
- ka ← kelastic
- fa ← felastic(εa)
- if εa > εy
  - ka ← kplastic(εa)
  - fa ← fplastic(εa)
- kb ← kelastic
- fb ← felastic(εb)
- if εb > εy
  - kb ← kplastic(εb)
  - fb ← fplastic(εb)
- kc ← kelastic
- fc ← felastic(εc)
- if εc > εy
  - kc ← kplastic(εc)
  - fc ← fplastic(εc)
- kd ← kelastic

```
    fd ← fplastic(εd)
ke ← kelastic
fe ← felastic(εe)
if  εe > εy
    ke ← kplastic(εe)
    fe ← fplastic(εe)
(fa
 fb
 fc
 fd
 fe
 ka
 kb
 kc
 kd
 ke)
```

Spherical Arc Length Method

```
SA(q2, q3, q4, num, ψ, Δl) := t ← 1
                              Δl ← √Δl
                              ψ ← ψ
                              z ← 0
                              k ← 0
```

$n \leftarrow 0$

$\gamma \leftarrow 1$

$P_0 \leftarrow \begin{pmatrix} 0 \\ 0 \\ 0 \end{pmatrix}$

$Pconv \leftarrow \begin{pmatrix} 0 \\ 0 \\ 0 \end{pmatrix}$

$\lambda_0 \leftarrow 0$

$\lambda c \leftarrow 0$

$Jac \leftarrow Jinitial$

$qe \leftarrow \begin{pmatrix} q2 \\ q3 \\ q4 \end{pmatrix}$

$\omega \leftarrow \begin{pmatrix} 0 \\ 0 \\ 0 \end{pmatrix}$

$Det_0 \leftarrow Deti$

$Dconv_0 \leftarrow Deti$

$Jacc \leftarrow Jinitial$

$Iter_0 \leftarrow 0$

$P2_0 \leftarrow 0$

$P3_0 \leftarrow 0$

$P4_0 \leftarrow 0$

for $m \in 0..num$

while $t = 1$

if $n = 0$

$$\Delta\lambda_{k+1} \leftarrow \gamma \cdot \frac{\Delta l}{\sqrt{\left[(Jacc)^{-1} \cdot qe\right]^T \cdot \left[(Jacc)^{-1} \cdot qe\right]}}$$

$$\Delta P_{k+1} \leftarrow \Delta\lambda_{k+1} \cdot \left[(Jacc)^{-1} \cdot qe\right]$$

$$P_{k+1} \leftarrow \Delta P_{k+1} + Pconv$$

$$PP \leftarrow P_{k+1}$$

$$P2_{k+1} \leftarrow PP_0$$

$$P3_{k+1} \leftarrow PP_1$$

$$P4_{k+1} \leftarrow PP_2$$

$$\lambda_{k+1} \leftarrow \Delta\lambda_{k+1} + \lambda c$$

$$SF \leftarrow force\_and\_stiffness\left(P2_{k+1}, P3_{k+1}, P4_{k+1}\right)$$

$$Jac \leftarrow J\left(SF_5, SF_6, SF_7, SF_8, SF_9\right)$$

$$\omega \leftarrow (G)^T \cdot \Lambda \cdot \begin{pmatrix} SF_0 \\ SF_1 \\ SF_2 \\ SF_3 \end{pmatrix}$$

$$\left(SF_4\right)$$

$Iter_{k+1} \leftarrow k + 1$

$k \leftarrow k + 1$

$n \leftarrow n + 1$

$\delta pe \leftarrow (Jac)^{-1} \cdot qe$

$a1 \leftarrow \left(\delta pe^{T} \cdot \delta pe\right) + \left(\psi^{2} \cdot qe^{T} \cdot qe\right)$

$\delta p \leftarrow -1 \cdot (Jac)^{-1} \cdot \left(\omega - qe\,\lambda_k\right)$

$a2 \leftarrow \left[2 \cdot \delta pe \cdot \left[\left(\Delta P_k\right) + \delta p\right]\right] + \left(2 \cdot \Delta\lambda_k \cdot \psi^{2} \cdot qe^{T} \cdot qe\right)$

$a3 \leftarrow \left[\left(\Delta P_k\right) + \delta p\right]^{T} \cdot \left[\left(\Delta P_k\right) + \delta p\right] - \Delta I^{2} + \left[\left(\Delta\lambda_k\right)^{2} \cdot \psi^{2} \cdot qe^{T} \cdot qe\right]$

$\delta\lambda \leftarrow \text{polyroots}\left(\begin{pmatrix} a3 \\ a2 \\ a1 \end{pmatrix}\right)$

$a4 \leftarrow \Delta P_k^{T} \cdot \delta p + \Delta P_k^{T} \cdot \Delta P_k$

$a5 \leftarrow \Delta P_k^{T} \cdot \delta pe$

$cos1 \leftarrow a4 + \left(a5 \cdot \delta\lambda_0\right)$

$cos2 \leftarrow a4 + \left(a5 \cdot \delta\lambda_1\right)$

$\delta\lambda\lambda \leftarrow \delta\lambda_0$

$\delta\lambda\lambda \leftarrow \delta\lambda_1 \quad \text{if} \quad cos2 > cos1$

$\Delta P_{k+1} \leftarrow \Delta P_k + \left[\delta p + \left(\delta\lambda\lambda \cdot \delta pe\right)\right]$

$$\Delta\lambda_{k+1} \leftarrow \Delta\lambda_k + \delta\lambda\lambda$$

$$P_{k+1} \leftarrow \Delta P_{k+1} + Pconv$$

$$\lambda_{k+1} \leftarrow \Delta\lambda_{k+1} + \lambda c$$

$$PP \leftarrow P_{k+1}$$

$$P2_{k+1} \leftarrow PP_0$$

$$P3_{k+1} \leftarrow PP_1$$

$$P4_{k+1} \leftarrow PP_2$$

$$n \leftarrow n + 1$$

$$SF \leftarrow force\_and\_stiffness\left(P2_{k+1}, P3_{k+1}, P4_{k+1}\right)$$

$$Jac \leftarrow J\left(SF_5, SF_6, SF_7, SF_8, SF_9\right)$$

$$Det_{k+1} \leftarrow |Jac|$$

$$\gamma \leftarrow -1 \quad \text{if} \quad Det_{k+1} < 0$$

$$\omega \leftarrow (G)^T \cdot \Lambda \cdot \begin{pmatrix} SF_0 \\ SF_1 \\ SF_2 \\ SF_3 \\ SF_4 \end{pmatrix}$$

$$\text{if} \left(\left|\omega_0 - qe_0 \cdot \lambda_{k+1}\right| \le \rho\right) \wedge \left(\left|\omega_1 - qe_1 \cdot \lambda_{k+1}\right| \le \rho\right) \wedge \left(\left|\omega_2 - qe_2 \cdot \lambda_{k+1}\right| \le \rho\right)$$

$$t \leftarrow 2$$

$Pconv \leftarrow PP$

$\lambda c \leftarrow \lambda_{k+1}$

$Nc \leftarrow n$

$res2 \leftarrow \left|\omega_0 - qe_0 \cdot \lambda_{k+1}\right|$

$res3 \leftarrow \left|\omega_1 - qe_1 \cdot \lambda_{k+1}\right|$

$res4 \leftarrow \left|\omega_2 - qe_2 \cdot \lambda_{k+1}\right|$

$Detc \leftarrow Det_{k+1}$

$Jacc \leftarrow Jac$

$Iter_{k+1} \leftarrow k + 1$

$k \leftarrow k + 1$

$nlast \leftarrow n$

break if $t = 2$

break if $n > 20$

$z \leftarrow z + 1$

$P2conv_z \leftarrow Pconv_0$

$P3conv_z \leftarrow Pconv_1$

$P4conv_z \leftarrow Pconv_2$

$\lambda conv_z \leftarrow \lambda c$

$Nconv_z \leftarrow Nc$

$F2conv_z \leftarrow qe_0 \cdot \lambda conv_z$

$F3conv_z \leftarrow qe_1 \cdot \lambda conv_z$

$F4conv_z \leftarrow qe_2 \cdot \lambda conv_z$

$Res2_z \leftarrow res2$

$Res3_z \leftarrow res3$

$Res4_z \leftarrow res4$

$Dconv_z \leftarrow Detc$

$Inc_z \leftarrow z$

$Inclast \leftarrow z$

$t \leftarrow 1$

$n \leftarrow 0$

break if $z \geq 50000$

break if $P4conv_z \geq 1$

$$\begin{pmatrix} P2conv \\ P3conv \\ P4conv \\ F2conv \\ F3conv \\ F4conv \\ Nconv \\ Inc \\ Iter \end{pmatrix}$$

$$\begin{pmatrix} \lambda conv \\ Res2 \\ Res3 \\ Res4 \\ Dconv \\ P2 \\ P3 \\ P4 \\ \lambda \end{pmatrix}$$

$ans := SA(2.294283 \times 10^5, 6.848022 \times 10^4, 1.908459 \cdot 10^5, 1600, .0000001, .01)$

$d2 := ans_0 \quad d3 := ans_1 \quad d4 := ans_2 \quad f2 := ans_3 \quad f3 := ans_4 \quad f4 := ans_5$

$N := ans_6 \quad Inc := ans_7 \quad Iter := ans_8 \quad \lambda c := ans_9 \quad Res2 := ans_{10}$

$Res3 := ans_{11} \quad Res4 := ans_{12} \quad Detc := ans_{13} \quad P2 := ans_{14}$

$P3 := ans_{15} \quad P4 := ans_{16} \quad \lambda := ans_{17} \quad F2 := 2.294283 \times 10^5 \cdot \lambda$

$F3 := 6.848022 \times 10^4 \cdot \lambda \quad F4 := 1.908459 \cdot 10^5 \cdot \lambda$

Critical Point Percent Difference Error:

$$\frac{2.294283 \cdot 10^5 - \max(f2)}{2.294283 \cdot 10^5} \cdot 100 = 0.032$$

Model Equation Max Forces:

$\max(f2m) = 2.29428200 \times 10^5$

$\max(f3m) = 6.84802130 \times 10^4$

$\max(f4m) = 1.90845862 \times 10^5$

$$\frac{6.848022 \times 10^4 - \max(f3)}{6.848022 \times 10^4} \cdot 100 = 0.032$$

$$\frac{1.908459 \cdot 10^5 - \max(f4)}{1.908459 \cdot 10^5} \cdot 100 = 0.032$$

LIST OF REFERENCES

ASM International. Atlas of Stress-Strain Curves. 2nd ed. Materials Park, Ohio: ASM International, 2002.

Batoz, J.L., and Dhatt, G. "Incremental Displacement Algorithm for Nonlinear Problems." International Journal for Numerical Methods in Engineering 14.8 (1979): 1262-1267.

Crisfield, M.A. “A fast incremental/iterative solution procedure that handles snap-through.” Computers and Structures 13 (1981): 55-62.

Crisfield, M.A. Non-linear Finite Element Analysis of Solids and Structures. Chichester, England: John Wiley & Sons, 1991.

Dahlquist, G., and Björck, Å. Numerical Methods. Englewood Cliffs, New Jersey: Prentice-Hall, Inc., 1974.

Geers, M.G.D.-a. "Enhanced Solution Control for Physically and Geometrically Nonlinear Problems. Part I-The Subplane Control Approach." International Journal for Numerical Methods in Engineering 46.2 (1999): 177-204.

Geers, M.G.D.-b. "Enhanced Solution Control for Physically and Geometrically Nonlinear Problems. Part II-Comparative Performance Analysis." International Journal for Numerical Methods in Engineering 46.2 (1999): 205-230.

Logan, Daryl L. A First Course in the Finite Element Method. Toronto, Ontario, Canada: THOMSON, 2007.

MATHCAD ver 15, available at www.PTC.com/MATHCAD, 2011.

Memon, B.A., Su, X. “Arc-length technique for nonlinear finite element analysis.” Journal of Zhejiang University Science 5(2004): 618-628.

Nicholson, David W. “Stiff arc length constraint in nonlinear FEA.” Acta Mechanica 175 (2004): 123-137.

Nicholson, David. W. Finite Element Analysis Thermomechanics of Solids. Boca Raton: CRC Press, 2008.

Posada, Luis M. "Stability Analysis of Two-Dimensional Truss Structures." MS Thesis Universität Stuttgart, 2007.

Ramm, E. “Strategies for Tracing the Nonlinear Response near Limit Points.” Nonlinear Finite Element Analysis in Structural Mechanics ed. by Wunderlich, W., Stein, E. and Bathe, K.J., Springer-Verlag, Berlin, (1981): 63-89.

Ramm, E. “The Riks/Wempner approach – an extension of the displacement control method in non-linear analysis.” Non-linear Computational Mechanics ed. by Hilton, E. et al., Pineridge, Swansea, (1982): 63-86.

Rao, Singiresu S. Applied Numerical Methods for Engineers and Scientists. Upper Saddle River, New Jersey: Prentice Hall, 2002.

Riks, E. “The application of Newton’s method to the problem of elastic stability.” Journal of Applied Mechanics 39 (1972): 1060-1065.

Riks, E. “An incremental approach to the solution of snapping and buckling problems.” International Journal of Solids and Structures 15 (1979): 529-551.

Rowe, G.W., et al. Finite-Element Plasticity and Metalforming Analysis. New York: Cambridge University Press, 1991.

Tummers, B. "DataThief III version 1.6”, available at http://datathief.Org, 2005.

Verhoosel, C.V., Remmers, Joris J.C., and Gutiérrez, M.A. "A Dissipation-Based Arc Length Method for Robust Simulation of Brittle and Ductile Failure." International Journal for Numerical Methods in Engineering 77.9 (2008): 1290-1321.

Wempner, G.A. “Discrete approximation related to nonlinear theories of solids.” International Journal of Solids and Structures 7 (1971): 1581-1599.

Zill, Dennis G. A First Course in Differential Equations. Pacific Grove: BROOKS/COLE, 2001.